STUDY OF PHOTOINDUCED ELECTRON TRANSFER IN HYDROGEN BONDED DONOR ACCEPTOR SYSTEMS

THESIS SUBMITTED TO
THE UNIVERSITY OF KERALA
IN FULFILMENT OF THE REQUIREMENTS
FOR THE DEGREE OF
DOCTOR OF PHILOSOPHY
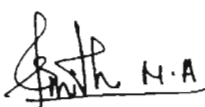IN CHEMISTRY
UNDER THE FACULTY OF SCIENCE

BY
M. A. SMITHA

STATEMENT

I hereby declare that the matter embodied in this thesis is the result of investigations carried out by me at the Photochemistry Research Unit of the Regional Research Laboratory (CSIR), Trivandrum, under the guidance of Dr. K. R. Gopidas and the same has not been submitted elsewhere for a degree.

In keeping with the general practice of reporting scientific observations, due acknowledgement has been made wherever the work described is based on the findings of other investigators.

M. A. Smitha

iii

Dr. K. R. GOPIDAS
SCIENTIST

PHOTOCHEMISTRY RESEARCH UNIT
REGIONAL RESEARCH LABORATORY (CSIR)
TRIVANDRUM-695 019, INDIA

Telephone: 91-471-515318   Fax: 91-471-490186
E. Mail: gopidaskr@rediffmail.com

October 4, 2001

CERTIFICATE

Certified that the work embodied in this thesis entitled: **"STUDY OF PHOTOINDUCED ELECTRON TRANSFER IN HYDROGEN-BONDED DONOR-ACCEPTOR SYSTEMS"** has been carried out by Ms. M. A. Smitha under my supervision and the same has not been submitted elsewhere for a degree.

K. R. Gopidas

(Thesis Supervisor)

iv

ACKNOWLEDGEMENTS

CONTENTS

PREFACE

Over the past decades, significant emphasis has been placed on developing an understanding of the dependence of electron transfer rate constants on donor-acceptor distance, orientation, free energy of reaction and electronic coupling. In this context, a large number of covalently bound donor-acceptor systems have been synthesized and studied. The present trend, however is to study the electron transfer processes in non-covalently bound supramolecular systems. Such systems act as models for studies of artificial photosynthesis. Accordingly, the last few years has seen a surge of interest in the use of supramolecular methods to synthesize chromophore quencher complexes using noncovalent interactions, both as models for the naturally occurring photosynthetic reaction centers and to explore new unnatural systems for light harvesting.

Of the various means of supramolecular assembly, hydrogen bonding is the most important. This is primarily because of the two important properties of hydrogen bonds, which are directionality and selectivity. Though a large number of donors and acceptors were assembled by hydrogen bonding interactions and electron transfer processes in these systems were studied in detail, several aspects of electron transfer processes in these systems remains to be explored. For example, the effects of factors such as solvent, distance, temperature etc. on the

rate of electron transfer in hydrogen-bonded systems have not been studied. Dealing with these aspects of electron transfer has become a necessary criterion to yield clear answers to questions concerning the mechanism of electron transfer reactions in biological systems. In the present thesis, some aspects of photoinduced electron transfer reactions in hydrogen-bonded donor-acceptor systems are reported. The first chapter gives a general introduction of the subject and describes the significant advances that have been made in this area.

In Chapter 2 of the thesis. we have investigated the photoinduced electron transfer processes in donor-acceptor systems containing arylacetic acid moieties. Because of the presence of acetic acid moieties in them, a small fraction of the donors and acceptors are present as hydrogen-bonded self assembled systems in non-polar solvents. Upon excitation two types of electron transfers can take place: (1) the activation controlled electron transfer within the hydrogen-bonded fraction and (2) the diffusion controlled electron transfer taking place in the free molecules as shown in Scheme 2.3. The rate constants for both these processes were determined as a function of free energy in chloroform solution. Our studies showed that electron transfer within the hydrogen-bonded fraction follows the Marcus behavior and electron transfer in the free moving segment obeys the Rehm-Weller behavior. We could thus establish unequivocally that the non-observance of the inverted region in bimolecular photoinduced electron transfer

reactions is due to diffusion. We also observed that the maximum in the Marcus plot for the hydrogen-bonded fraction was shifted to less negative free energy values in chloroform compared to that in dichloromethane. This further confirms the Marcus type electron transfer in these systems. In toluene solution in addition to electron transfer, exciplex formation was also observed for some systems. This complicated the analysis of the fluorescence decay profiles.

In Chapter 3, we have carried out the distance dependence studies in the normal and inverted regions using compounds shown in Chart 3.5. The rate constant for the electron transfer depends very much on the distance between the donor and acceptor moieties. Based on the theoretical consideration it was predicted that the rate constant decreases exponentially with distance in the normal region but is expected to show an increase followed by a decrease in the inverted region. The latter suggestion has not been verified. This has prompted us to undertake a study of distance dependence of electron transfer reactions in hydrogen-bonded systems. We found that for the system in the normal region the rate constants decreased exponentially with distance and for the system in the inverted region the rate constant showed a small initial increase followed by a decrease.

Chapter 4 of the thesis deals with the study of temperature dependence in the normal and inverted region in hydrogen-bonded systems. 5, 6 and 7 were used

as quenchers. Analysis of the results showed that the Marcus treatment provides a reasonably good estimate of the temperature dependence of electron transfer rates for the system in the normal region. For systems in the inverted region electron transfer rates were nearly independent of temperature and could not be explained by the Marcus equation. These however, could be adequately described by the golden rule expression, which takes in to account the nuclear tunneling via one or more high frequency vibrational modes.

Note: The compound numbers and schemes listed in this preface refer to those given in different chapters of this thesis.

CHAPTER 1

PHOTOINDUCED ELECTRON TRANSFER REACTIONS IN HYDROGEN-BONDED DONOR-ACCEPTOR SYSTEMS: AN OVERVIEW

1.1. Introduction

Photoinduced electron transfer (PET) is of fundamental importance because it plays a crucial role in the natural photosynthetic process. Much of the current interest in PET processes stems from the exciting advances made in the past decade in understanding the primary processes involved in photosynthesis. In photosynthesis solar light is absorbed and transformed into bio-energy by the reduction of carbon dioxide and in the process water is oxidized to molecular oxygen. The whole process is brought about by an initial absorption of light followed by a series of electron transfers between donors and acceptors that are placed at specific distances and orientations relative to one another by the surrounding protein matrix in the photosynthetic reaction centre. A fundamental understanding of the processes taking place in natural photosynthesis is also required for the development of efficient, artificial photosynthetic systems for the conversion and storage of solar energy.

The photosynthetic apparatus in both bacteria and plants consists of two distinct units called antennae and the reaction centre. Antennae are the light gathering complexes consisting of chlorophyllous pigments as well as carotenoids

arranged in the protein matrix. These pigment-protein complexes absorb light and

efficiently transfer the excitation to the reaction centre. The reaction centre

consists mainly of organic donor and acceptor molecules embedded within a

protein matrix. The reaction centre of *Rhodobacter sphaeroides* comprises of four

bacteriochlorophylls (BChl), two bacteriopheophytins (BPh), two quinones (Q_A

and Q_B) and a carotenoid polyene. The spatial arrangement of these components

within the reaction centre is shown in Figure 1.1.[1]
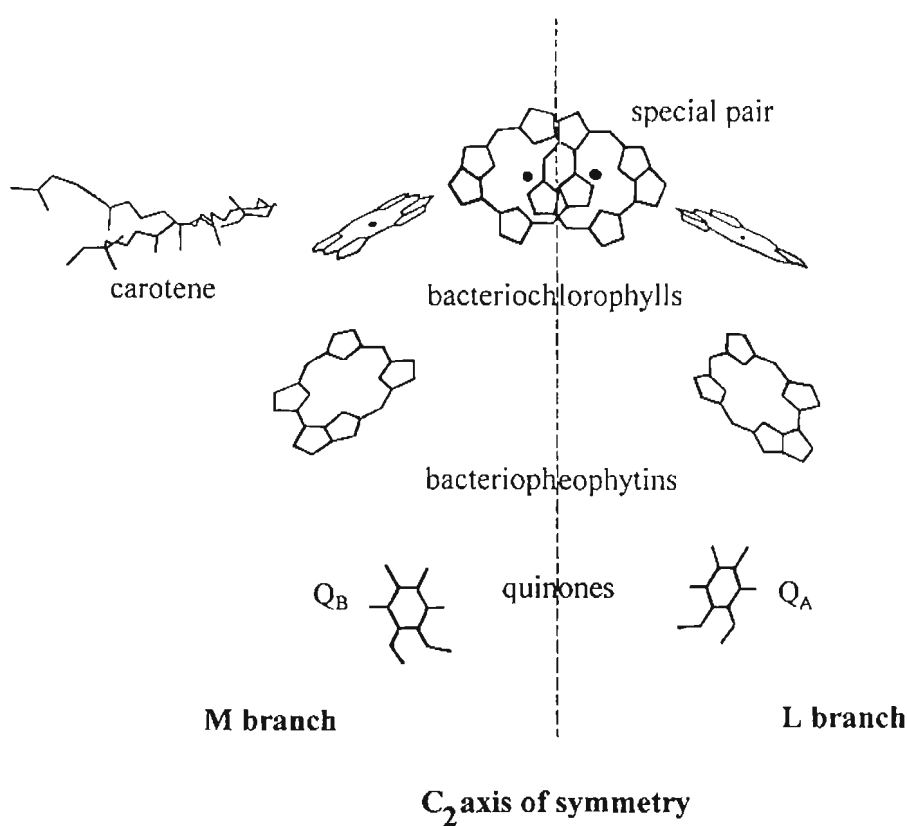
Figure 1.1. Arrangement of the chromophores, electron donors and electron acceptors in the bacterial reaction centre of *Rhodobacter sphaeroides.*

It can be seen from Figure 1.1 that with the exception of carotenoid, the molecules occur in pairs and the reaction centre has approximate C_2 symmetry. Of the four BChl molecules, two are positioned very close. Hence they are very strongly coupled electronically and are termed "special pair" of BChls.

The photosynthetic process within the reaction centre begins with the excitation of the special pair BChls by excitation transfer from the antennae units. Within 2 - 4 ps of excitation, the singlet excited state of the special pair donates an electron to the BPh molecule on the L-branch, leading to the formation of the special pair radical cation and BPh radical anion.[2-6] The accessory BChl on the L-branch plays the role of an intermediate acceptor in this process.[7] The M-branch of the reaction centre in Figure 1.1 is almost inactive in the electron transfer process. The BPh radical anion formed by electron transfer from the special pair transfers an electron to the nearby quinone (Q_A) in 200 ps. This electron is subsequently transferred to quinone Q_B in about 100 μs. The positive charge remaining on the special pair is quenched by electron transfer from an iron porphyrin on the outer side of the membrane. The net result of this multistep electron transfer is the generation of a trans-membrane charge separated state with a quantum yield of near unity. Since the positive and negative charges are separated by the thickness of the lipid bilayer, back electron transfer, which would waste the stored energy, is precluded.

Considerable effort has been devoted to mimicking the natural photosynthetic process in the laboratory and this area of electron transfer

chemistry is known as artificial photosynthesis. It involves the construction and study of PET processes in model systems in which pigments, donors and acceptors are held at proper distances and orientations. The first approach used in the construction of model systems has been to link the various constituents by covalent bonds. Following this approach, a large number of covalently linked donor-bridge-acceptor systems were synthesized and studied as model systems for artificial photosynthesis and these studies have contributed a great deal to our understanding of the fundamental processes taking place in photosynthesis.[8-18]

In the covalent approach to artificial photosynthesis, the constituents are held in place by chemical bonds. In the natural photosynthetic reaction centre, however, the constituents are not held together by covalent bonds. The complex array of components in the natural photosynthetic reaction centre are held in a spatially well-defined arrangement by the surrounding protein using a collection of weak non-covalent interactions. These non-covalent interactions not only hold the components in place but also help in the mediation of electron and energy transfer processes.[19-21] Realization of this aspect has led to a surge of interest in the use of non-covalent interactions to assemble donor-acceptor systems for artificial photosynthesis and light harvesting. Research in this area has lead to the preparation of several highly sophisticated supramolecular systems for energy and electron transfer reactions.[21-26] A non-covalent approach is indeed a novel and feasible way to augment our understanding of photosynthesis and metabolism related electron transfer reactions.

Non-covalent or supramolecular assembling of components relies on the principles of molecular recognition. The non-covalent interactions of interest in the present context are coordinate bonds, hydrogen bonds, van der Waals interactions, aromatic π-stacking and ionic interactions.[25-29] The propensity of the metal centres in metalloporphyrins to coordinate with suitable electron donating moieties was first recognized by Sanders and co-workers as a useful tool to build donor-acceptor assemblies.[30] Subsequently, coordinate bonds were widely used to assemble a number of chromophore-quencher systems to study intramolecular electron transfer reactions.[31-35] Nocera and co-workers have assembled donors and acceptors by association involving salt bridges and studied the PET processes in these systems.[36-39] Hydrophobic encapsulation of guest molecules in cyclodextrin (CD) cavities provides yet another method to assemble donors and acceptors. For example, Bolton and co-workers described a system in which electron transfer occurred from a porphyrin unit covalently linked to the periphery of the β-CD to a quinone unit encapsulated within the hydrophobic cavity of the same CD.[40]

Of the various means of supramolecular assembly, hydrogen bonding is the most important. This is primarily because of the two important properties of hydrogen bonds, which are directionality and selectivity. The directional nature makes it possible to know the separation and relative orientation between the two components associated *via* hydrogen bonding. The selectivity helps to exert considerable control over the association process by careful use of exactly complementary components. By a judicious choice of hydrogen bonding moieties

one can design linear arrays or three-dimensional networks of hydrogen-bonded

assemblies. The fact that these self-assemblies can exist in solution as well as in

solid phase is of special interest. Although hydrogen bonds are relatively weak

when compared to covalent bonds, multiple hydrogen bonds can hold together

assemblies of chromophores and quenchers very efficiently. Consequently a large

number of donors and acceptors were assembled by hydrogen bonding interactions

and electron transfer processes in these systems were studied in detail.

In the present thesis, some aspects of PET reactions in hydrogen-bonded

donor-acceptor systems are reported. In order to put our work in proper

perspective, a review of the literature in this area is attempted here. Origin of the

present work and outline of the thesis is then briefly discussed. It is hoped that the

work presented here will shed some light on the various aspects of biological

electron transfer processes.

1.2. Survey of Photoinduced Electron Transfer Reactions in Hydrogen-Bonded Donor-Acceptor Systems

PET in a synthetic hydrogen-bonded assembly was first reported by

Harriman, Sessler and co-workers in 1992.[41] In the system (1, Chart 1.1) designed

by these authors, a Zn-porphyrin donor and a quinone acceptor were assembled at

approximately 20 Å apart by hydrogen bonding interactions involving guanine

and cytosine residues. Association of the donor and acceptor components in 1 was

established by ^{1}H NMR and electron transfer was probed by fluorescence lifetime

measurements. In the absence of the quinone component the fluorescence decay of the Zn-porphyrin was monoexponential with a lifetime (τ_0) of 1.5 ± 0.2 ns. When the cytosine appended quinone derivative was added, fluorescence decay became biexponential with τ_1 = 0.94 ± 0.07 ns and τ_2 = 1.5 ± 0.2 ns. The longer component τ_2 is the unquenched Zn-porphyrin decay and the shorter component τ_1 results from electron transfer to the quinone in the hydrogen-bonded assembly. The rate constant for this process was calculated using the expression k_{et} = (1/τ_1 - 1/τ_0) and the value obtained was k_{et} = (4.2 ± 0.7) x 10^8 s^{-1}.
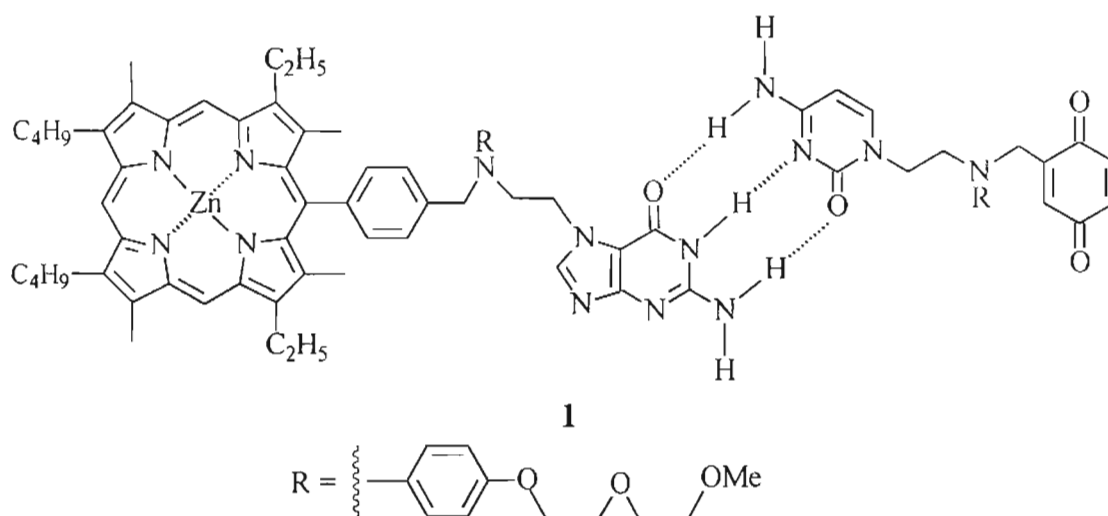
Chart 1.1

Several control experiments were carried out to show that the short lifetime component was due to the hydrogen-bonded species. Addition of a hydrogen bonding solvent such as ethanol led to the disruption of the hydrogen-bonded assembly resulting in the disappearance of the short lifetime component. The short

component also disappeared when the recognition units responsible for hydrogen bonding were removed.

A major drawback of the assembly **1** is its flexibility. Because of the flexibility the donor and acceptor units in **1** can approach each other in space and this can result in through-space electron transfer. The observed rate constant can not be then attributed to through-hydrogen bond electron transfer. Sessler and co-workers had later designed a very rigid system (**2**, Chart 1.2) to address this issue.[42]

2
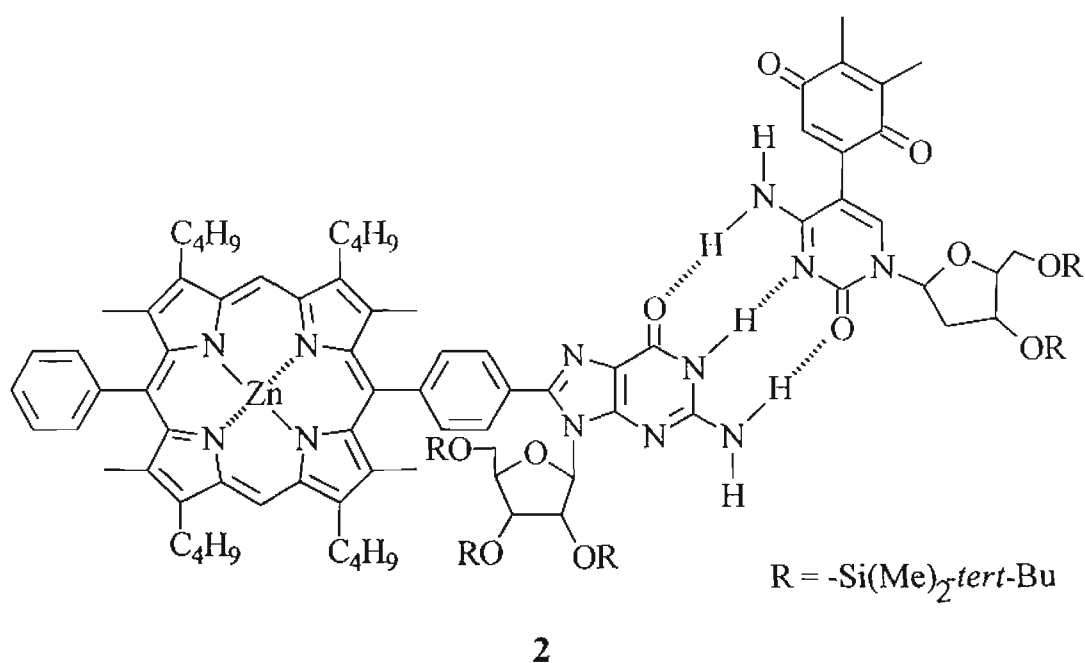
Chart 1.2

The rigidity of the hydrogen bond framework in **2** prevents the donor and acceptor from interacting in space. Time resolved fluorescence studies as in the case of **1** showed that electron transfer in **2** is very fast and efficient. In this case

also appropriate control experiments were carried out to establish that electron transfer is taking place through the hydrogen bond interface.

Another system designed by Sessler and co-workers is shown in Chart 1.3.[43] In this case through-hydrogen bond as well as through-space electron transfer pathways are possible. Time resolved fluorescence studies in dry dichloromethane showed that in the absence of added benzoquinone, the decay of the singlet excited state of the calixarene bound porphyrin was single exponential with a lifetime of 1.6 ns. Addition of benzoquinone resulted in biexponential decay, and the shorter component of this decay was attributed to the intra-ensemble electron transfer. The observed rate constant of $(8.0 \pm 0.2) \times 10^8$ s^{-1} in this case may have substantial contributions from through-space or through-solvent electron transfer reactions.
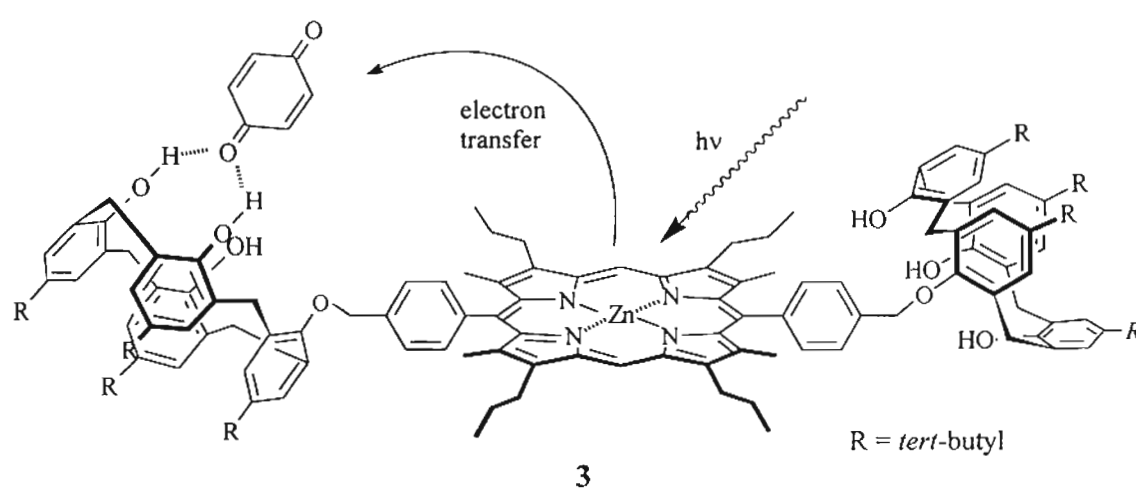
Chart 1.3

Sessler *et al.* had recently designed the coplanar hydrogen-bonded system **4** (Chart 1.4) consisting of a chlorin donor and naphthalene diimide acceptor.[44] The edge-to-edge distance between the donor and acceptor in **4** is 7 Å. Fluorescence lifetime measurements yielded a rate constant of 7.6×10^8 s^{-1} for the electron transfer process. Unfortunately, all efforts to observe the diimide derived radical anion using time resolved spectroscopy met with failure in this case. This was attributed to extremely fast back electron transfer taking place in the system.

Ar = 3,5-di-*tert*-butylphenyl
R = *tert*-butyl

4
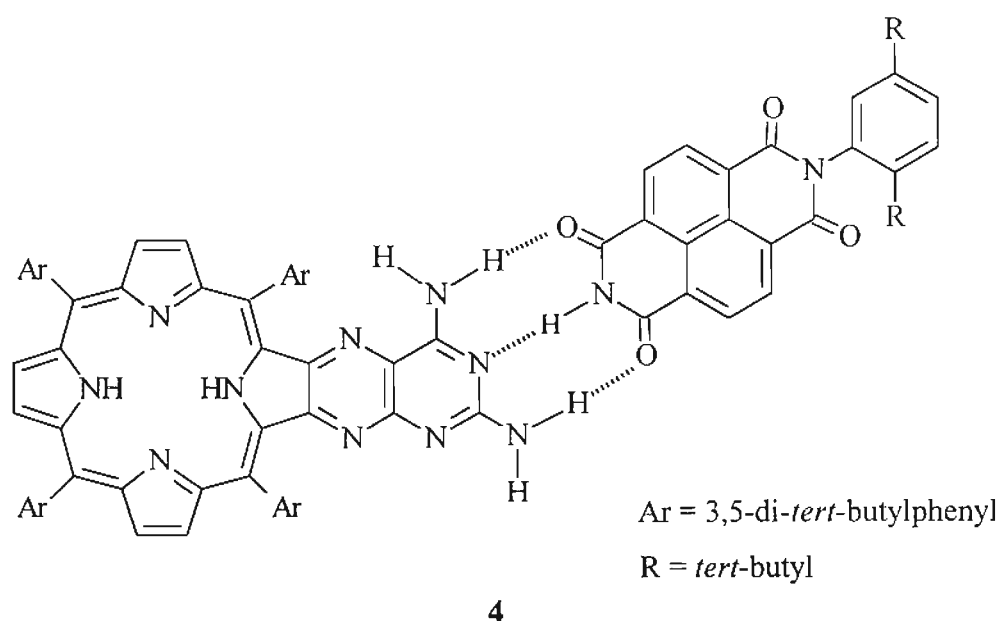
Chart 1.4

PET in hydrogen-bonded donor-acceptor systems has also been probed by time resolved electron paramagnetic resonance spectroscopy (TREPR).[45-47] Sessler and co-workers, for example, had assembled the porphyrin-dinitrobenzene system **5** (Chart 1.5) in a liquid crystal medium.[46] It is recognized that liquid crystals as

solvents attenuate intramolecular electron transfer rates by 2 - 3 orders of magnitude by slowing down the rotational diffusion rate relative to organic solvents. This reduction in electron transfer rates, in turn, enables us to detect radical pair states directly by TREPR. Selective photoexcitation of the Zn-porphyrin moiety in **5** yielded a narrow derivative like signal, which was assigned to a long-distance charge-separated state. Electron transfer in this case takes place from the lowest triplet state of Zn-porphyrin to the dinitrobenzene. No EPR signal was observed when the complementary hydrogen bonding units were absent and this confirmed the intra-ensemble nature of the electron transfer reaction.
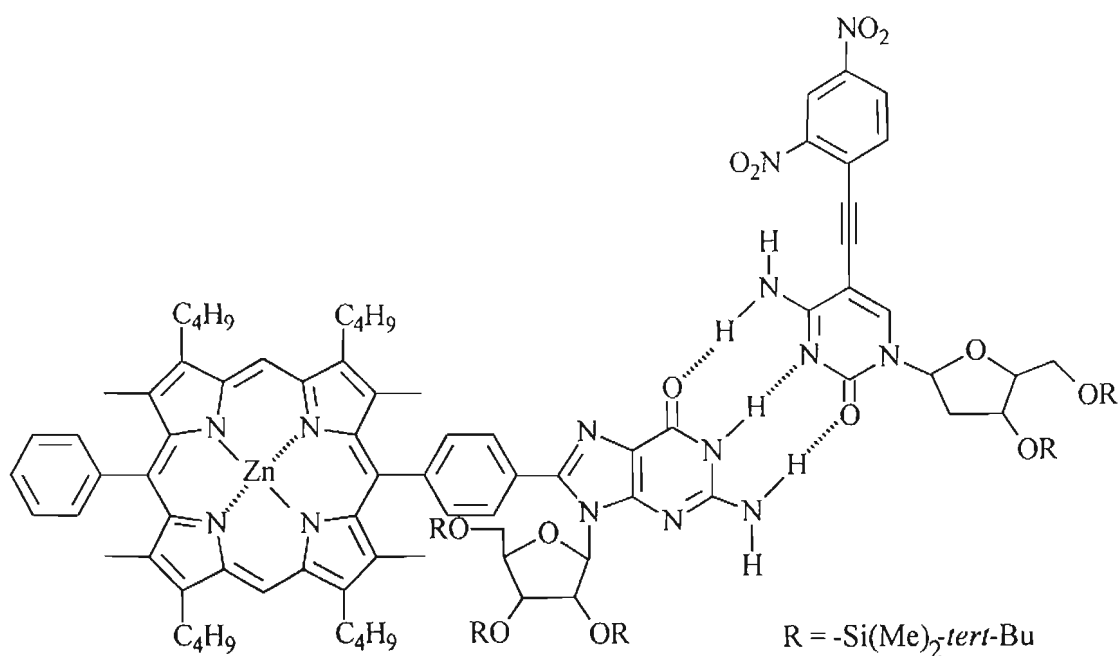
5

Chart 1.5

In a very recent paper, Sessler *et al.* studied a hydrogen-bonded anthracene-dimethylaniline dyad, held together by guanine-cytidine Watson-Crick base pair interactions.[48] Upon excitation at 420 nm, PET from the dimethylaniline donor to the singlet excited state of the anthracene acceptor occurs, as inferred from a combination of time resolved fluorescence quenching and transient absorption measurements. In toluene, at room temperature, rate constants for photoinduced intra-ensemble electron transfer (k_{et}) and subsequent back electron transfer (k_{CR}) were $3.5 \times 10^{10} \text{ s}^{-1}$ and $1.42 \times 10^9 \text{ s}^{-1}$, respectively.

The propensity of carboxylic acid groups to form hydrogen-bonded dimers in non-polar solvents was exploited by Nocera and co-workers to design the donor-acceptor system 6 (Chart 1.6).[49] The association constant for the formation of 6 was determined by infrared spectroscopy and the value obtained was 552 M^{-1} in dichloromethane solution. The free energy change for the intra-ensemble PET in 6 is -0.73 eV. Photoexcitation of the Zn-porphyrin resulted in transfer of an electron to the nitroaromatic acceptor moiety, which was monitored using steady state and time resolved experiments. The rate constant for electron transfer in this case ($k_{et} = 5.0 \times 10^{10} \text{ s}^{-1}$) was only slightly lower than that in the covalently linked system 7 (Chart 1.6), having similar donor-acceptor separation and driving force.[50] Several other systems were studied by Nocera and co-workers and these are discussed later in this chapter in the section dealing with proton coupled electron transfer reactions.

6

7
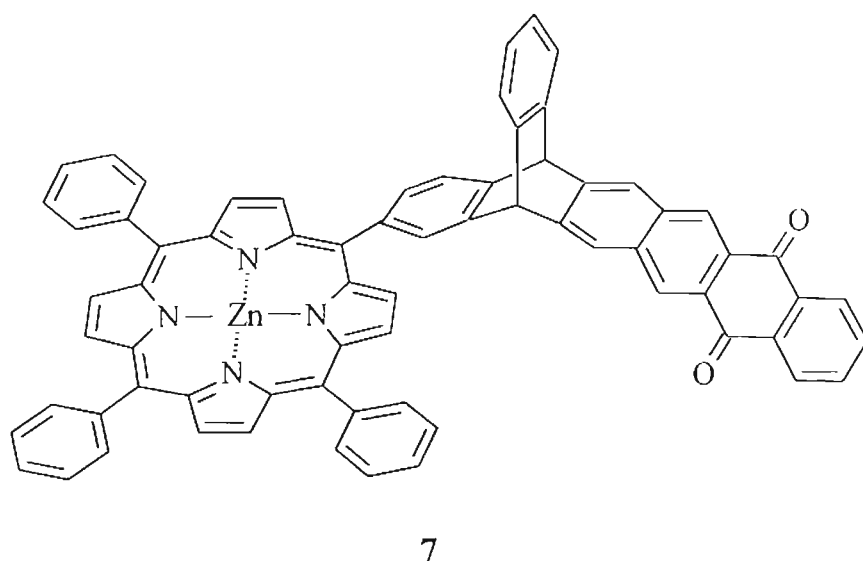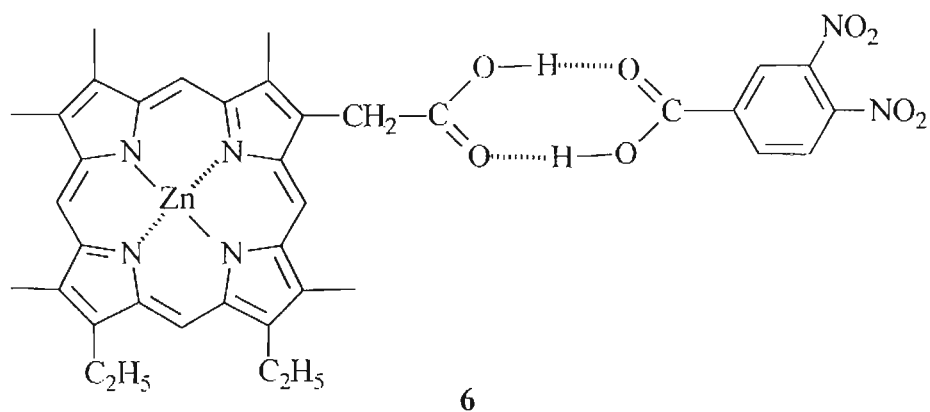
Chart 1.6

Osuka *et al.* had studied electron transfer processes in the porphyrin-naphthalenediimide supramolecular system **8** (Chart 1.7).[51] The centre-to-centre distance between the donor and acceptor in **8** is 14.7 Å. Picosecond transient absorption studies provided clear evidence for the formation of the diimide radical anion at 474 nm and the Zn-porphyrin radical cation at 655 nm. For the ensemble **8**, rate constants for charge separation k_{CS} = 4.1 x 10^{10} s^{-1} and charge recombination k_{CR} = 3.7 x 10^9 s^{-1} were obtained. The authors had compared this

with the covalently linked model system **9** having similar driving force and centre-to-centre distance. For this system measured k_{CS} and k_{CR} values were 9.9×10^{10} s^{-1} and 6.7×10^8 s^{-1}, respectively. Based on this study, the authors concluded that: (1) the electronic coupling across hydrogen-bonded interface needed for the charge separation is comparable to that across two C-C single bonds and (2) the ion-pair across a hydrogen-bonded interface is considerably short-lived when compared to a covalently linked ion pair.

8

R = -Si(Me)$_2$*tert*-Bu
R' = *tert*-butyl

9
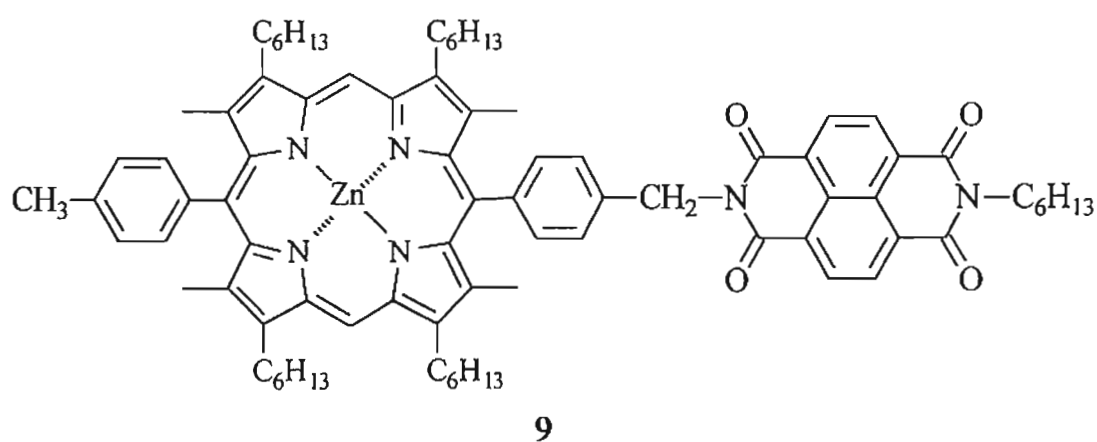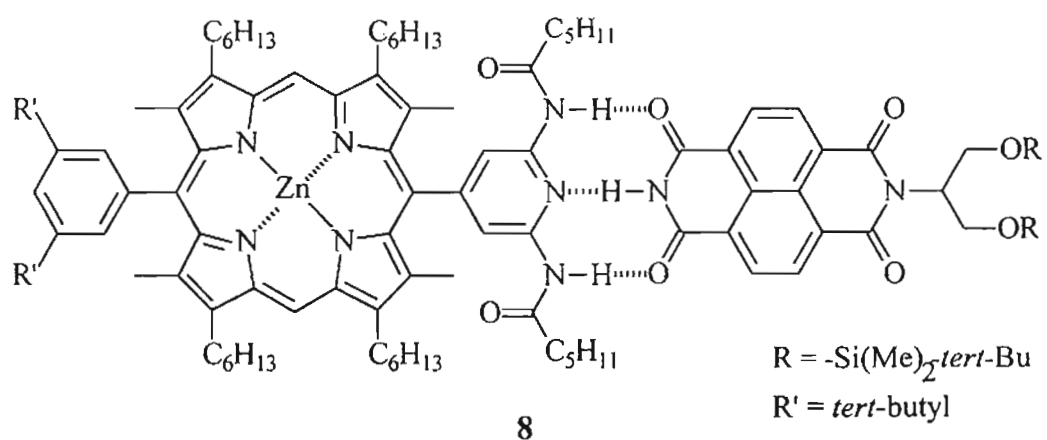
Chart 1.7

All the above studies had established very clearly that hydrogen bonds can act as effective conduits for the transfer of electrons from a donor to an acceptor moiety. It is however not clear as to whether the electronic coupling pathways provided by the hydrogen bond is better or worse compared to that by a covalent bond. Since hydrogen bonds are much weaker than covalent bonds, it was generally believed that the electronic coupling provided by a hydrogen bond is very weak compared to that by a covalent bond. In order to clarify this issue, Therien and co-workers had designed and studied the elegant set of donor-acceptor systems (**10 - 12**) shown in Chart 1.8.[52] Compounds **10, 11,** and **12** have Zn-porphyrin as donor and Fe-porphyrin as acceptor units. The bridging units in these cases changed from the unsaturated covalent in **10** to saturated covalent in **11** to hydrogen-bonded non-covalent in **12**. In all these bridging groups, there are two equivalent electron transfer pathways, which contribute to the overall electronic coupling. The donor-acceptor distances and free energy changes were similar in **10** - **12**. The electron transfer rate constants obtained in these cases (see Chart for k_{et} values) showed that the electronic coupling in the hydrogen-bonded donor-acceptor system **12** is larger than that in **11**. This interesting study evinces the result that electronic interaction modulated by the hydrogen bond interface is superior to that provided by an analogous interface composed entirely of carbon-carbon sigma bonds.

10
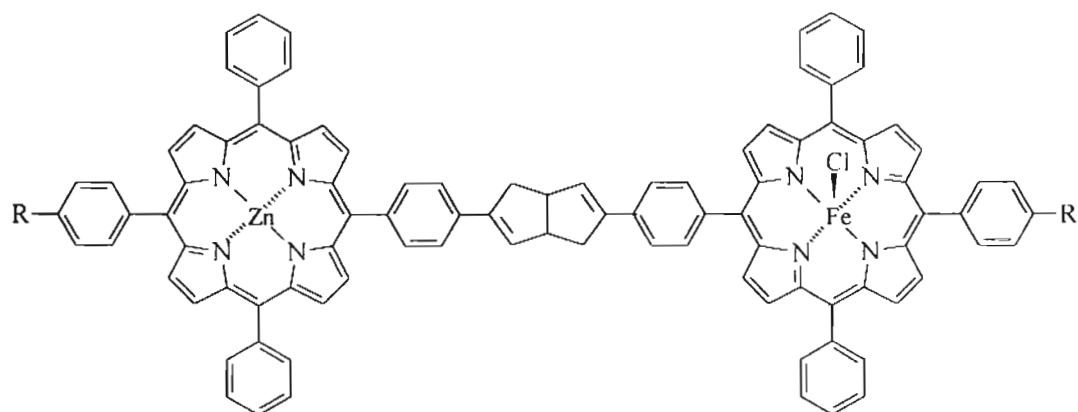
$\Delta G^\circ = -0.87$ eV, $k_{et} = 8.8 \times 10^9$ s^{-1}

11
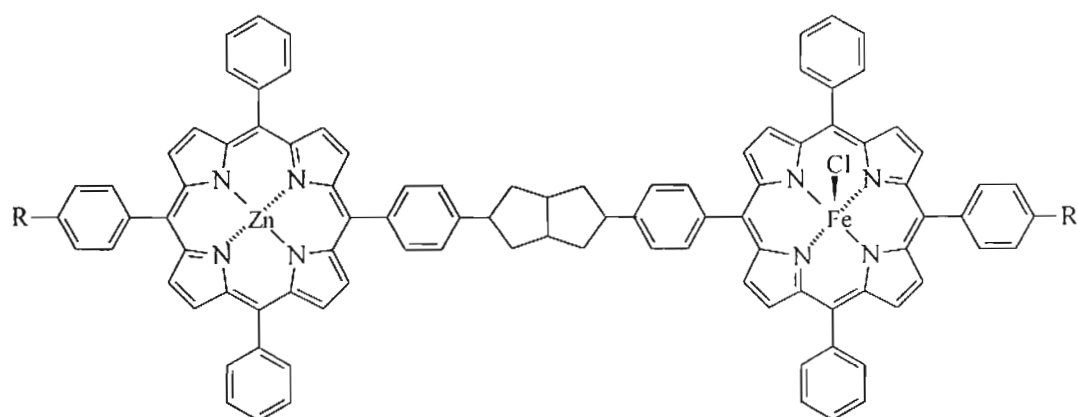
$\Delta G^\circ = -0.87$ eV, $k_{et} = 4.3 \times 10^9$ s^{-1}

12
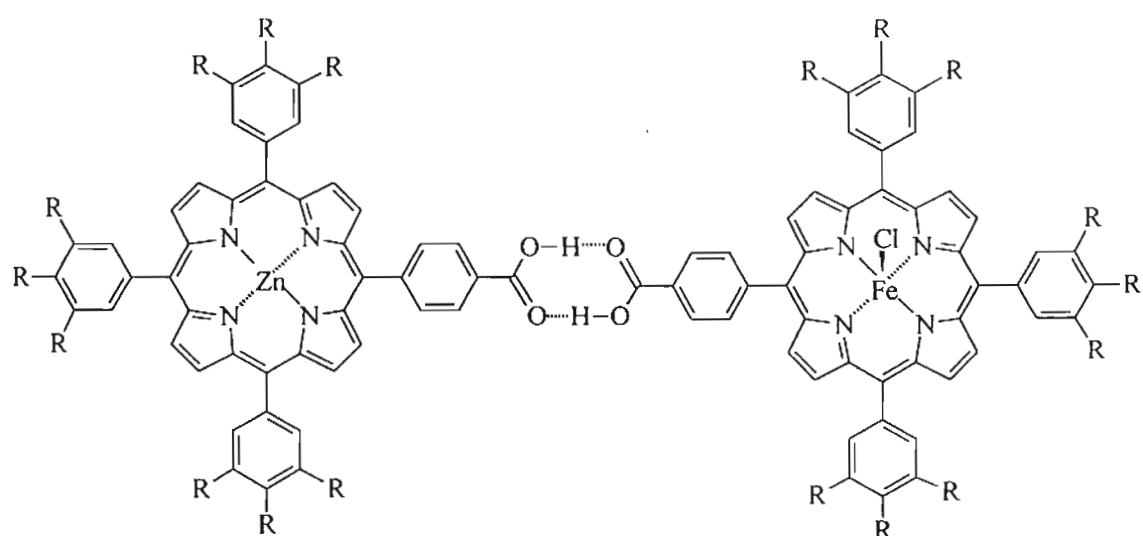
R = OCH$_3$

$\Delta G^\circ = -0.70$ eV, $k_{et} = 8.1 \times 10^9$ s^{-1}

Chart 1.8

Tamiaki and Maruyama had reported a donor-acceptor system (**13**, Chart 1.9) capable of forming a β-turn structure often found in proteins.[53] The electron transfer from the porphyrin to the quinone was studied using fluorescence lifetime measurements and a value of 2.1×10^8 s^{-1} was obtained for k_{et} in this system. Though the study turned out to be a stepping stone in the study of electron transfer in protein, it had two major setbacks. In **13**, the central amide linkage can lead to a γ-turn formation and this may complicate interpretation of the results. Secondly the question whether the non-covalent short-cuts were preferred over covalent pathways remained unaddressed, since in both the pathways the donor and acceptor were separated by a distance of 8 bonds.
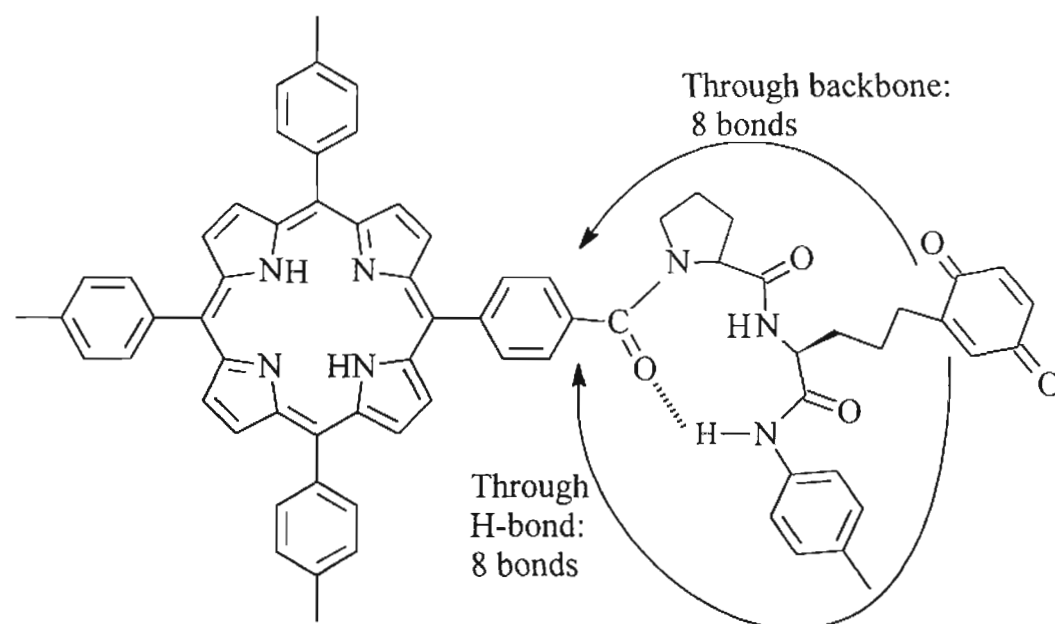
13

Chart 1.9

In a recent study Williamson and Bowler addressed the above issues using
the donor-acceptor system **14** (Chart 1.10).[54] In this system the central amide
linkage was replaced by an ester group, which ensures the β-turn folding and

14

15
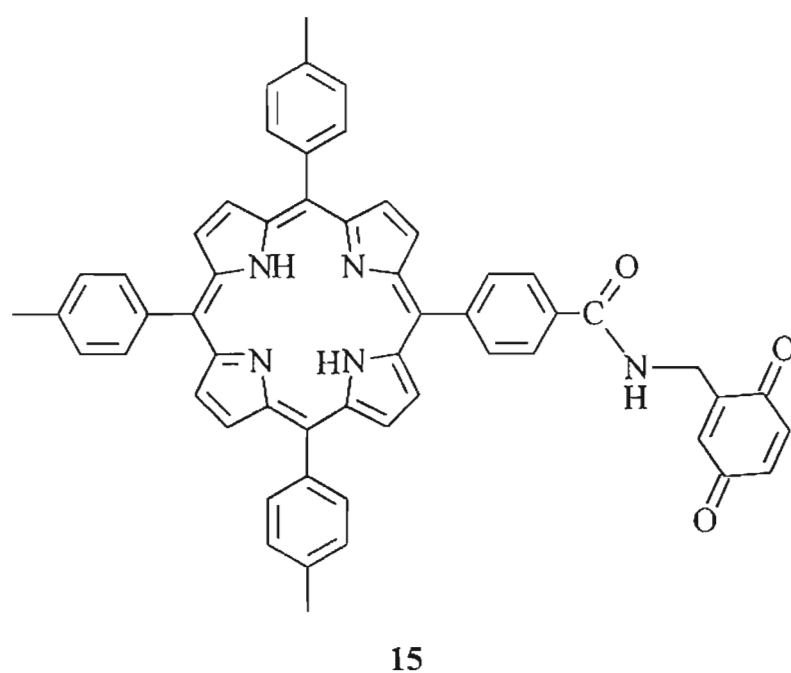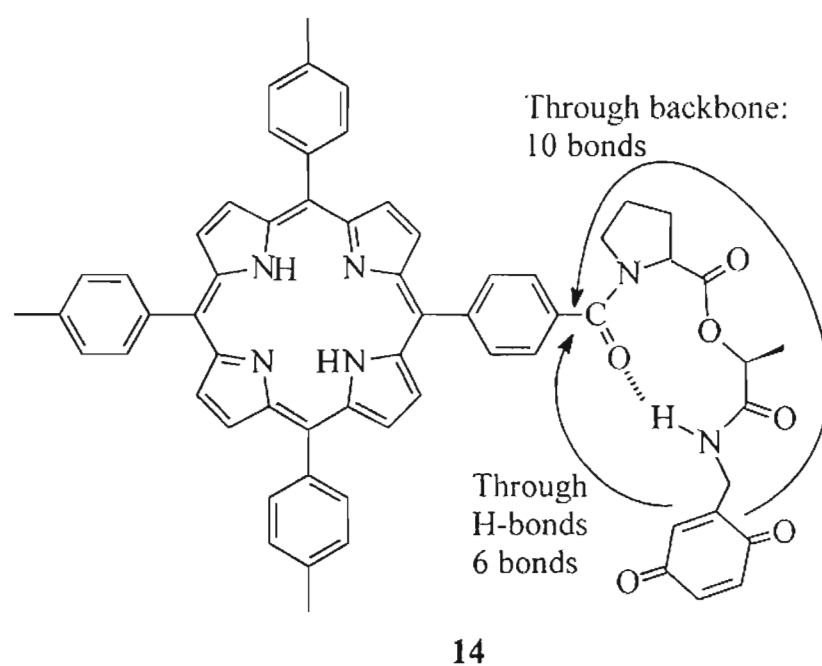
Chart 1.10

eliminated the possibility of γ-turn folding. In **14,** electron transfer pathway through the hydrogen bond involves only 6 bonds, whereas, the pathway through covalent bonds involves 10 bonds. The authors also had compared the electron transfer in **14** with that in **15** studied earlier by Bolton and co-workers.[55] Three out of the four covalent bonds in the shortest electron transfer pathway in **14** and **15,** are identical. Thus, by comparing the electron transfer rates in **14** and **15** one can evaluate the electronic coupling due to a single hydrogen bond. For **15,** Bolton and co-workers had reported a rate constant of 8.0×10^8 s^{-1}. If only the covalent pathway is considered, then k_{et} in **14** is expected to be 200 - 1000 times slower. In contrast, very fast electron transfer was observed for **14** in dichloromethane solution ($k_{et} = (1.1 \pm 0.1) \times 10^9$ s^{-1}). This was attributed to the short-cut provided by the hydrogen-bonded pathway in the β-turn conformation. When DMSO was used as solvent, β-turn structure was disrupted and electron transfer was no longer competitive with the intrinsic fluorescence decay. This study has shown very clearly that hydrogen bonds present in the system can act as a short-cut pathway for electron transfer reactions.

Williamson and Bowler recently extended their study to **16** (Chart 1.11) in which the porphyrin donor and quinone acceptor are separated by 13 covalent bonds.[56] But **16** can undergo a α-helical turn, which leads to a hydrogen-bonded short-cut involving only 6 bonds. Fluorescence lifetime measurements showed that electron transfer is very efficient in this system with $k_{et} = (5.6 \pm 0.3) \times 10^8$ s^{-1}. The

electronic coupling matrix element observed for this compound was 100 fold larger than the value expected for electron transfer along the covalent pathway. The study clearly indicates that non-covalent contacts, such as that provided by hydrogen bonds, are very adequate to compensate for increasing covalent separation between the electron donors and acceptors in biological systems.
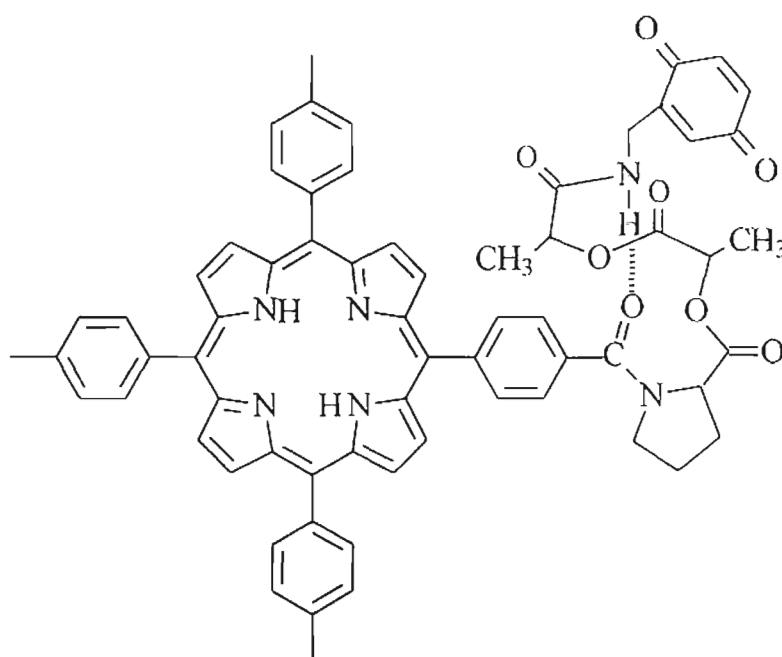
16

Chart 1.11

Several authors have assembled porphyrins and quinones in a co-facial manner using hydrogen bonding interactions and studied the electron transfer processes in these systems.[57-63] For example, Hayashi *et al.* had studied the ensemble **17** shown in Chart 1.12.[63] The distance between the porphyrin and quinone rings in **17** is estimated to be 3.5 Å from CPK models. Extremely fast

electron transfer (k_{et} = 4.0 x 10^{11} s^{-1}) was observed in **17** and this may have contributions from through-space electron jumps. Studies of this type are important as they help in understanding the electron transfer processes in biological systems.
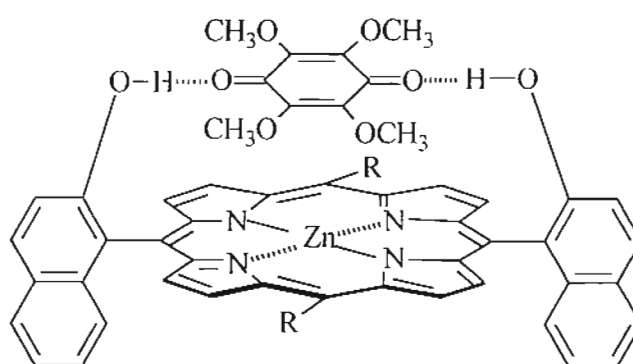
17
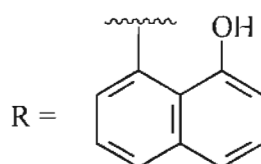
Chart 1.12

Hydrogen bonding interactions have also been utilized to facilitate heterogeneous electron transfer. In the ensemble shown in Chart 1.13, a TiO_2 particle is encapsulated by a diamidopyridine derivative having long alkyl chains, which in turn is hydrogen-bonded to a complementary uracil based component containing a covalently linked viologen moiety.[63,64] Irradiation of the TiO_2 fragment of complex **18** at 355 nm resulted in promotion of electrons from the

valence band to the conduction band. The conduction band electron was then transferred to the viologen moiety across the triple hydrogen bond interface. Control experiments had shown that in the absence of hydrogen bonds electron transfer does not occur.
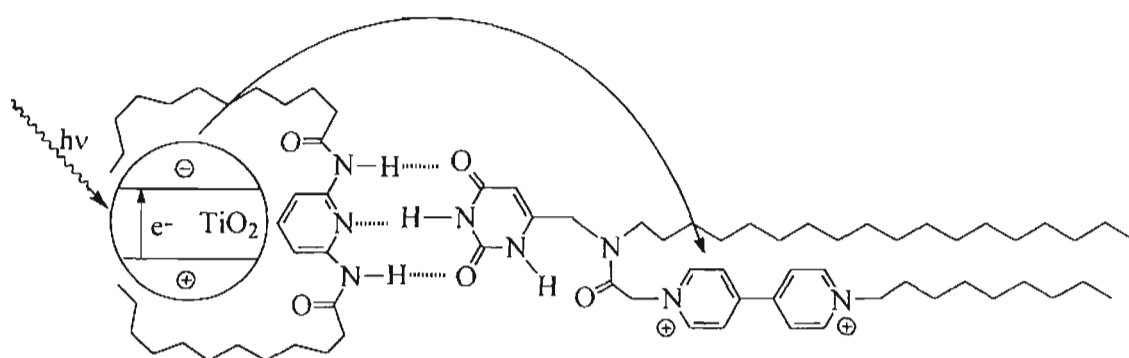
18

Chart 1.13

The dependence of electron transfer rates upon free energy in hydrogen-bonded donor-acceptor systems was addressed by Prasad and Gopidas[65] and also by Isied and co-workers[66]. The work described in this thesis is a continuation of the work by Prasad and Gopidas and this will be described later in Chapter 2 of the thesis. Isied and co-workers had studied the PET and thermal back electron transfer in the hydrogen-bonded ensemble **19** (Chart 1.14). By using different combinations of Ru and Os bipyridine derivatives, the free energy change in these systems could be varied from -0.39 to -1.68 eV. A comparison of electron transfer rates in **19** with those in related but covalently linked systems **20** (Chart 1.14) showed that the rates are only modestly slower in the former case.

19

$M = Ru^{2+}, Os^{2+}$
$M' = Ru^{3+/2+}$ } $R = \textit{tert}\text{-butyl}$
$M' = Os^{3+/2+}$ $R = \text{methyl}$

20

$M = Ru^{2+}, Os^{2+}$
$M' = Os^{3+}$
$M' = Ru^{3+}$
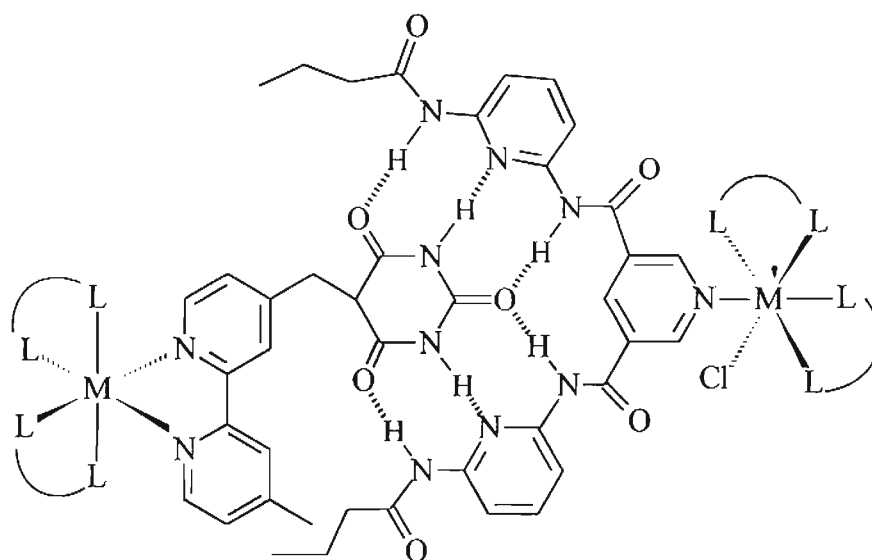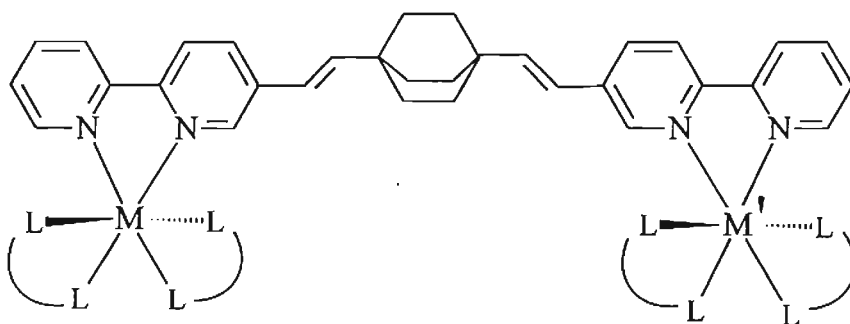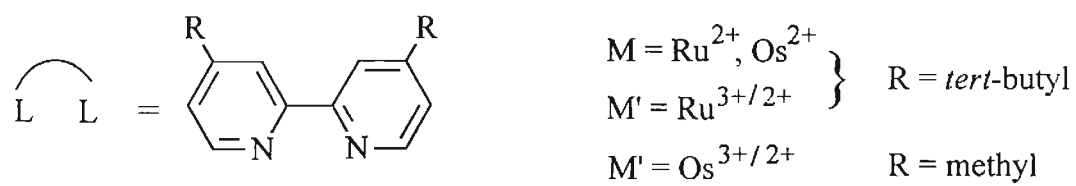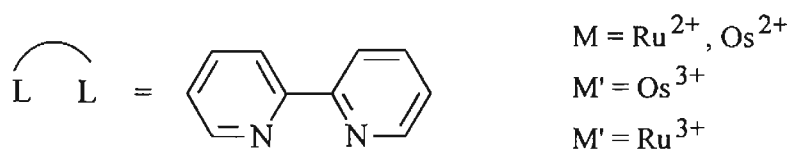
Chart 1.14

A photoswitchable hydrogen-bonded PET system was recently designed by Myles and Branda.[67] This is shown in Scheme 1.1. The system consisted of a photochromic phenoxynaphthacenequinone (NQ) unit linked to a porphyrin (P) through a hydrogen bond interface. The photochromic group is capable of undergoing reversible photoisomerization between its *trans* (irradiation by $\lambda > 434$ nm) and *ana* (irradiation by 365 nm) forms (the *trans* and *ana* moieties are highlighted in the boxes in Scheme 1.1). Both the *trans* and *ana* forms are capable of accepting an electron from the excited porphyrin moiety. The free energy change for the *P $\rightarrow$ *ana*-NQ electron transfer is more negative ($\Delta G = -10.67$ kcal M^{-1}) compared to that for the *P $\rightarrow$ *trans*-NQ electron transfer process ($\Delta G = -0.94$ kcal M^{-1}). Thus electron transfer in the ensemble **22** is expected to be faster than that in **21**. Consequently the porphyrin fluorescence is quenched much more efficiently in **22** than in **21** and the authors have claimed that this difference in the fluorescence yield of **21** and **22** can form the basis of a non-destructive read/write system in which both reading and writing are photoinduced.

A discussion on electron transfer across hydrogen bonds remains incomplete without a brief mention of proton coupled electron transfer (PCET) reactions. Proton coupled electron transfer is a process in which inter-component electron transfer across a hydrogen-bonded interface is accompanied by proton transfer across the same interface. The interface can be a symmetric one as found in carboxylic acid dimers or an asymmetric one as in guanine-cytosine base pairs.

21

560 nm

365 nm | >434 nm

trans-isomer

560 nm

22

ana-isomer

R =   ⌇─〈 〉─O-*n*-C$_4$H$_9$
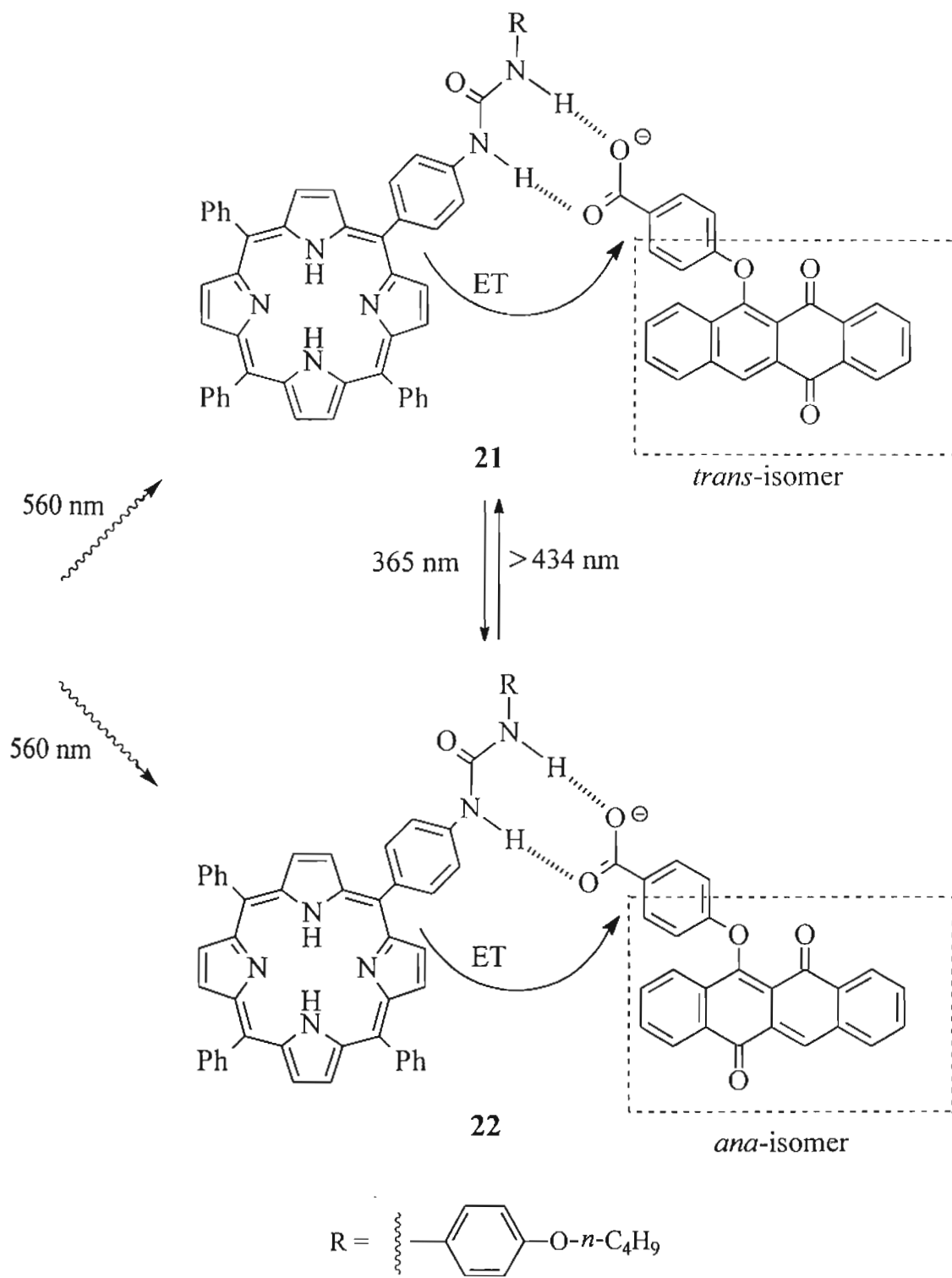
Scheme 1.1

The amidinium-carboxylate salt-bridged interface is a convenient system to study PCET reactions. This interface is very attractive since it models the arginine - aspartane salt-bridge found in many biological structures including RNA stem loops and DNA complexes. Since the interface is formed through molecular recognition of the negatively charged carboxylate and positively charged amidinium units, it is highly stable and persist in solution even when the dielectric constant of the solvent is very high. In donor-acceptor systems assembled by amidinium-carboxylate salt-bridges (**23**, Scheme 1.2), the electron and proton may transfer consecutively (path 'a', Scheme 1.2) or concertedly (path 'b', Scheme 1.2). Nocera and co-workers have studied PCET reactions in great detail and their studies have revealed several interesting aspects of PET reactions.[36-39, 68-71]

Scheme 1.2
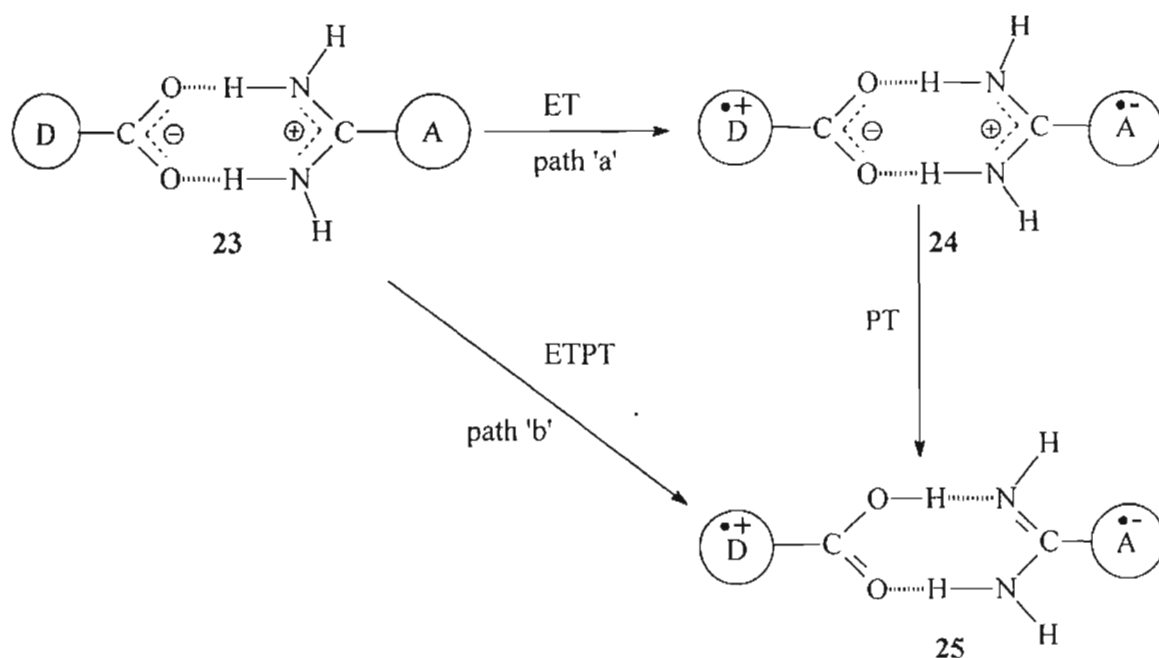
In an early study Nocera and co-workers had compared the electron transfer rates for donor-acceptor ensembles **26a** and **27a** (Chart 1.15).[36] In both the cases, $Ru^{II}(bpy)_3$ acted as the electron donor and the 3,5-dinitrobenzene as the acceptor. The free energies for PET in **26a** and **27a** were -0.14 eV and -0.21 eV, respectively. Intra-ensemble electron transfer rate constants obtained for **26a** and **27a** were 8.0 x 10^6 and 4.3 x 10^6 s^{-1}, respectively. An examination of the rate constants showed that electron transfer in **26a** is twice faster than that in **27a** even though the ΔG° value is more negative for **27a**. In both cases the electron transfer process is coupled to proton transfer. The authors have claimed that for the symmetric-hydrogen bond interface **26a**, proton displacement on one side of the dicarboxylic acid interface is compensated by displacement of a proton on the other side. As a result the proton transfer is overall symmetrical and does not require any charge redistribution in the bridge. Hence solvent interactions in the region of the bridge remain the same and activation barrier for proton transfer is low. On the other hand, the proton transfer in **27a** is accompanied by charge redistribution bringing about an activation barrier on the proton transfer process. Since proton transfer and electron transfer are coupled, the electron transfer is also slowed in the asymmetric-bridge system.

To better understand the relationship between electron transfer and proton motion, a comparative study of PCET process in a donor-amidinium-carboxylate-acceptor ensemble (**27b**) and its switched interface isomer (donor-carboxylate-
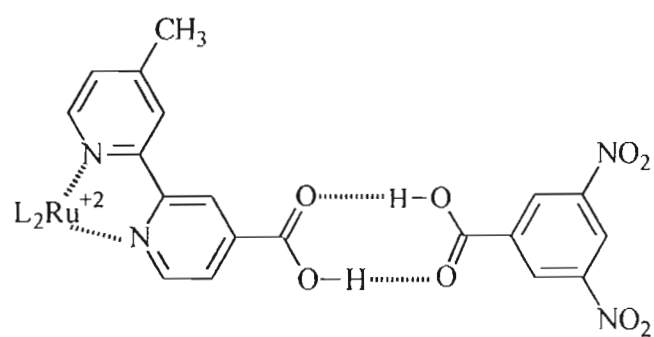
26 a, b
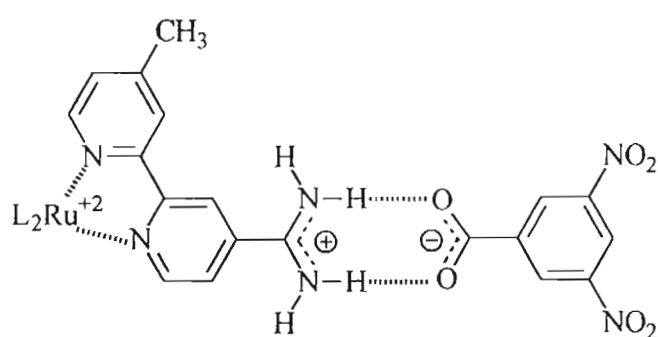
27 a, b

a: L = 2,2'-bipyridyl

b: L= 3,3',4,4'-tetramethyl-2,2'-bipyridyl
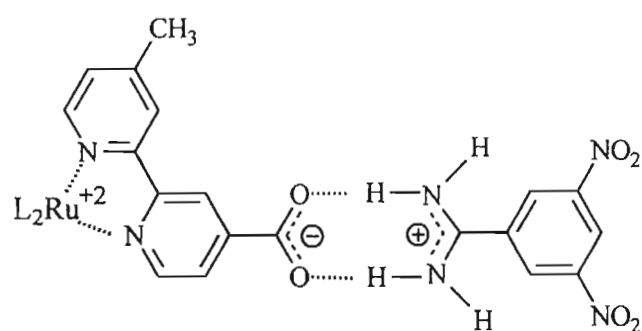
28

L= 3,3',4,4'-tetramethyl-2,2'-bipyridyl

Chart 1.15

amidinium-acceptor ensemble **28**) was undertaken.[37] Free energy changes for PET in **27b** and **28** were -0.14 and -0.34 eV, respectively. Intra-ensemble electron transfer rate constants obtained for **27b** and **28** were 8.4 x 10^6 s^{-1} and 3.1 x 10^8 s^{-1} respectively. The authors had put forward several reasons to explain this difference in the rate constants. In **27b**, electron is transferred from the positively charged side of the interface to the negatively charged side and this process may be opposed by electrostatic forces resulting in lower values of k_{et}. In contrast, electron transfer in **28** occurs from the negative side of the interface to the positive side of the interface, which is favored by electrostatic forces. This may enhance the rate constant. Difference in the strength of the hydrogen bonding in **27b** and **28** can also contribute to the difference in the rates. The electron withdrawing nitro group can stabilize the negative charge on the carboxylate resulting in a weaker hydrogen bond between the components in **27b**. Weak hydrogen bonds lead to weak electronic coupling between donor and acceptor and reduce the rate constant for electron transfer. This study suggested that unlike symmetric bridge, the PET across asymmetric interface can be affected by electrostatic potential, Frank-Condon factors and electronic coupling arising from the asymmetric charge distribution.

In order to establish that a proton transfer is actually taking place in these reactions, deuterium isotope effects on the rates of electron transfer in **26a** and **27a** were studied using deuterated bridges. In both these cases electron transfer rate

constants obtained were approximately 1.4 times slower for the deuterated systems. This means that cleavage of the O-D or N-D bond is involved in the rate-determining step. If the proton did not move with the electron, rate constants would have been identical in the protonated and deuterated systems. Similar studies were carried out using porphyrin-dinitrobenzene donor-acceptor assemblies linked via an amidinium-carboxylate salt bridge.[38,39] Deuteration of the hydrogen-bonded bridge slowed down the PET by a factor of 1.7 in this case.

1.3. Origin of the Present Work

The above survey has clearly demonstrated that significant advances have been made in the field of electron transfer in hydrogen-bonded systems. However, several aspects of electron transfer in these systems still remain unclarified. For example, the effects of factors like solvent, distance, temperature etc. on the rate of electron transfer in hydrogen-bonded systems have not been studied. Dealing with these aspects of electron transfer has become a necessary criterion to yield clear answers to questions concerning the mechanism of electron transfer reactions in biological systems. In this thesis some of these issues are addressed.

A systematic study of the dependence of electron transfer rate on free energy change in hydrogen-bonded donor-acceptor systems was carried out earlier in our laboratory.[65] Since solvent plays a crucial role in electron transfer reactions we have now looked into the effects of solvent on the free energy dependence. Since hydrogen-bonded association of the donor and acceptor could be observed

only in non-polar solvents, such studies could be carried out only in very few solvents. In Chapter 2 of this thesis, free energy dependence studies in chloroform solution are reported. The dynamics of electron transfer in a few hydrogen-bonded donor-acceptor systems in toluene solution are also reported in this chapter.

Distance between the donor and acceptor affects the rate of electron transfer profoundly. A large number of covalently bound donor-acceptor systems have been designed to study the distance dependence of electron transfer reactions. In Chapter 3 of this thesis an attempt is made to study the distance dependence of electron transfer reactions in hydrogen-bonded systems. We have looked into the distance dependence in both the normal and inverted free energy regions in hydrogen-bonded systems.

Study of temperature dependence is one of the tools available to the chemist to analyze mechanistic details of a given reaction. In this context several biological electron transfer reactions have been examined and a variety of behaviours, namely Arrhenius type, non-Arrhenius type or temperature independent, were observed. Thus there is no consensus on the type of temperature dependence expected in these systems. In this context we thought it is essential to probe the temperature dependence in the normal and inverted regions in hydrogen-bonded systems. The results of this study are reported in Chapter 4 of this thesis. All these studies were undertaken to clearly understand the various factors that control electron transfer reactions in non-covalently bound donor-acceptor

systems. This in turn is expected to throw some light into the mechanistic details of electron transfer processes in biological systems.

1.4. References

1. Gust, D.; Moore, A. T. in *Topics in Current Chemistry. Photoinduced Electron Transfer, Part III, Vol. 159;* Mattay, J. Ed.; Springer Verlag: Berlin, 1991; p 106.

2. Woodbury, N. W.; Becker, M.; Middendorf, D.; Parson, W. W. *Biochemistry* **1985**, *24,* 7516.

3. Martin, J.-L.; Breton, J.; Hoff, A. J.; Migus, A.; Antonetti, A. *Proc. Natl. Acad. Sci. USA* **1986**, *83,* 957.

4. Breton, J.; Martin, J.-L.; Migus, A.; Antonetti, A.; Orszag, A. *Proc. Natl. Acad. Sci. USA* **1986**, *83,* 5121.

5. Wasielewski, M. R.; Tiede, D. M. *FEBS Lett.* **1986**, *204,* 368.

6. Fleming, G. R.; Martin, J.-L.; Breton, J. *Nature* **1988**, *333,* 190.

7. Arlt, T.; Schmidt, S.; Kaiser, W.; Lauterwasser, C.; Meyer, M.; Scheer, H.; Zinth, W. *Proc. Natl. Acad. Sci. USA* **1993**, *90,* 11757.

8. Wasielewski, M. R. in *Photoinduced Electron Transfer, Part D;* Fox, M. A., Channon, M. Eds.; Elsevier: Amsterdam, 1988; p 303.

9. Wasielewski, M. R. *Chem. Rev.* **1992**, *92,* 435.

10. Jordan, K. D.; Paddon-Row, M. N. *Chem. Rev.* **1992**, *92,* 395.

11. Paddon-Row, M. N. *Acc. Chem. Res.* **1994**, *27,* 18.

12. Kurreck, H.; Huber, M. *Angew. Chem. Int. Ed. Engl.* **1995**, *34*, 849.

13. Harriman, A.; Sauvage, J.-P. *Chem. Soc. Rev.* **1996**, *26*, 41.

14. Gust, D.; Moore, A. L. *Pure Appl. Chem.* **1998**, *70*, 2189.

15. Blanco, M.-J.; Jimenez, M. C.; Chambron, J.-C.; Heitz. V.; Linke, M.; Sauvage, J.-P. *Chem. Soc. Rev.* **1999**, *28*, 293.

16. Verhoeven, J. W. in *Electron Transfer, Part 1*; Jortner, J., Bixon, M. Eds.; John Wiley and Sons: New York, 1999; p 603.

17. Guldi, D. M.; Prato, M. *Acc. Chem. Res.* **2000**, *33*, 695.

18. Gust, D.; Moore, T. A.; Moore, A. L. *Acc. Chem. Res.* **2001**, *34*, 40.

19. Deisenhofer, J.; Epp, O.; Miki, K.; Huber, R.; Michel, H. *Nature* **1985**, *318*, 618.

20. Barber, J. *Nature* **1988**, *333*, 114.

21. Kühlbrandt, W. *Nature* **1995**, *374*, 497.

22. Lehn, J.-M. *Supramolecular Chemistry: Concepts and Perspectives*; VCH: New York, 1995.

23. Philip, D.; Stoddart, J. F. *Angew. Chem. Int. Ed. Engl.* **1996**, *35*, 1154.

24. Schneider, H.-J., Dürr, H. Eds.; *Frontiers in Supramolecular Organic Chemistry and Photochemistry*; VCH: New York, 1991.

25. Sessler, J. L.; Wang, B.; Springs, S. L.; Brown, C. T. in *Comprehensive Supramolecular Chemistry, Vol.4*; Atwood, J. L., Davies, J. E. D., Macnicol, D. D., Vögtle, E., Murakami, Y. Eds.; Pergamon: UK, 1996; p 311.

26. Balzani, V.; Scandola, F. In *Comprehensive Supramolecular Chemistry, Vol.10;* Atwood, J. L., Davies, J. E. D., Macnicol. D. D., Vogtle. F.. Reinhoudt, D. N. Eds.; Pergamon: UK, 1996; p 687.

27. Hayashi, T.; Ogoshi, H. *Chem. Soc. Rev.* **1997**, *26*. 355.

28. Ward, M. D. *Chem. Soc. Rev.* **1997**, *26*, 365.

29. Piotrowiak, P. *Chem. Soc. Rev.* **1999**, *28*, 143.

30. Hunter, C. A.; Sanders, J. K. M.; Beddard, G. S.; Evans. S. *J. Chem. Soc., Chem. Commun.* **1989**, 1765.

31. Anderson, H. L.; Hunter, C. A.; Sanders, J. K. M. *J. Chem. Soc., Chem. Commun.* **1989**, 226.

32. Chambron, J.-C.; Harriman, A.; Heitz, V.; Sauvage. J.-P. *J. Am. Chem. Soc.* **1993**, *115*, 7419.

33. Imahori, H.; Yoshizawa, E.; Yamada, K.; Hagiwara, K.; Okada, T.; Sakata, Y. *J. Chem. Soc., Chem. Commun.* **1995**, 1133.

34. Hunter, C. A.; Hyde, R. K. *Angew. Chem. Int. Ed. Engl.* **1996**, *35*, 1936.

35. Hunter, C. A.; Shannon, R. J. *Chem. Commun.* **1996**, 1361.

36. Roberts, J. A.; Kirby, J. P.; Nocera, D. G. *J. Am. Chem. Soc.* **1995**, *117*, 8051.

37. Kirby, J. P.; Roberts, J. A.; Nocera, D. G. *J. Am. Chem. Soc.* **1997**, *119*, 9230.

38. Kirby, J. P.; van Dantzig, N. A.; Chang, C. K.; Nocera, D. G. *Tetrahedron Lett.* **1995**, *36*, 3477.

39. Deng, Y.; Roberts, J. A.; Peng, S.; Chang, C. K.; Nocera, D. G. *Angew. Chem. Int. Ed. Engl.* **1997**, *36*, 2124.

40. Gonzalez, M.; McIntosh, A.; Bolton, J.; Weedon, A. *J. Chem. Soc., Chem. Commun.* **1984**, 1138.

41. Harriman, A.; Kubo, Y.; Sessler, J. L. *J. Am. Chem. Soc.* **1992**, *114*, 388.

42. Sessler, J. L.; Wang, B.; Harriman, A. *J. Am. Chem. Soc.* **1993**, *115*, 10418.

43. Arimura, T.; Brown, C. T.; Springs, S. L.; Sessler, J. L. *Chem. Commun.* **1996**, 2293.

44. Sessler, J. L.; Brown, C. T.; O'Connor, D.; Springs, S. L.; Wang, R.; Sathiosatham, M.; Hirose, T. *J. Org. Chem.* **1998**, *63*, 7370.

45. Berman, A.; Izraeli, E. S.; Levanon, H.; Wang, B.; Sessler, J. L. *J. Am. Chem. Soc.* **1995**, *117*, 8252.

46. Someda, M. A.; Levanon, H.; Sessler, J. L.; Wang, R. *Mol. Phys.* **1998**, *95*, 935.

47. Berg, A.; Shauli, Z.; Someda, M. A.; Levanon, H.; Fuhs, M.; Mobius, K.; Wang, R.; Brown, C.; Sessler, J. L. *J. Am. Chem. Soc.* **1999**, *121*, 7433.

48. Sessler, J. L.; Sathiosatham, M.; Brown, C. T.; Rhodes, T. A.; Wiederrecht, G. *J. Am. Chem. Soc.* **2001**, *123*, 3655.

49. Turro, C.; Chang, C. K.; Leroi, G. E.; Cukier, R. I.; Nocera, D. G. *J. Am. Chem. Soc.* **1992**, *114*, 4013.

50. Wasielewski, M. R.; Niemczyk, M. P.; Svec, W. A.; Pewitt, E. B. *J. Am. Chem. Soc.* **1985**, *107*, 1080.

51. Osuka, A.; Yoneshima, R.; Shiratori, H.; Okada, T.; Taniguchi. S.; Mataga, N. *Chem. Commun.* **1998**, 1567.

52. de Rege, P. J. F.; Williams, S. A.; Therien. M. J. *Science* **1995**, *269*, 1409.

53. Tamiaki, H.; Maruyama, K. *Chem. Lett.* **1993**, 1499.

54. Williamson, D. A.; Bowler, B. E. *J. Am. Chem. Soc.* **1998**, *120*, 10902.

55. Liu, J.-Y.; Schmidt, J. A.; Bolton, J. R. *J. Phys. Chem.* **1991**, *95*, 6924.

56. Williamson, D. A.; Bowler, B. E. *Inorg. Chim. Acta* **2000**, *297*, 47.

57. Aoyama, Y.; Asakawa, M; Matsui, Y.; Ogoshi, H. *J. Am. Chem. Soc.* **1991**, *113*, 6233.

58. Hayashi, T.; Miyahara, T.; Hashizume, N.; Ogoshi, H. *J. Am. Chem. Soc.* **1993**, *115*, 2049.

59. Hayashi, T.; Asai, T.; Hokazono, H.; Ogoshi, H. *J. Am. Chem. Soc.* **1993**, *115*, 12210.

60. Hayashi, T.; Miyahara, T.; Aoyama, Y.; Kobayashi, M.; Ogoshi, H. *Pure Appl. Chem.* **1994**, *66*, 797.

61. Hayashi, T.; Miyahara, T.; Aoyama, Y.; Nonoguchi, M.; Ogoshi, H. *Chem. Lett.* **1994**, 1749.

62. Hayashi, T.; Miyahara, T.; Kumazaki, S.; Ogoshi, H.; Yoshihara, K. *Angew. Chem. Int. Ed. Engl.* **1996**, *35*, 1964.

63. Cusack, L.; Nagaraja Rao, S.; Wenger, J.; Fitzmaurice, D. *Chem. Mater.* **1997**, *9*, 624.

64. Cusack, L.; Nagaraja Rao, S.; Fitzmaurice, D. *Chem. Eur. J.* **1997**, *3*, 202.

65. Prasad, E.; Gopidas, K. R. *J. Am. Chem. Soc.* **2000**, *122*, 3191.

66. Ghaddar, T. H.; Castner, E. W.; Isied, S. S. *J. Am. Chem. Soc.* **2000**, *122*, 1233.

67. Myles, A. J.; Branda, N. R. *J. Am. Chem. Soc.* **2001**, *123*, 177.

68. Cukier, R. I.; *J. Phys. Chem.* **1994**, *98*, 2377.

69. Cukier, R. I. *J. Phys. Chem.* **1996**, *100*, 15428.

70. Cukier, R. I.; Nocera, D. G. *Annu. Rev. Phys. Chem.* **1998**, *49*, 337.

71. Cukier, R. I. *J. Phys. Chem. A* **1999**, *103*, 5989.

72. Soudackov, A.; Schiffer, S. H. *J. Am. Chem. Soc.* **1999**, *121*, 10598.

CHAPTER 2

FREE ENERGY AND SOLVENT DEPENDENCE OF PHOTOINDUCED ELECTRON TRANSFER REACTIONS IN HYDROGEN-BONDED DONOR-ACCEPTOR SYSTEMS

2.1. Abstract

In this chapter we have investigated the photoinduced electron transfer processes in donor-acceptor systems containing arylacetic acid moieties. Because of the presence of acetic acid moieties in them, a small fraction of the donors and acceptors are present as hydrogen-bonded self-assembled systems in non-polar solvents as shown in Scheme 2.4. Upon excitation two types of electron transfers can take place: (1) the activation controlled electron transfer within the hydrogen-bonded fraction and (2) the diffusion controlled electron transfer taking place in the free molecules. The rate constants for both these processes were determined as a function of free energy in chloroform solution. Our studies showed that electron transfer within the hydrogen-bonded fraction follows the Marcus behaviour and electron transfer in the free moving segment obeys the Rehm-Weller behaviour. We could thus establish unequivocally that the non-observance of the inverted region in bimolecular photoinduced electron transfer reactions is due to diffusion. We also observed that the maximum in the Marcus plot for the hydrogen-bonded fraction was shifted to a less negative free energy value in chloroform compared to that in dichloromethane. This further confirms the Marcus type electron transfer in

these systems. In toluene solution in addition to electron transfer, exciplex formation was also observed for some systems. This complicated the analysis of the fluorescence decay profiles.

2.2. Introduction

Photoinduced electron transfer (PET) involves the use of light to induce electron transfer from the donor (D) to the acceptor (A). A general reaction scheme involving the excitation of D is given in Scheme 2.1. The ion pairs formed in the electron transfer step may recombine by the back electron transfer step to regenerate the starting materials as shown in equation 2.3.[1]

$$D \xrightarrow{\text{h}\nu} D^* \tag{2.1}$$

$$D^* + A \xrightarrow{\text{ET}} D^{\bullet +} + A^{\bullet -} \tag{2.2}$$

$$D^{\bullet +} + A^{\bullet -} \xrightarrow{\text{BET}} D + A \tag{2.3}$$
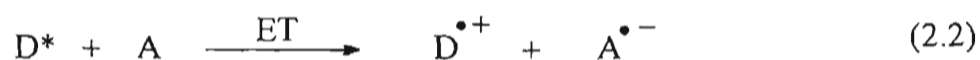
Scheme 2.1

PET in solution involves several steps and intermediates. A schematic representation of the various processes taking place in PET is shown in Scheme 2.2. In Scheme 2.2, k_{diff} and k_{-diff} are the diffusion controlled rate constants for the formation and dissociation of the encounter complex. k_{et} is the unimolecular electron transfer rate constant within the complex, k_{-et} is the rate constant for

reverse electron transfer and k_{bet} is the rate constant for back electron transfer. A steady state treatment of the reaction leads to equation 2.4.[1]
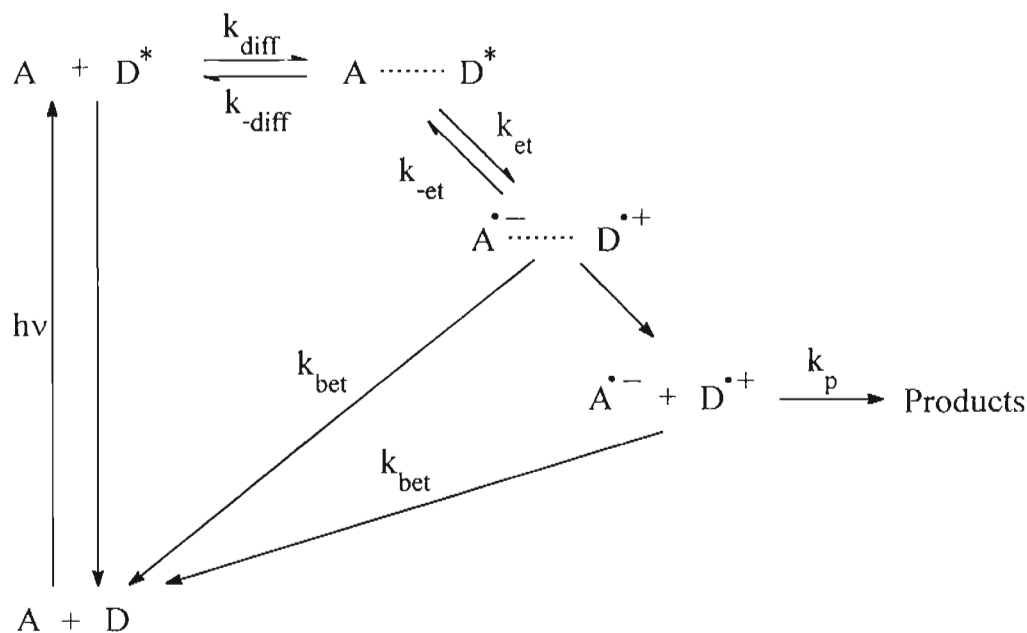
Scheme 2.2

$$k_q = \cfrac{k_{diff}}{1 + \cfrac{k_{-diff}}{k_{et}} + \cfrac{k_{-diff}}{k_{et}} \cfrac{k_{-et}}{(k_p + k_{bet})}} \qquad (2.4)$$

where, k_q is the quenching rate constant. It can be shown that equation 2.4 reduces to equation 2.5.[2,3]

$$\frac{1}{k_q} = \frac{1}{k_{et}} + \frac{1}{k_{diff}} \qquad (2.5)$$

Under conditions of fast electron transfer, (*ie.*, $k_{et} \gg k_{dif}$), the observed rate of quenching is given by the diffusion rate constants for the reactants in the particular solvent. The reaction is then dominated by diffusion dynamics and said to be

diffusion controlled. When the electron transfer is very slow, (*ie.*, $k_{et} \ll k_{diff}$), electron transfer is said to be activation controlled.

The rate constant for activation controlled electron transfer is given by

$$k_{et} = \nu \kappa_n \kappa_{el} \tag{2.6}$$

where, ν is the frequency factor, κ_{el} is defined as the electronic factor and κ_n as the nuclear factor. Classical theories assume that the donor and acceptor are within contact distance during electron transfer. In this case $\kappa_{el} = 1$ and the rate constant for electron transfer is given by the Marcus equation

$$k_{et} = \nu \exp\left[\frac{-(\lambda + \Delta G^\circ)^2}{4\lambda RT}\right] \tag{2.7}$$

where, ΔG° is the free energy associated with the electron transfer reaction and λ is called the reorganization energy. When the separation distance is more than 7 Å, $\kappa_{el} \neq 1$ and electronic or nuclear barriers may be rate limiting. The rate constant for electron transfer in this case is given by the semiclassical expression[3-7]

$$k_{et} = (2\pi/\hbar) \, H_{el}^2 \, (4\pi\lambda k_B T)^{-1/2} \exp[-(\lambda + \Delta G^\circ)^2/4\lambda k_B T] \tag{2.8}$$

where, $\hbar$ is the Planck's constant divided by 2π, H_{el} is the electronic coupling matrix element between the donor and acceptor, k_B is the Boltzmann constant, and T is the temperature. If the electronic coupling is large the reaction will be adiabatic ($k_{el} = 1$) and if the electronic coupling is weak the reaction will be non-adiabatic.

According to the Marcus equation (classical or semiclassical), a plot of k_{et} *vs.* ΔG° will be bell-shaped (Figure 2.1).[4-10] The bell-shaped dependence predicts three kinetic regimes for electron transfer reactions: (1) A "normal" regime for small driving forces $(\Delta G^\circ > -\lambda)$ where the process is thermally activated and is favored by an increase in the driving force; (2) an "activationless" regime $(\Delta G^\circ = -\lambda)$ and (3) an "inverted" regime for strongly exergonic reactions $(\Delta G^\circ < -\lambda)$ where, the rate actually decreases with increasing driving force. Existence of the Marcus inverted region (MIR) was very controversial and it took nearly twenty years to obtain the first evidence to support it. Over the years considerable amount of work was carried out to establish the existence of the inverted region in various types of electron transfer reactions. A brief account of these studies is given here with the hope that this will help in a better understanding of the relevance of the work reported here.

The first detailed investigation of the dependence of rate of electron transfer on free energy was carried out by Rehm and Weller.[11,12] They have determined the fluorescence quenching rate constants for a series of aromatic compounds using large number of donors and acceptors. Although the free energies of the PET reactions span the range of 0.26 to -2.7 eV in this study, the inverted region was not observed here. They found that the rate constant rapidly rises in the normal region, reaches a limiting value and stays there no matter how exergonic the process becomes. Similar observations were made by several others.[13-18]

The behaviour, where the rate constant for electron transfer increases with decrease in free energy, reaches a maximum and remains pegged to the maximum with further decrease in free energy, came to be known as the "Rehm-Weller behaviour" (Figure 2.1). The Rehm-Weller behaviour seems to be the rule for processes of luminescence quenching through electron transfer in homogeneous solution.
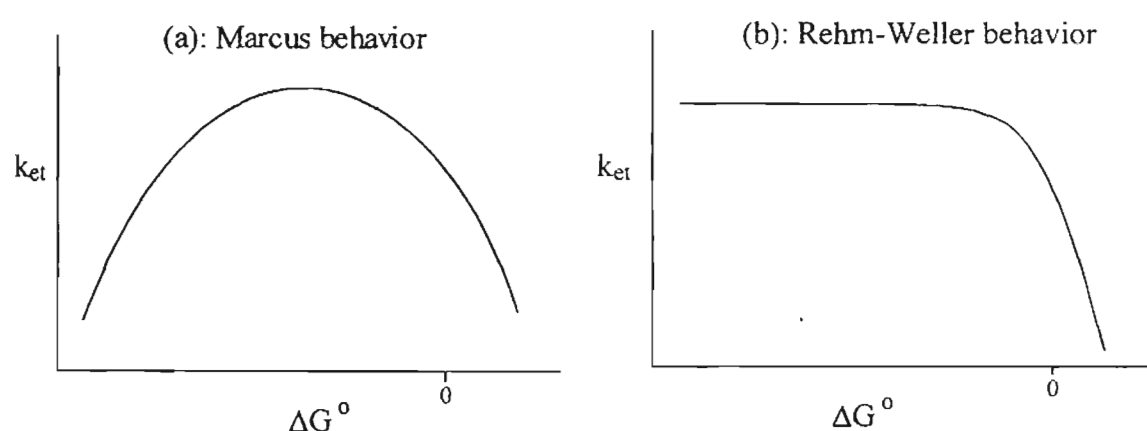
Figure 2.1. Shapes of the rate constant *vs.* free energy plots according to (a) Marcus and (b) Rehm-Weller equations.

The first clear indication of any reduction of the electron transfer rate with increasing driving force (decreasing free energy) was observed by Miller and co-workers.[19,20] They had studied the electron transfer from radiolytically generated radical anions to aromatic hydrocarbons in frozen solution. The reaction covered the free energy range 0.01 to -2.75 eV and the rates were found to decrease at high exothermicities. This experiment had some drawbacks. The studies were carried out in rigid glasses and analysis of the data was based on random distance dependence between the donor and the acceptor. Subsequently, experiments were

designed to circumvent these difficulties. Diffusion was eliminated by linking the donor (biphenyl) radical anion and acceptor through a rigid spacer.[21,22] By changing the acceptor molecule, the free energy was varied from 0 to -2.38 eV. The rate constants of electron transfer in these molecules were found to follow the prediction of the Marcus theory including the appearance of the inverted region at high exothermicities. This was the first unambiguous confirmation of the existence of the MIR.

Existence of the MIR is now firmly established in electron transfer reactions. Most of these pertain to charge shift reactions in solid matrices[19] or charge recombination reactions in covalently linked donor-acceptor systems.[23-30] The MIR is also seen in back electron transfer reactions of contact and solvent separated ion pairs.[31-41] All these reactions are unimolecular thermal electron transfer processes. The MIR, however, is not observed in bimolecular PET reactions and in these cases one normally observes the Rehm-Weller behaviour.

At this juncture it is very relevant to ask as to why some electron transfer systems follow the Marcus model and others follow the Rehm-Weller model? This is a fundamental question, which has been addressed by several authors in recent times. It has been suggested that the absence of the MIR in PET reactions is due to the following four reasons:[42-46] (1) Limiting of rate constants by diffusion; (2) formation of products in the excited state; (3) lack of truly homogenous series of donors and acceptors and (4) presence of other reaction channels. All these explanations were offered several years ago, but no serious efforts were made to

prove or disprove any of these. We have initiated our research on electron transfer in hydrogen-bonded donor-acceptor systems in order to specifically address the role of diffusion in PET reactions.

We reasoned that the role of diffusion in masking the MIR can be proved or disproved conclusively by a study of PET reaction in donor-acceptor systems having complementary hydrogen bonding moieties. These molecules when dissolved in a non-polar solvent associate to form hydrogen-bonded systems in which the donor and acceptor are separated by the length of the hydrogen bond interface. If the equilibrium constant for association (K_a) is small, then only a small fraction of the molecules will be present as the hydrogen-bonded complex and the remaining will be free to diffuse in solution. The strategy we have used to resolve the diffusion problem takes advantage of the incomplete association of the donors and acceptors and this strategy is outlined in Scheme 2.3.

$$P + Q \; \underset{}{\overset{K_a}{\rightleftharpoons}} \; P \sim Q$$

Bimolecular Quenching
Diffusion Mediated

Unimolecular Quenching
No Diffusion
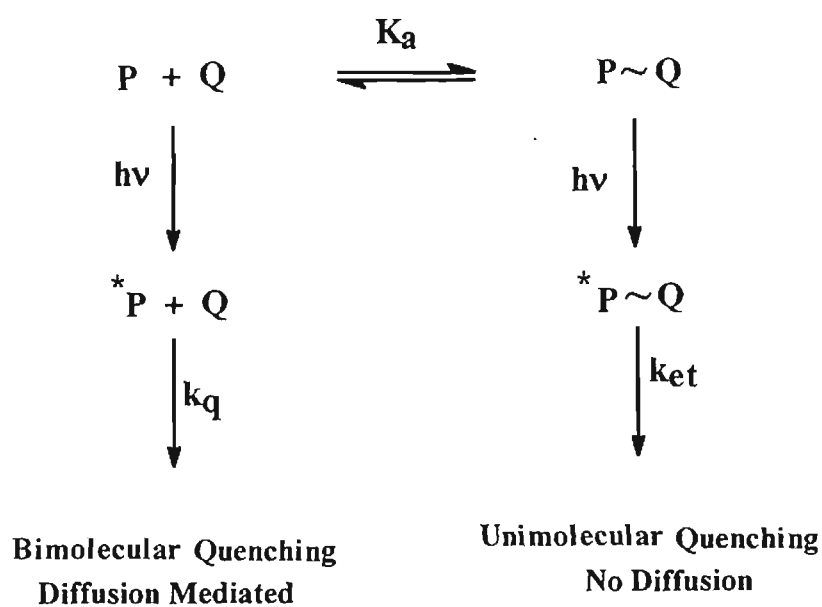
Scheme 2.3

In Scheme 2.3, **P** is a probe molecule and **Q** is the quencher. Both **P** and **Q** contain hydrogen bonding moieties and ~ stands for the hydrogen bond interface. Upon irradiation both the associated and unassociated probe molecules are excited. Fluorescence of the associated probes will be quenched by unimolecular, fixed distance electron transfer involving the associated quencher, whereas, fluorescence of the unassociated probes will be quenched by diffusion mediated bimolecular electron transfer. The rate constants for both these reactions can be obtained simultaneously by fluorescence lifetime measurements (vide infra). The role of diffusion in masking the inverted region will be proved unequivocally if Marcus behaviour is observed for quenching in the associated fraction and Rehm-Weller behaviour is observed for quenching in the freely moving segment. If Rehm-Weller behaviour is observed for both the cases, it can be concluded that diffusion has no role in masking the observation of the inverted region. Thus, by studying the electron transfer process in hydrogen-bonded systems one can analyse the role of diffusion in these reactions.

Study of the free energy dependence of PET in hydrogen-bonded systems was initiated in our laboratory by Dr. E. Prasad.[47] In this study, the propensity of carboxylic acids to undergo hydrogen-bonded dimer formation was exploited to assemble donors and acceptors in dichloromethane solution. This study revealed that electron transfer in the hydrogen-bonded fraction follows Marcus behaviour. An important confirmation of the Marcus theory comes from the solvent dependence of the Marcus plot. According to Marcus equation the maximum rate

occurs when $\Delta G^\circ = -\lambda$. The reorganization energy λ is expected to vary with solvent. Hence the maximum in the Marcus plot is expected to shift to less negative free energy values in less polar solvents and to more negative free energy values in more polar solvents.[7] In order to examine this aspect we have carried out a study of the free energy dependence of electron transfer in hydrogen-bonded systems in a less polar solvent such as chloroform. Some of the systems were studied in toluene solution also. These studies could not be carried out in polar solvents such as acetonitrile, methanol etc. because hydrogen-bonded association did not occur in these solvents.

2.3. Results

Structures of the compounds we have used for the study and their redox potentials in acetonitrile (*vs.* SCE) are shown in Chart 2.1. All these molecules contain an acetic acid moiety for hydrogen bonding association. Among these, pyreneacetic acid (**PA**) and anthraceneacetic acid (**AA**) are highly fluorescent and hence used as probe molecules. These probe molecules can act as donors or acceptors depending on the quenchers used. When **1** and **2** are used as quenchers the probe molecules act as acceptors and when **3 - 5** are used as quenchers the probes act as donors. It is already reported in the literature that the quenchers shown in Chart 2.1 (without the CH_2COOH) can quench the fluorescence of pyrene or anthracene by an electron transfer mechanism.[48-52] Hence we have not made any attempt to detect the radical ions formed in these reactions and thus ascertain the electron transfer pathway for fluorescence quenching.
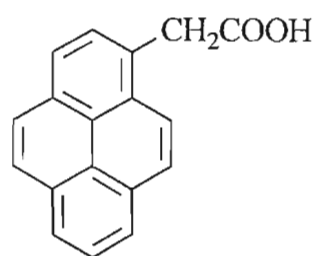
PROBES

PA

$E_{ox} = 1.08$ V

$E_{red} = -2.12$ V
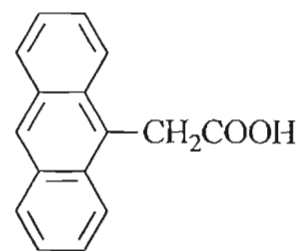
AA

$E_{ox} = 0.94$ V

$E_{red} = -1.99$ V

QUENCHERS

DONORS
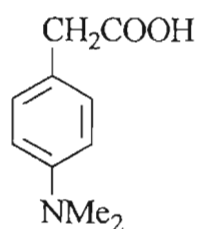
1

$E_{ox} = 0.85$ V
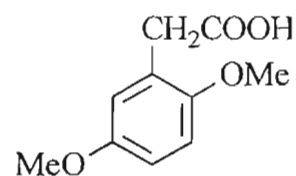
2

$E_{ox} = 1.33$ V

ACCEPTORS
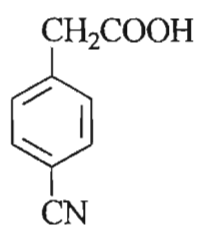
3

$E_{red} = -2.46$ V
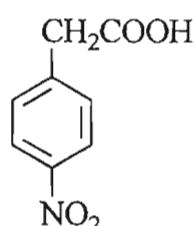
4

$E_{red} = -1.23$ V
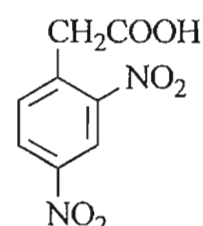
5

$E_{red} = -0.99$ V

Chart 2.1. Structures and redox potentials of the probes and quenchers used in the present study.

2.3.1. Absorption and emission properties of PA and AA

Figure 2.2 shows the absorption and emission spectra of **PA** in chloroform solution and Figure 2.3 shows the same for **AA**. Spectra taken in solvents such as dichloromethane and toluene were similar. The absorption and fluorescence spectra of these compounds were almost identical to those of the parent hydrocarbon, which indicated that the acetic acid moiety is not a part of the chromophore. The singlet energy $E_{0,0}$ of these probes were calculated from the point of intersection of the normalized absorption and emission spectra. Relevant photophysical parameters of **PA** and **AA** are given in Table 2.1.
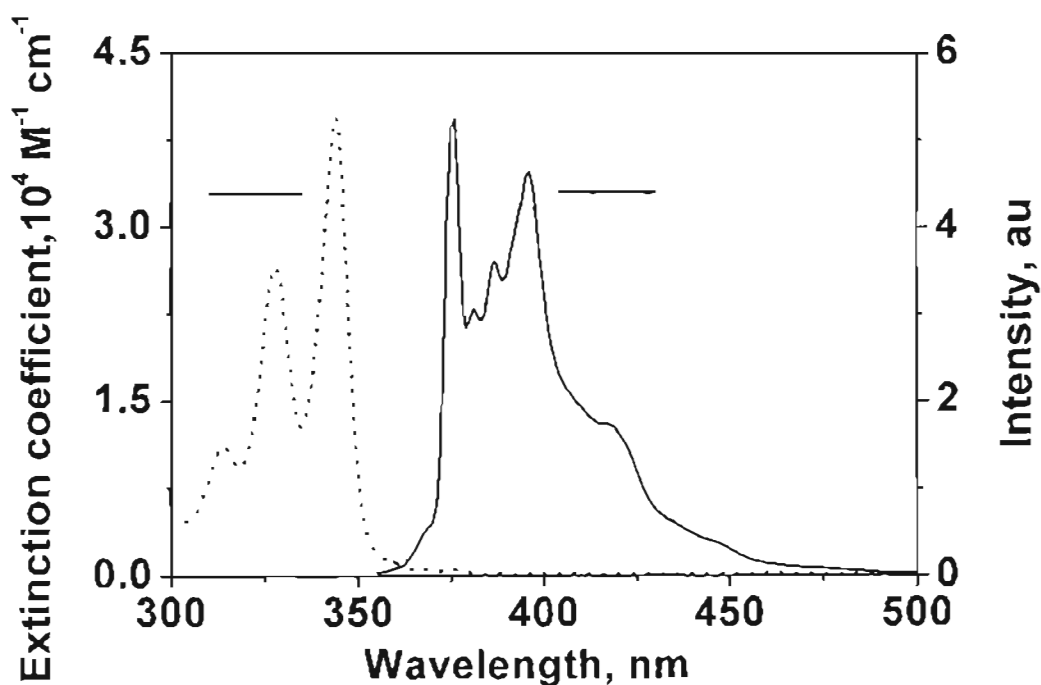
Figure 2.2. Absorption and emission spectra of pyrene-1-acetic acid in chloroform. For emission spectrum, excitation was at 345 nm.

G/2031
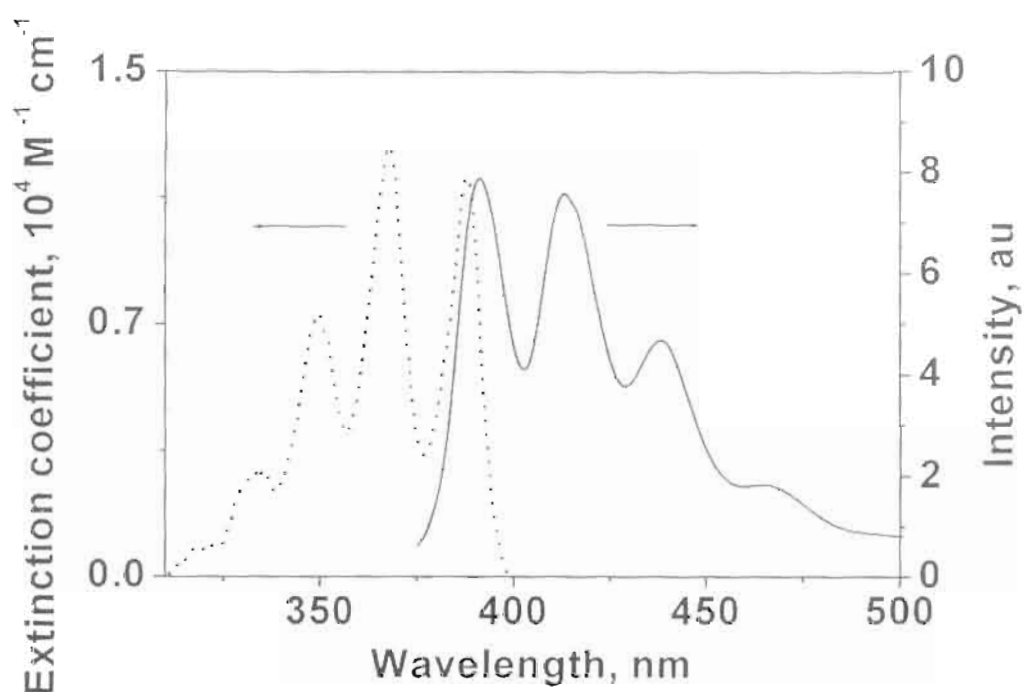
Figure 2.3. Absorption and emission spectra of anthracene-9-acetic acid in chloroform. For emission spectrum, excitation was at 350 nm.

Table 2.1. Absorption maxima (λ_{ab}), emission maxima (λ_{em}), singlet energies $(E_{0.0})$ and fluorescence lifetimes (τ_0) of PA and AA in chloroform. Values in parenthesis are those in toluene.

Probes	λ_{ab} nm	λ_{em} nm	$E_{0.0}$ eV	τ_0 ns
PA	345	375	3.6	100 ± 10 (150 ± 10)
AA	385	420	3.2	6 ± 0.2 $(7 + 0.1)$

2.3.2. Fluorescence lifetime quenching studies

2.3.2.1. Theory

The concentration of the probe used in our study is 1×10^{-5} M. Concentrations of the quenchers were varied in the range $(1 - 5) \times 10^{-3}$ M. Under these conditions a small fraction of the probes and quenchers associate to give the hydrogen-bonded donor-acceptor system shown in Scheme 2.4.
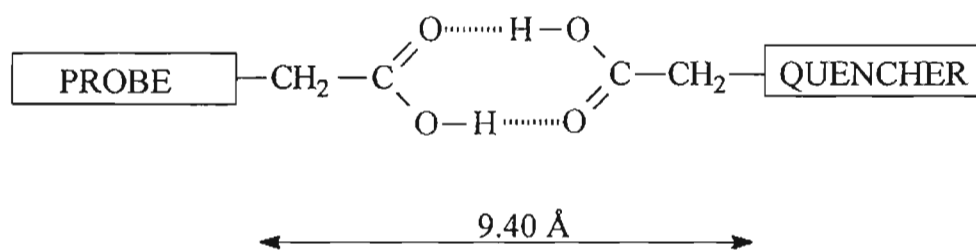
Scheme 2.4

The length of the acetic acid dimer is 6.94 Å.[53,54] In our system an additional single bond is present on either side of the hydrogen-bonded interface and hence the edge-to-edge distance between the probe and quencher is about 9.4 Å. As indicated in Scheme 2.3, a major fraction of the probe remains free and this fraction is quenched by diffusion mediated electron transfer.

The free energy for PET reactions is given by the Weller equation[1]

$$\Delta G^{0} = E_{ox} - E_{red} - E_{00} - \frac{e^2}{2}\left(\frac{1}{r_P} + \frac{1}{r_Q} \right)\left(\frac{1}{37} - \frac{1}{\varepsilon} \right) - \frac{e^2}{\varepsilon\, d_c} \qquad (2.9)$$

where, E_{ox} is the oxidation potential of the donor, E_{red} is the reduction potential of the acceptor, ε is the dielectric constant of solvent used, r_P and r_Q are the radii of the probe and quencher molecules and d_c is the centre-to-centre distance separating

these partners. The fourth term in equation 2.9 is the solvent correction term. r_P and r_Q were taken as 6 and 4 Å, respectively in the calculations. For the calculation of $\Delta G°$ for electron transfer within the hydrogen-bonded assembly, we have taken d_c as 12 Å. For calculation of $\Delta G°_{diff}$ for the diffusive quenching, d_c is taken as the contact distance of 10 Å. The calculated $\Delta G°$ and $\Delta G°_{diff}$ values are presented later in Table 2.11.

As mentioned in Scheme 2.3 both unimolecular and bimolecular quenching pathways exist and this results in a biexponential decay of the probe that can be expressed by equation 2.10.

$$I_{(t)} = \chi_{(P-Q)} \exp(-t/\tau_1) + \chi_{(P)} \exp(-t/\tau_2) \tag{2.10}$$

where,

$$\tau_1 = (k_0 + k_{et})^{-1} \tag{2.11}$$

$$\tau_2 = (k_0 + k_q[Q])^{-1} \tag{2.12}$$

$\chi_{(P-Q)}$ and $\chi_{(P)}$ are the mole fractions of the associated and unassociated probe molecules, respectively, k_0 ($= 1/\tau_0$) is the intrinsic decay rate of the probe, k_{et} is the unimolecular rate constant of electron transfer within the associated complex and k_q is the bimolecular quenching rate constant for the unassociated probe molecules. According to equations 2.10 to 2.12, the short lifetime component (τ_1) is independent of the quencher concentration and the long lifetime component (τ_2) is dependent on quencher concentration. From the short lifetime component, the

rate constant for electron transfer within the hydrogen-bonded complex can be calculated using equation 2.13.

$$k_{et} = 1/\tau_1 - 1/\tau_0 \tag{2.13}$$

The quenching rate constant k_q for the bimolecular process can be obtained from the slope of the Stern-Völmer plot of τ_0/τ_2 *vs.* quencher concentration.

$$\tau_0/\tau_2 = 1 + k_q\tau_0[Q] \tag{2.14}$$

It was observed that probe-quencher association takes place only in less polar solvents such as dichloromethane, chloroform and toluene. The association constants of these hydrogen-bonded donor-acceptor systems can be determined from the fractional contributions of the associated ($\chi_{(P-Q)}$) and the unassociated ($\chi_{(P)}$) probe molecules. These values are proportional to the concentration of the associated and unassociated forms of the probe, respectively. Since the quencher concentration is very large compared to the probe concentration, we can write

$$K_a = \frac{\chi_{(P-Q)}}{\chi_P[Q]} \tag{2.15}$$

Thus a plot of $\chi_{(P-Q)}/\chi_{(P)}$ *vs.* [Q] will be linear and gives K_a as the slope. It is to be mentioned here that association constants for some of these systems were determined earlier by NMR techniques.[47]

2.3.2.2. Fluorescence lifetime quenching studies in chloroform

Our aim is to obtain k_{et} and k_q values as a function of free energy using the fluorescence lifetime measurements. In the following section, the methodology we have used is illustrated in detail using the probe/quencher system **PA/1**. For other probe/quencher systems, which showed the same trend, only the decay traces and relevant data tables are given. For some of the systems we could not observe biexponential decays and one such case is also described in this section.

For the **PA/1** system, **PA** acts as the excited state acceptor and **1** acts as the donor. The absorption spectrum of the **PA/1** system is the sum of the absorption spectra of the individual components and this ruled out the possibility of any ground state electronic interaction between the components. The fluorescence of **PA** in chloroform solution is quenched by addition of millimolar quantities of **1**. Fluorescence quenching did not lead to the formation of any bands that can be attributed to exciplexes. Figure 2.4 shows a plot of I_0/I for the above quenching. The Stern-Völmer plot shows an upward curvature, which clearly indicates that static as well as dynamic quenching are taking place in this system. Static quenching occurs in the pre-associated donor-acceptor pairs and dynamic quenching occurs in the freely diffusing donor and acceptor molecules.

For the **PA/1** system, $\Delta G°$ and $\Delta G°_{diff}$ values calculated using equation 2.9 were -0.33 and -0.39 eV, respectively. The fluorescence decay profiles of **PA** in chloroform were recorded in the presence of varying amounts of **1** and these are given in Figure 2.5.
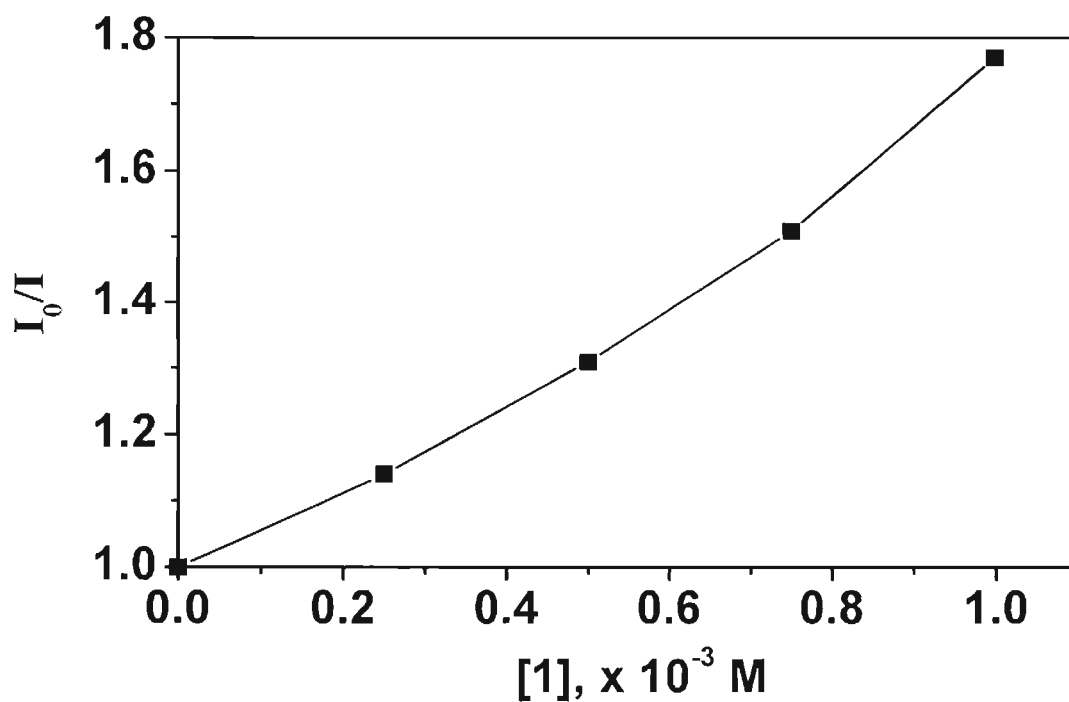
Figure 2.4. Plot of I_0/I for the steady state quenching of PA by 1.
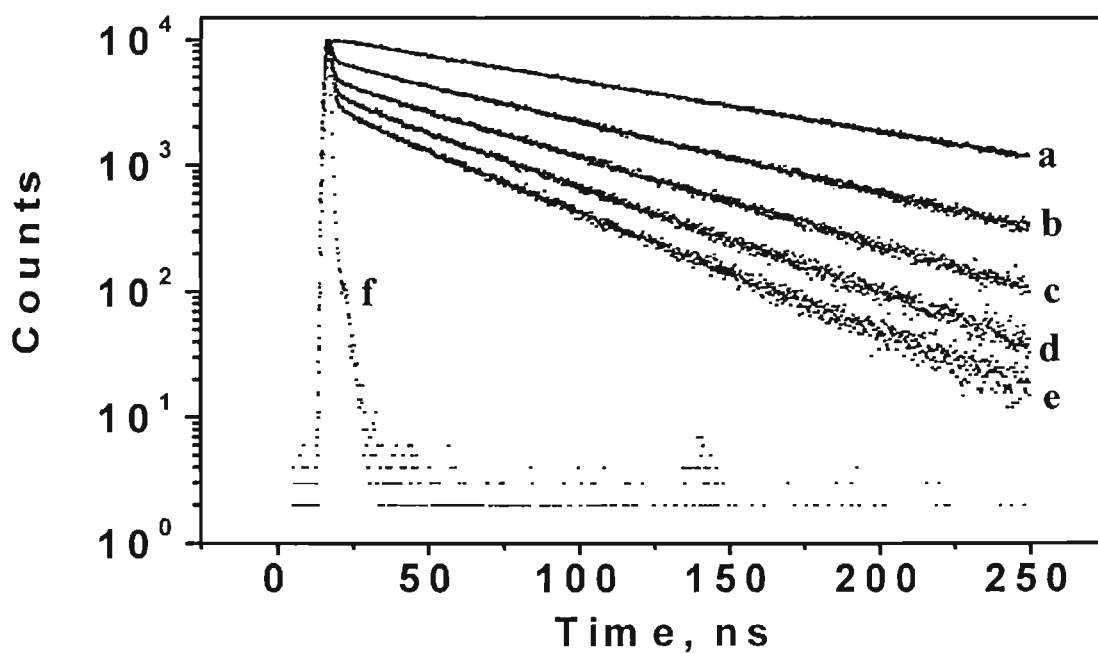
Figure 2.5. The fluorescence decay profiles of PA in the absence (a) and in presence (b - e) of 1 (0.5 - 2 mM). (f) is the lamp profile.

In the absence of the quencher the decay was monoexponential. In the presence of **1**, the florescence decay became biexponential. Upon increasing the quencher concentration, the short lifetime component (τ_1) remained the same but its relative contribution ($\chi_{(P-Q)}$) increased. This is clearly seen in Figure 2.5. The long lifetime component (τ_2), on the other hand, decreased and its contribution (($\chi_{(P)}$) also decreased. The decay profiles shown in Figure 2.4 were fitted using Edinburgh Instruments deconvolution programme and the values of τ_1, τ_2, $\chi_{(P-Q)}$ and $\chi_{(P)}$ thus obtained are given in Table 2.2 along with χ^2 values for the fits. χ^2 values below 1.3 indicate good fit of the data.

To ascertain that the short lifetime component in the fluorescence decay profile is due to electron transfer quenching within the hydrogen-bonded assembly some control experiments were carried out. When methanol was added (15%), the short lifetime component disappeared. Methanol, being a hydroxylic solvent, is a hydrogen bond competitor. Addition of methanol disrupts the hydrogen-bonded assembly between the probes and quenchers and this leads to disappearance of the short lifetime component. This study confirmed that the short lifetime component was due to the hydrogen-bonded fraction of the probe.

The rate constant of electron transfer within the hydrogen-bonded assembly, k_{et}, was calculated from the values of τ_1 and τ_0 using equation 2.13. The value obtained was 1.27×10^9 s^{-1}. The bimolecular quenching rate constant k_q was calculated from a plot of τ_0/τ_2 *vs.* [**1**] (see Figure 2.6). The slope of this graph gave $k_q\tau_0$ from which k_q was calculated. The value obtained was 6.8×10^9 $M^{-1}s^{-1}$.

Table 2.2. Fluorescence lifetimes (τ_1 and τ_2), fractional contributions (χ_{P-Q} and χ_P) and χ^2 values obtained for the fluorescence quenching of PA by 1. [PA] was 1×10^{-5} M.

[1], M	τ_1, ns	χ_{P-Q} %	τ_2, ns	χ_P, %	χ^2
0	-	-	106	100	1.3
0.25×10^{-3}	0.78	2.82	86.66	97.8	1.2
0.50×10^{-3}	0.78	6.21	77.37	93.79	1.3
0.75×10^{-3}	0.77	10.43	67.09	89.57	1.2
1.00×10^{-3}	0.78	15.14	59.55	84.86	1.2
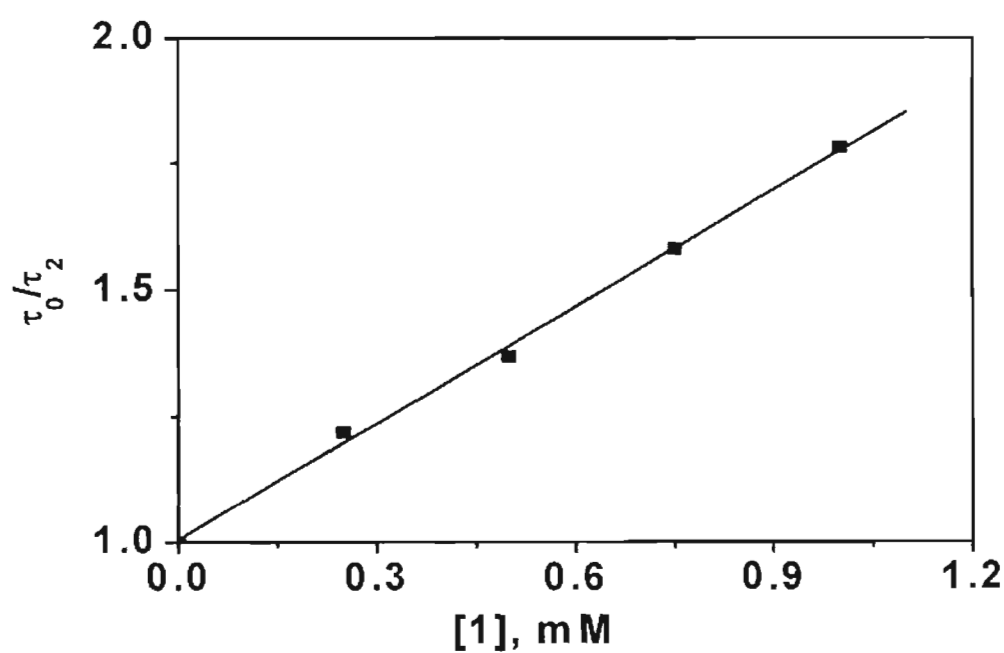
Figure 2.6. Stern-Völmer plot for the fluorescence lifetime quenching of PA by 1.

The association constant K_a was calculated from a plot of $\chi_{(P-Q)}/\chi_{(P)}$ *vs.* concentration of **1**. The plot is shown in Figure 2.7. From the slope of this graph. the value of 199 M^{-1} was obtained as K_a. This value is very close to the value (207 M^{-1}) obtained by NMR method.[47]
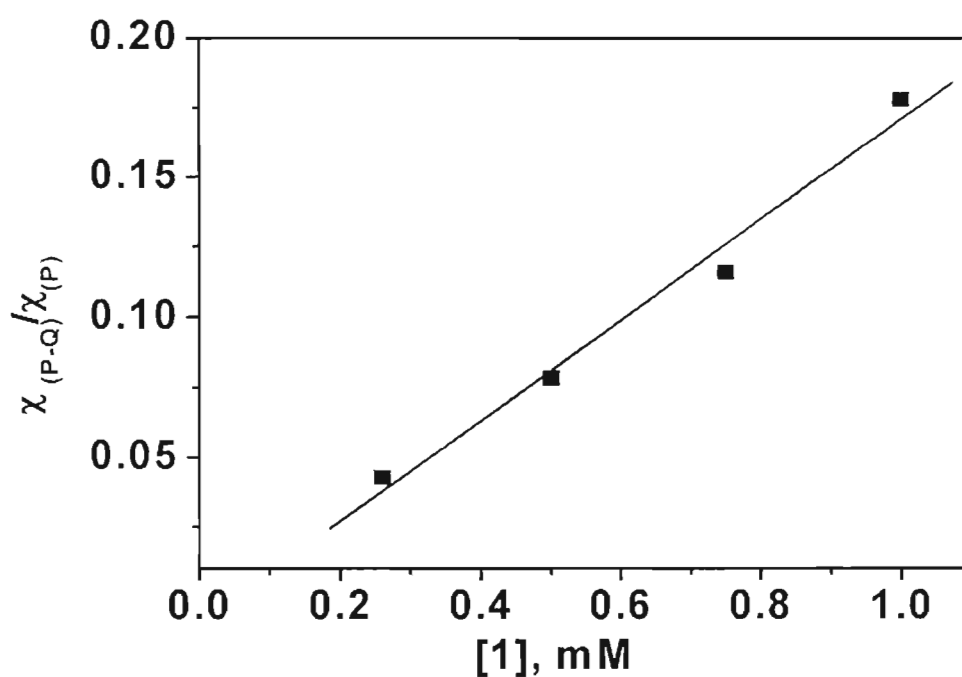
Figure 2.7. Plot of $\chi_{(P-Q)}/\chi_{(P)}$ *vs.* [1]. K_a obtained from this plot was 199 M^{-1}.

Experiments similar to those described above for **PA/1** system were carried out for **PA/2**, **PA/3**, **PA/4**, **PA/5**, **AA/1** and **AA/4** systems in chloroform solution. The decay profiles for these systems are shown in Figures 2.8 - 2.13 and the data obtained are presented in Tables 2.3 - 2.8. τ_0/τ_2 *vs.* quencher concentration for each systems are shown in Figures 2.14 - 2.19. k_{et} and k_q values obtained for are presented later in Table 2.11.

Figure 2.8. The fluorescence decay profiles of PA in the absence (a) and in presence (b - e) of 2 (1 - 4 mM). (f) is the lamp profile.
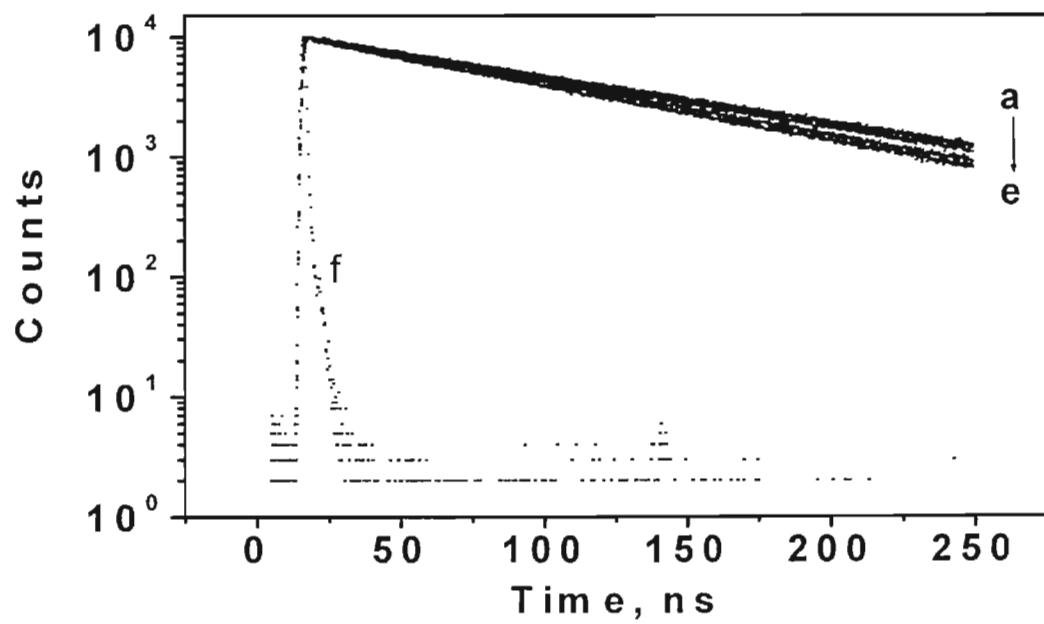
Figure 2.9. The fluorescence decay profiles of PA in the absence (a) and in presence (b - e) of 3 (1 - 4 mM). (f) is the lamp profile.
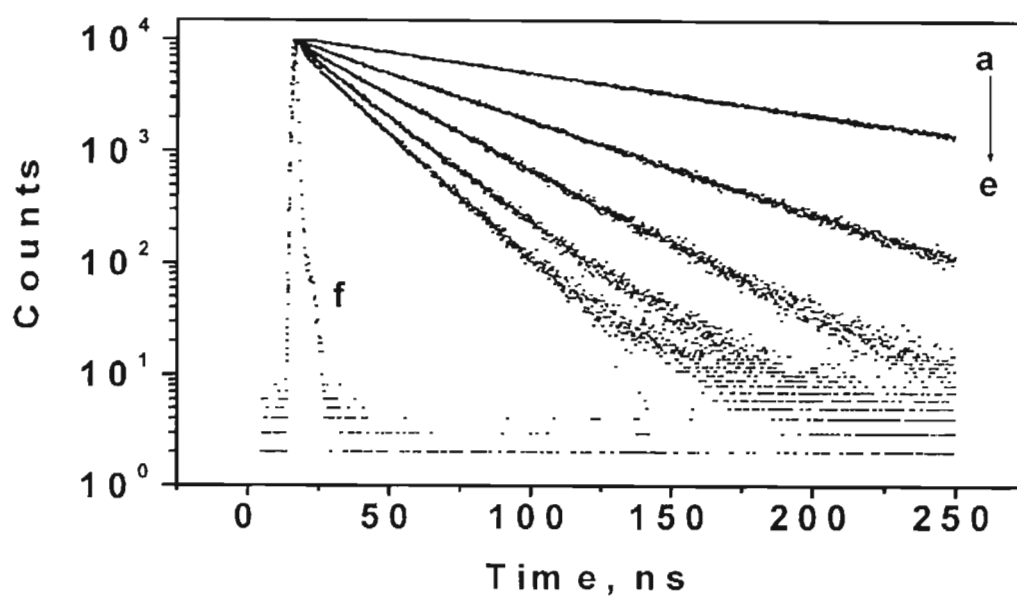
Figure 2.10. The fluorescence decay profiles of PA in the absence (a) and in presence (b - e) of 4 (1 - 4 mM). (f) is the lamp profile.
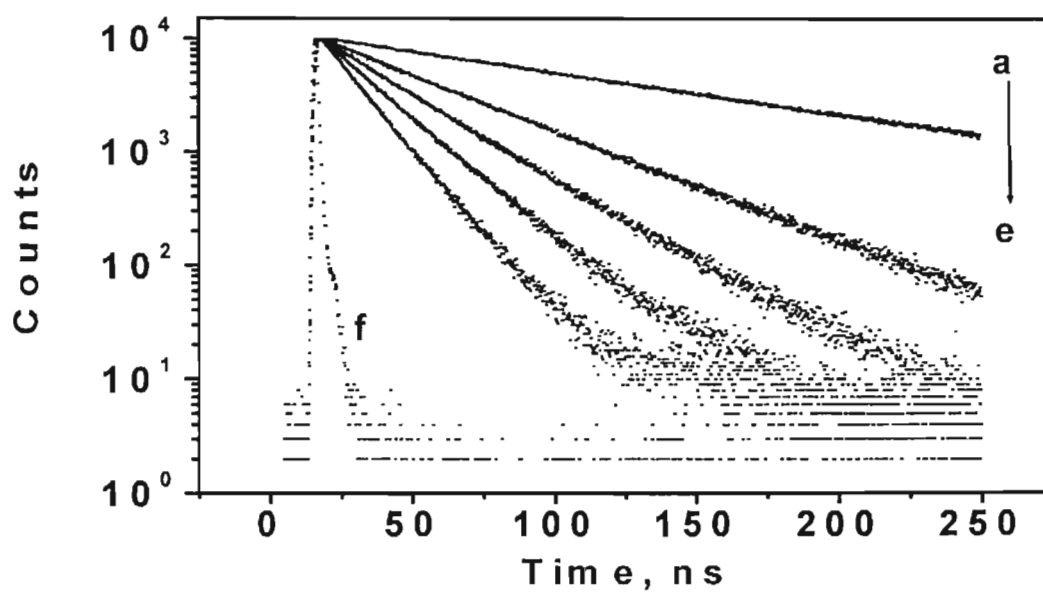
Figure 2.11. The fluorescence decay profiles of PA in the absence (a) and in presence (b - e) of 5 (1 - 4 mM). (f) is the lamp profile.
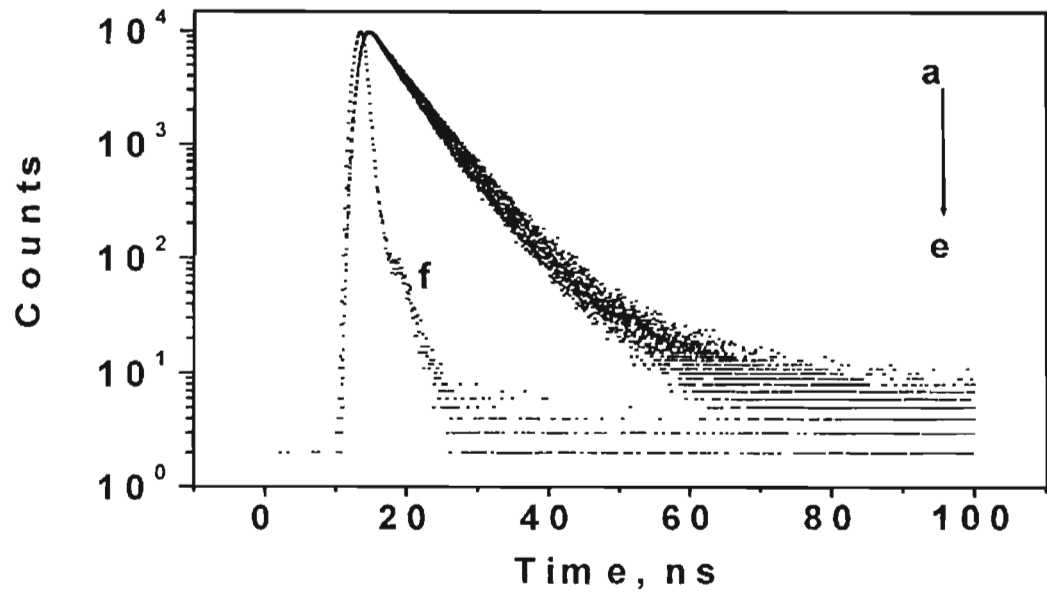
Figure 2.12. The fluorescence decay profiles of AA in the absence (a) and in presence (b-e) of 1 (1 - 4 mM). (f) is the lamp profile.
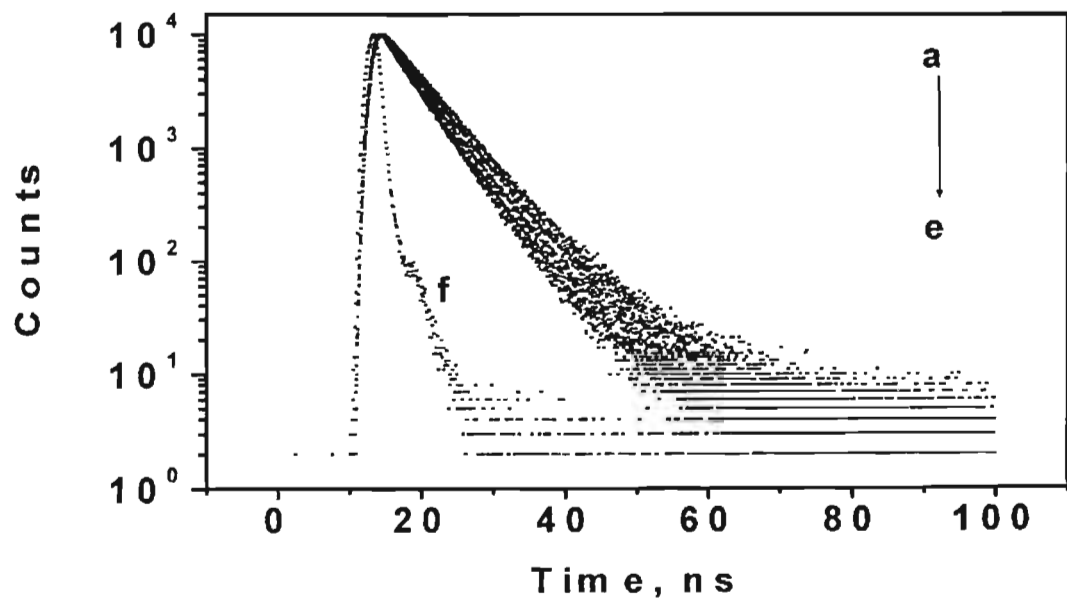
Figure 2.13. The fluorescence decay profiles of AA in the absence (a) and in presence (b - e) of 4 (1 - 4 mM). (f) is the lamp profile.

Table 2.3. Fluorescence lifetimes (τ_1 and τ_2), fractional contributions (χ_{P-Q} and χ_P) and χ^2 values obtained in the fluorescence quenching of PA by 2. [PA] was 1×10^{-5} M.

[2], M	τ_1, ns	χ_{P-Q}, %	τ_2, ns	χ_P, %	χ^2
0	-	-	106	100	1.1
1×10^{-3}	20.0	0.43	102.9	99.57	1.1
2×10^{-3}	17.5	0.50	99.06	99.50	1.1
3×10^{-3}	17.0	0.56	96.36	99.44	1.0
4×10^{-3}	17.5	0.65	94.20	99.35	1.2

Table 2.4. Fluorescence lifetimes (τ_1 and τ_2), fractional contributions (χ_{P-Q} and χ_P) and χ^2 values obtained in the fluorescence quenching of PA by 3. [PA] was 1×10^{-5} M.

[3], M	τ_1, ns	χ_{P-Q}, %	τ_2, ns	χ_P, %	χ^2
0	-	-	110	100	1.1
1×10^{-3}	9.0	0.15	100.9	99.85	1.3
2×10^{-3}	9.0	0.25	93.20	99.75	1.1
3×10^{-3}	9.0	0.40	86.60	99.60	1.1
4×10^{-3}	10.0	0.47	82.09	99.53	1.0

Table 2.5. Fluorescence lifetimes (τ_1 and τ_2), fractional contributions (χ_{P-Q} and χ_P) and χ^2 values obtained in the fluorescence quenching of PA by 4. [PA] was 1 x 10^{-5} M.

[4], M	τ_1, ns	χ_{P-Q}, %	τ_2, ns	χ_P, %	χ^2
0	-	-	101	100	1.1
1 x 10^{-3}	1.5	1.02	47.86	98.98	1.0
2 x 10^{-3}	1.5	2.53	30.79	97.47	1.1
3 x 10^{-3}	1.5	4.26	22.95	95.74	1.1
4 x 10^{-3}	1.6	6.46	18.19	93.54	1.1

Table 2.6. Fluorescence lifetimes (τ_1 and τ_2), fractional contributions (χ_{P-Q} and χ_P) and χ^2 values obtained in the fluorescence quenching of PA by 5. [PA] was 1 x 10^{-5} M.

[5], M	τ_1, ns	χ_{P-Q}, %	τ_2, ns	χ_P, %	χ^2
0	-	-	110	100	1.1
1 x 10^{-3}	48.0	4.63	45.60	95.37	1.2
2 x 10^{-3}	35.0	12.00	27.14	88.00	1.2
3 x 10^{-3}	33.0	15.00	19.65	85.00	1.1
4 x 10^{-3}	40.0	17.47	14.40	82.53	1.0

Table 2.7. Fluorescence lifetimes (τ_1 and τ_2), fractional contributions (χ_{P-Q} and χ_P) and χ^2 values obtained in the fluorescence quenching of AA by 1. [AA] was 1×10^{-5} M.

[1], M	τ_1, ns	χ_{P-Q}, %	τ_2, ns	χ_P, %	χ^2
0	-	-	6	100	1.2
1×10^{-3}	2.3	14.17	4.50	85.83	1.0
2×10^{-3}	2.1	27.68	3.60	72.32	1.0
3×10^{-3}	2.1	38.14	2.98	61.86	1.0
4×10^{-3}	2.4	42.0	2.55	57.00	1.0

Table 2.8. Fluorescence lifetimes (τ_1 and τ_2), fractional contributions (χ_{P-Q} and χ_P) and χ^2 values obtained in the fluorescence quenching of AA by 4. [AA] was 1×10^{-5} M.

[4], M	τ_1, ns	χ_{P-Q}, %	τ_2, ns	χ_P, %	χ^2
0	-	-	6.0	100	1.2
1×10^{-3}	0.95	5.16	5.71	94.84	1.1
2×10^{-3}	0.95	7.11	5.40	92.89	1.0
3×10^{-3}	0.98	8.20	5.12	91.80	1.0
4×10^{-3}	1.00	10.13	4.87	89.87	1.0
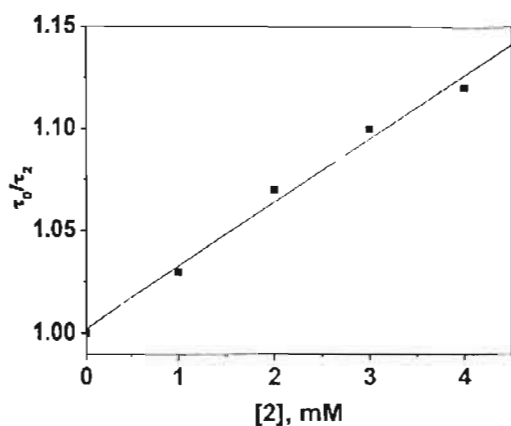
Figure 2.14. Stern-Völmer plot for the fluorescence lifetime quenching of PA by 2.
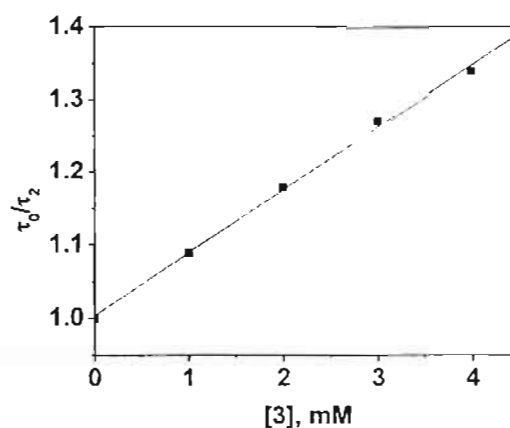
Figure 2.15. Stern-Völmer plot for the fluorescence lifetime quenching of PA by 3.
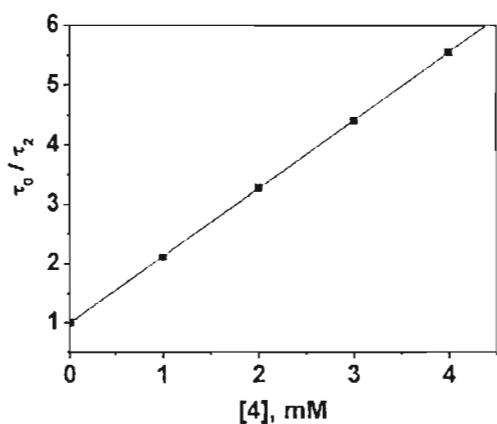
Figure 2.16. Stern-Völmer plot for the fluorescence lifetime quenching of PA by 4.
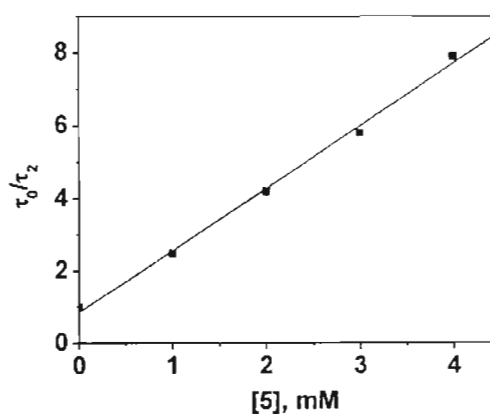
Figure 2.17. Stern-Völmer plot for the fluorescence lifetime quenching of PA by 5.
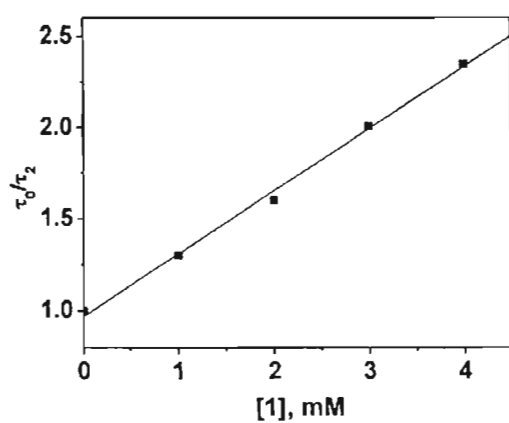
Figure 2.18. Stern-Völmer plot for the fluorescence lifetime quenching of AA by 1.
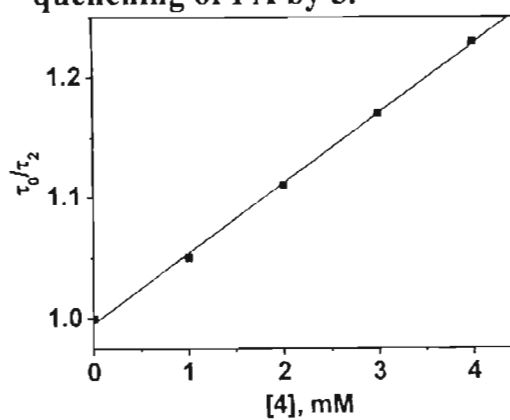
Figure 2.19. Stern-Völmer plot for the fluorescence lifetime quenching of AA by 4.

We could not observe biexponential decays for **AA/2**, **AA/3**, and **AA/5** systems. As a representative case the **AA/5** system is described below. In this case **AA** acts as the excited state donor and **5** acts as the acceptor. The fluorescence decay profiles of **AA** in the absence and presence of (various concentrations of) **5** are shown in Figure 2.20. All these decays could be fitted well using single exponential functions. Fitting to biexponential functions resulted in large χ^2 values. Lifetimes (τ) obtained using single exponential fits are given in Table 2.9.

Absence of a biexponential decay prompted us to check the formation of hydrogen-bonded **AA/5** complex using NMR. For **AA** the carboxyl proton appeared as a broad singlet around 11 ppm in $CDCl_3$. Up on addition of small amount of **5**, this peak showed an upfield shift. Although we could not determine the association constant due to the very poor solubility of both **AA** and **5** in this solvent, NMR studies suggest that **AA** and **5** indeed associate in solution. We believe that the **AA/5** hydrogen-bonded complex is formed, but did not participate in the electron transfer process. Since quenching involved only the diffusional pathway, a plot of τ_0/τ (Figure 2.21) was made and a k_q value of 1.6×10^{10} $M^{-1}s^{-1}$ was obtained from this plot.
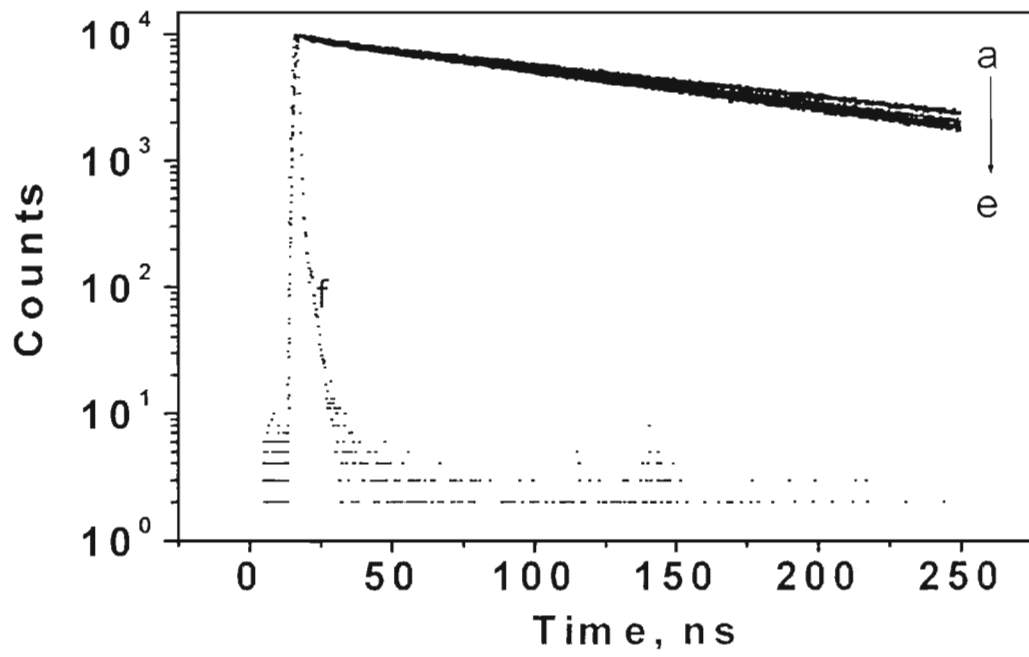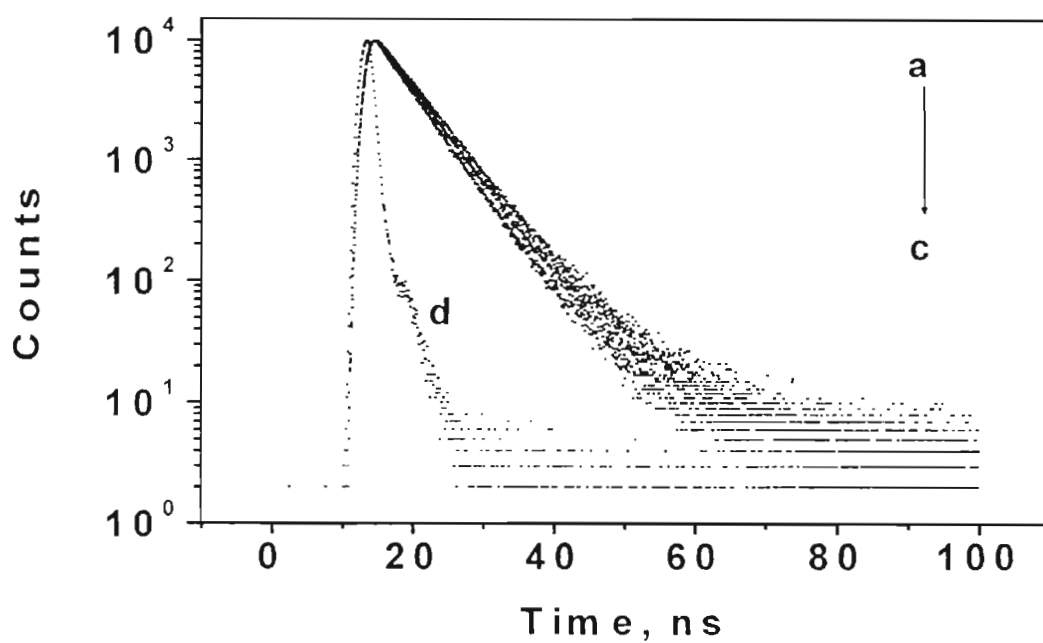
Figure 2.20. The fluorescence decay profiles of AA in the absence (a) and in presence (b, c) of 5 (2 and 4 mM). (d) is the lamp profile.

Table 2.9. Fluorescence lifetime τ and χ^2 values obtained for the fluorescence quenching of AA by 5. [AA] was 1 x 10^{-5} M.

[5], M	τ, ns	χ^2
0	5	1.2
1 x 10^{-3}	4.6	1.1
2 x 10^{-3}	4.2	1.1
3 x 10^{-3}	4.0	1.2
4 x 10^{-3}	3.7	1.2
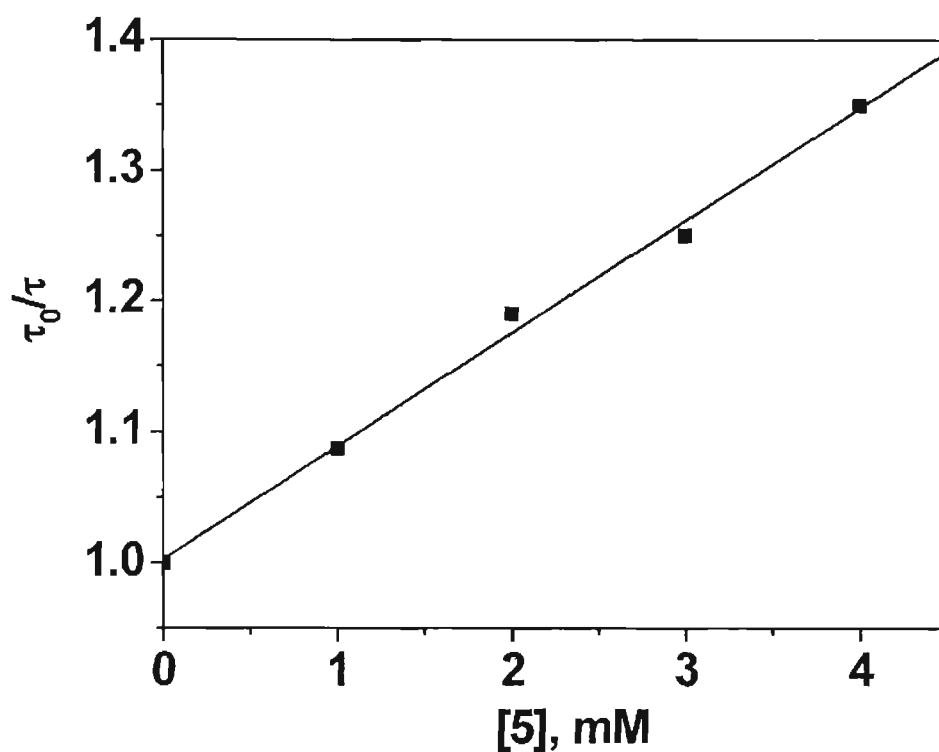
Figure 2.21. Stern-Völmer plot for the fluorescence lifetime quenching of AA by 5.

2.3.2.3. Fluorescence lifetime quenching studies in toluene

We have looked at the fluorescence quenching of **PA/1** and **PA/4** systems in toluene solution. In toluene, the fluorescence intensity of **PA** was highly quenched by addition of submillimolar concentrations of **1**, but this is accompanied by the formation of a broad band around 500 nm as shown in Figure 2.22. Based on literature this band was assigned to an exciplex formed between pyrene and dimethylaniline. It can be noticed from Figure 2.22 that the exciplex band increases in intensity with increase in the concentration of **1**.
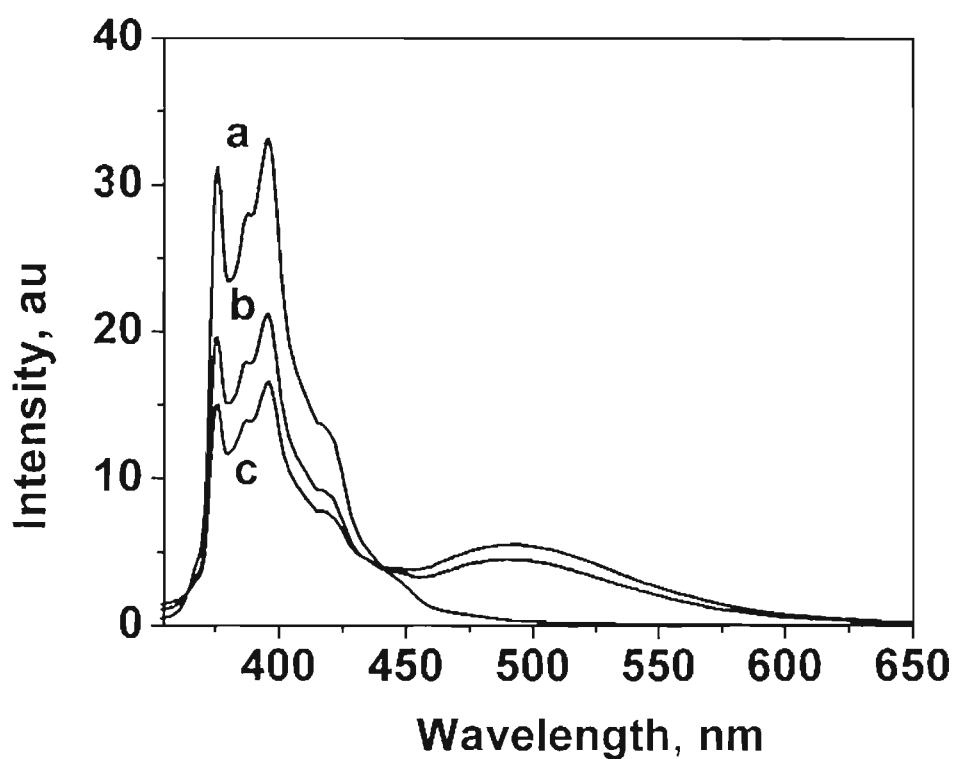
Figure 2.22. Fluorescence spectra of PA in the absence of quencher (a) and in the presence of (b - c) [1]. [1] varies from (b) 0.5 x 10^{-3} to (c) 1 x 10^{-3} M.

The fluorescence decay profiles of **PA** in toluene in the absence and presence of different concentrations of **1** is shown in Figure 2.23. The decay profiles in the presence of **1** could not be fitted using biexponential functions. These could, however, be fitted reasonably well with triexponential functions. This indicated that kinetics process in the **PA/1** system in toluene could not be described by the model shown in Scheme 2.3. Hence we have not made any serious effort to analyse this system in detail.
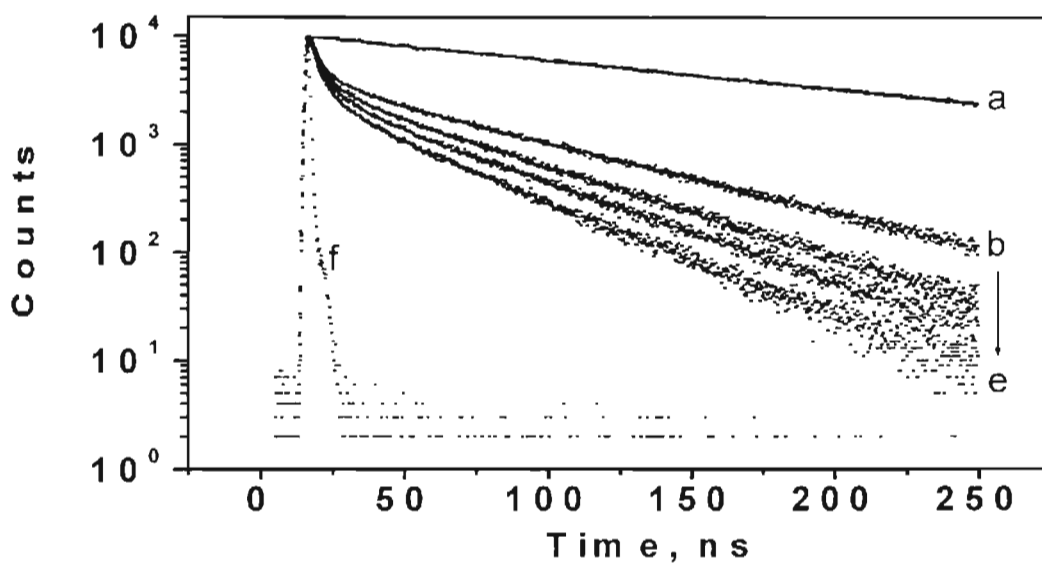
Figure 2.23. The fluorescence decay profiles of PA in the absence (a) and in presence (b - e) of 1 (1 - 4 mM). (f) is the lamp profile.

Photoprocesses in the **PA/4** system in toluene were very similar to those in chloroform solution. The fluorescence of **PA** was quenched upon addition of **4** and there was no indication of the formation of any exciplex. Fluorescence decays of **PA** in toluene in the presence of **4** were found to be biexponential (Figure 2.24) as demanded by Scheme 2.3. These were fitted to biexponential functions and the values of the parameters obtained are given in Table 2.10. Analysis of the data as described earlier gave $k_{et} = 3.9 \times 10^8$ s^{-1} and $k_q = 8.4 \times 10^9$ M^{-1} s^{-1} for this system. It is to be noted that k_{et} value obtained in this solvent is lower than that obtained in chloroform solution.
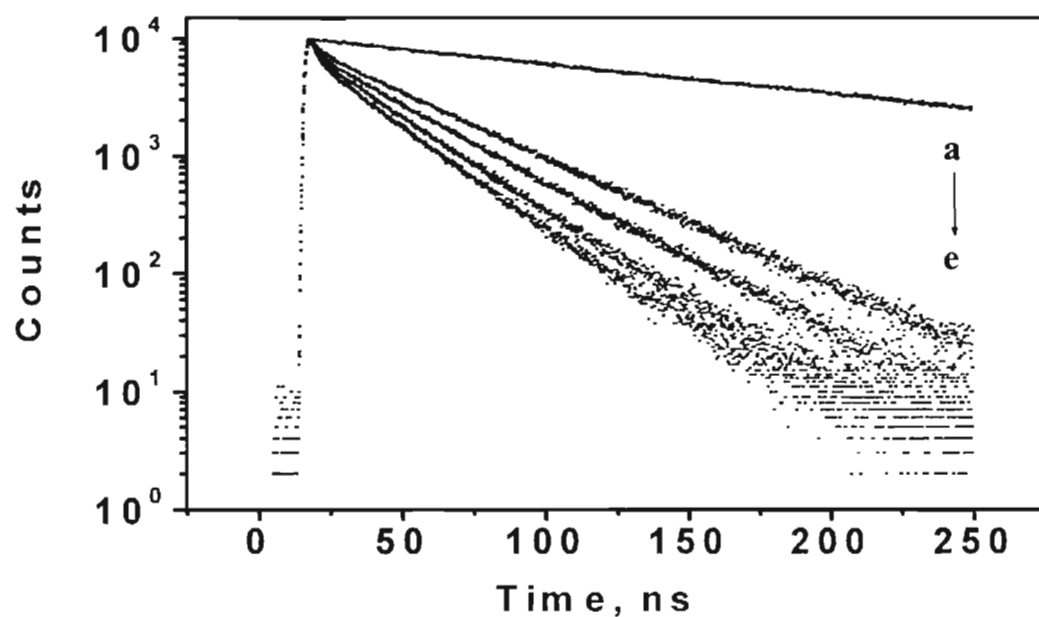
Figure 2.24. The fluorescence decay profiles of PA in the absence (a) and in presence (b - e) of 4 (1 - 4 mM).

Table 2.10. Fluorescence lifetimes (τ_1 and τ_2), fractional contributions (χ_{P-Q} and χ_P) and χ^2 values obtained in the fluorescence quenching of PA by 4 in toluene. [PA] was 1 x 10^{-5} M.

[4], M	τ_1, ns	χ_{P-Q}, %	τ_2, ns	χ_P, %	χ^2
0	-	-	158	100	1.2
1 x 10^{-3}	2.5	4.01	54.20	95.99	1.1
2 x 10^{-3}	2.4	5.52	38.99	94.48	1.2
3 x 10^{-3}	2.5	7.46	30.58	92.54	1.2
4 x 10^{-3}	2.5	9.81	24.30	90.19	1.1
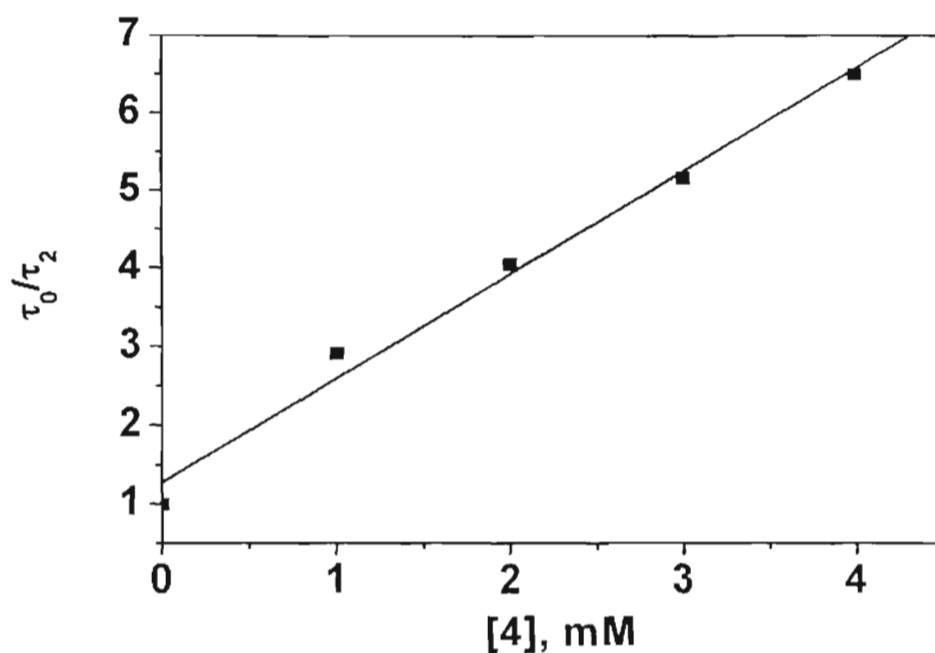
Figure 2.25. Stern-Völmer plot for the fluorescence lifetime quenching of PA by 4 in toluene.

2.3.3. Free energy dependence of electron transfer

The free energies for electron transfer in chloroform solution for our donor-acceptor systems calculated using Weller equation, and the rate constants obtained from the fluorescence lifetime measurements of these systems are presented in Table 2.11. $\Delta G°$ and k_{et} are the free energy and the rate constants, respectively for electron transfer in the hydrogen-bonded fraction and ΔG_{diff} and k_q are the corresponding values for the freely moving segment. The values in parenthesis are those reported earlier from our laboratory for these systems in dichloromethane solution and these values are reproduced here for a comparison.[47] It can be noticed from the table that the free energy varied from a slightly positive value of 0.15 eV

to a moderately negative value of - 1.23 eV and the rate constants obtained span a

range of two orders of magnitude.

Table 2.11. Free energies (ΔG° and ΔG_{diff}) and rate constants of electron transfer, k_{et} and k_q for the donor-acceptor assemblies. The numbers in column 1 corresponds to the number of the quenchers in Chart 2.1.

Probe-Quencher systems	ΔG°, eV	k_{et}, $10^7 s^{-1}$	ΔG°_{diff}, eV	k_q, $10^9 M^{-1}s^{-1}$
PA/1	-0.33 (-0.52)	128.0 ± 0.8 (89.9)	-0.39 (-0.56)	6.80 (9.29)
PA/2	0.15 (-0.04)	4.4 ± 0.4 (6.2)	0.09 (-0.07)	0.32 (0.04)
PA/3	0.24 (0.05)	9.7 ± 0.55 (1.9)	0.18 (0.02)	0.78 (0.21)
PA/4	-0.99 (-1.18)	63.5 ± 2.05 (39.0)	-1.05 (-1.21)	11.3 (12.80)
PA/5	-1.23 (-1.42)	1.7 ± 0.45 (5.2)	-1.29 (-1.45)	15.0 (12.80)
AA/1	-0.06 (-0.24)	27.9 ± 2.9 (43.0)	-0.12 (-0.28)	0.56 (7.36)
AA/4	-0.73 (-0.92)	89.9 ± 2.6 (144.0)	-0.79 (-0.95)	9.80 (16.60)

The values within parenthesis are those taken from reference 47.

In Figure 2.26 we have plotted the observed k_{et} values against ΔG°. It can

be seen from Figure 2.26 that as the free energy becomes more negative the rate

constants first increases, reaches a maximum and then decreases. This clearly is an

example of Marcus type electron transfer. We have attempted to fit the data to the

Marcus equation 2.8 using different combinations of H_{el} and λ values. A

reasonably good fit was obtained by using $H_{el} = 5$ cm^{-1} and $\lambda = 0.55$ eV. This fit is also shown along with the experimental data in Figure 2.26. An important result here is that the rate maximum shifted to less negative free energy values (-0.55 eV) in chloroform compared to -0.70 eV in dichloromethane and this is in very good agreement with Marcus theory.
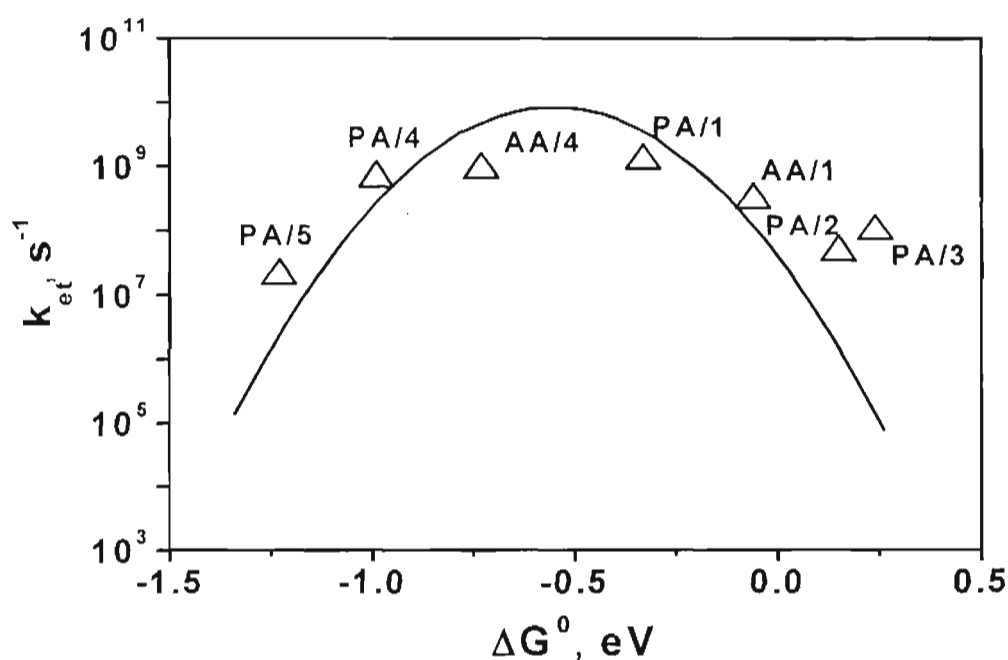
Figure 2.26. Dependence of electron transfer rates (k$_{et}$) in the hydrogen-bonded complex upon free energy in chloroform solution. Solid line is a fit to equation 2.8 with H$_{el}$ = 5 cm^{-1} and λ = 0.55 eV.

In Figure 2.27 we have plotted the experimental k_q values against ΔG°_{diff}. It can be seen from Figure 2.27 that as the driving force increases, k_q first increases, reaches a maximum and stays there. This clearly is an example of the Rehm-Weller behaviour. In the Rehm-Weller formalism, the overall quenching rate constant k_q in a bimolecular electron transfer reaction can be expressed by equation 2.24,[46]

$$k_q = 2 \times 10^{10} \left[1 + 0.23 \exp(\frac{\Delta G^{\#}}{RT}) + \exp(\frac{\Delta G^{o}}{RT}) \right]^{-1} \qquad (2.24)$$

$\Delta G^{\#}$ in equation 2.24 is the free energy of activation for electron transfer and is given by the equation 2.25.

$$\Delta G^{\#} = \Delta G^{o} + \frac{\Delta G^{\#}(0)}{\ln 2} \ln \left[1 + \exp \left(\frac{-\Delta G^{o} \ln 2}{\Delta G^{\#}(0)} \right) \right] \qquad (2.25.)$$

$\Delta G^{\#}(0)$ in the above expression is the free energy of activation when there is no driving force for the reaction. Normally $\Delta G^{\#}(0)$ is taken as equal to $\lambda/4$. Since $\lambda = 0.55$ eV in this case, a value of 0.138 eV was assumed for $\Delta G_0^{\#}$. The theoretical fit calculated using equation 2.25 is also shown in Figure 2.27.
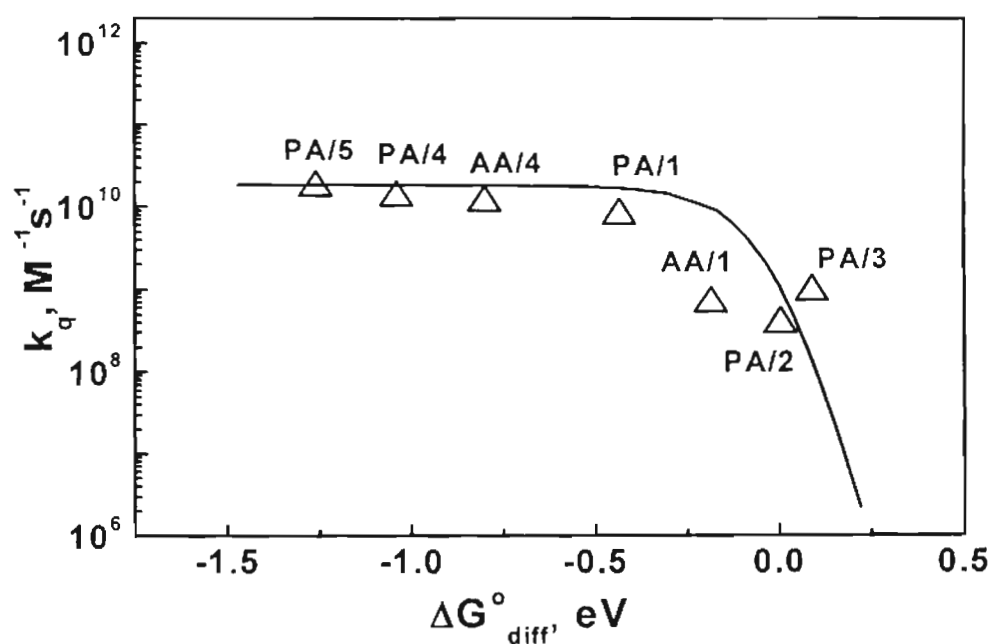
Figure 2.27. The plot of bimolecular quenching rate constants (k_q) *vs.* ΔG^o_{diff} in chloroform. The solid line is a fit to Rehm-Weller equation 2.24.

The strategy we have outlined in Scheme 2.3 thus allows for the simultaneous observation of the Marcus and Rehm-Weller behaviours of electron transfer. Where the partners are held at fixed distances and allowed to react under unimolecular condition, electron transfer follows the Marcus equation and when they are allowed to diffuse freely Rehm-Weller behaviour was observed. This clearly suggested that diffusion of the partners is the reason for not observing the MIR in bimolecular PET reactions.

2.4. Discussion

In this study arylacetic acids are used as electron donors and acceptors. Photophysical and electrochemical properties of the parent hydrocarbons are unaffected by substitution of the acetic acid moieties, which indicate that the acetic acid group is not a part of the chromophore in these molecules. Anthracene and pyrene derivatives were selected as probes because they can function as excited state acceptors as well as donors. All the quenchers listed in Chart 2.1 (without the CH_2COOH group) are known quenchers of pyrene or anthracene fluorescence by an electron transfer mechanism. The acetic acid moiety in these molecules serves to bring the donor and acceptor together through the two-point hydrogen bonding interaction of the carboxylic acid groups. Upon mixing the probe and the quencher in a non-polar solvent, probe-quencher association takes place as shown in Scheme 2.4. For hetero-dimers of carboxylic acids association constants reported are in the range of 300 - 700 M^{-1}.[55-58] In the systems we have used, one CH_2 group

on either side of the hydrogen bond interface, which brings some flexibility to the systems and reduce the association constants. By using NMR techniques it was shown in our laboratory earlier, that the association constants in these arylacetic acids are in the range of 20 - 200 M^{-1} in chloroform solution.[47] In fact a low association constant is required for the successful operation of Scheme 2.3.

The simplistic picture presented in Scheme 2.3 does not take into consideration the presence of **P~P** and **Q~Q** species. Since hydrogen bonding interactions are non-specific in nature, these species may also be present in solution. Since the concentration of **P** used is extremely small (10^{-5} M), concentration of **P~P** species will be extremely low and this does not present any problem in the analysis. Assuming a self-association constant of 100 M^{-1} for **Q**, we obtain a value of 10^{-4} M for the concentration of the **Q~Q** species when the quencher concentration used is 1 mM. Thus, about 10% of the quencher will be present as self associated species and the error in the value of diffusional quenching may be about 10%. This error limit may still be smaller because of the slower diffusion coefficient of the large associated species. In one of the earlier papers in this area, Nocera and coworkers studied the quenching of excited $(bpy)_2Ru(bpy\text{-}amidine)^{2+}$ by 3,5-dinitrobenzoic acid.[57] They have shown that the diffusional bimolecular quenching rate constants in the absence and presence of the hydrogen bond interface are similar. This shows that the error due to self-association of the quencher is small.

Excitation of the probe in the presence of the quencher leads to a biphasic decay in the fluorescence profile. The short lifetime component in the fluorescence decay is attributed to the electron transfer within the hydrogen-bonded assembly. Disappearance of the short lifetime component on addition of methanol proves that a fraction of the molecules are present indeed as hydrogen-bonded pairs. A close look at the decay profiles presented here shows that biexponential decay is clearly visible to the naked eye only in a few cases like **PA/1** and **PA/4**. For the **PA/3**, **PA/4** and **PA/5** systems, fluorescence decays looked more like monoexponential to the naked eye. This is due to the following reason. A bimolecular decay becomes clearly visible to the naked eye only if $\tau_1 \ll \tau_2$. Such systems lie at the top of the Marcus plot where rates are close to the maximum value. For systems in the normal and inverted regions τ_1 is relatively large and hence the difference between τ_1 and τ_2 is small. In the inverted region bimolecular quenching becomes diffusion controlled and leads to drastic reduction of τ_2 values with increase in quencher concentration. For these cases τ_1 and τ_2 have similar values. As the difference between τ_1 and τ_2 decreases, the decays progressively approach monoexponential in appearance. In these cases, although the decays did not appear distinctly biexponential to the naked eye, they fit well to biexponential functions and the reduced chi-square (χ^2) values obtained are all below 1.3. As described in the results section, the **AA/5** system did not show biexponential behaviour and possible reasons for this behaviour are discussed later in this section.

By employing the strategy outlined in Scheme 2.3 we could study and compare the unimolecular and bimolecular electron transfer reactions involving the same donor-acceptor systems. Free energy dependence studies showed that the unimolecular PET reaction obeys the Marcus equation and the bimolecular PET reaction obeys the Rehm-Weller equation. Here the only difference between a reaction that obeys the Marcus equation and one that obeys the Rehm-Weller equation is the free diffusion of the reactants in the latter case. Hence we conclude that the reason for not observing the MIR in bimolecular PET reactions is diffusion. Before discussing the implications of our results in detail, it is essential to describe the confusion that existed in the literature regarding the Marcus type and Rehm-Weller type of electron transfers. As mentioned previously several authors have tried to answer the question as to why the inverted region is generally not observed in PET reactions. In the following section an overview of their results is attempted.

The classical Marcus theory was reanalysed in the 1980's to include the influence of quantum effects, notably electron tunneling.[59] This treatment increases the rate constants when the thermally activated process becomes slow, but it was concluded that this treatment could not account for the discrepancies of the Marcus and Rehm-Weller type of plots. Later a new theory was put forward by Mataga and Kakitani (MK theory), which emphasized the role of solvent in controlling electron transfer processes in polar solvents.[60-62] This theory suggests that the difference in the Marcus and Rehm-Weller behaviours is the electric field,

which acts on the solvent. In the case of ions or ion pairs, the electric field leads to partial dielectric saturation of polar solvents and this will restrict solvent motion. In the case of neutral reactants no such dielectric saturation would exist and the solvent motion remain unhindered resulting in the observation of diffusion controlled rate constants. It was suggested later that the theory can not be applied to electron transfer reactions of relatively large organic molecules because the dielectric saturation becomes important only in the neighbourhood of small ions like Li^+ in water and is negligible for other cases.[63] Also according to the MK theory inverted region should not be observed in non-saturable solvents like toluene, which actually is not the case. Because of all these factors, the MK theory is not considered as the right approach in understanding the difference between Marcus and Rehm-Weller behaviours.

Recently Tachiya and Murata made a distinction between the Marcus and Rehm-Weller types of electron transfers.[64] According to them the Marcus equation gives the first order rate constant for a donor-acceptor pair with a fixed separation, while the Rehm-Weller equation gives a second order rate constant. They have calculated the second order diffusion mediated rate constant by using a recently developed theory of diffusion mediated reactions which takes into account the donor-acceptor distance of the first order rate constant. This theory also predicted an inverted region at very large driving forces, but this could not be verified experimentally.

Results from our laboratory unequivocally established that the MIR could be observed in forward electron transfer reactions and that the MIR is masked in bimolecular PET reactions due to diffusion. The fact that we are actually seeing the Marcus behaviour is confirmed by the dependence of the maximum of the Marcus plot on solvent. The maximum shifted from -0.70 eV in dichloromethane to -0.55 in chloroform and this is very well supported by the Marcus theory. According to this theory the rate constants in the normal region should increase and rate constants in the inverted region should decrease in non-polar solvents and this is found to be largely true in the present case.[7] Also note that k_{et} for the **PA/4** system decreases from 6.35 x 10^8 s^{-1} to 3.9 x 10^8 s^{-1} upon changing the solvent from chloroform to toluene. This is further indication that this system actually belongs to the inverted region.

Our conclusion is that free diffusion of the donors and acceptors is responsible for not observing the MIR in bimolecular PET reactions. This aspect can be further analysed as follows. It has been suggested in the literature that diffusion can mask the inverted region in two ways.[64-69] The first of this is by limiting the rate constant to the diffusion rate. This factor was recognised very early and is based on equation 2.5. When k_{act} is large, $1/k_{act}$ can be neglected and hence $k_q \approx k_{diff}$, which leads to limiting of the rate constants by diffusion. Using these arguments, it can be shown that the inverted region will be masked in the moderately large driving force regime because of diffusion, but should be

observable in bimolecular PET reactions at $\Delta G° < -2eV$. The original Rehm-Weller data did not, however, show any sign of inverted region even at $\Delta G° = -2.6$ eV.[12]

Rau and coworkers have suggested that the inverted region is not observed in bimolecular PET reactions because of the peculiar distance dependence of electron transfer in the inverted region.[70] The argument is that, in the inverted region the electron transfer is inefficient at contact distance, but will be highly efficient (and occur at diffusion controlled rates) at larger distances and this leads to the masking of the MIR (this aspect will be analysed in more detail in Chapter 3). To the best of our knowledge, the suggestion by Rau and coworkers has not been experimentally verified. Our experiments provide some indirect evidence for the above prediction. The first of such evidence comes from an analysis of the data presented in Table 2.11 and Figures 2.26 and 2.27.

Probe-quencher systems **PA/4** and **PA/5** fall in the inverted region. When these systems were allowed to undergo electron transfer at fixed distance (ie., in the hydrogen-bonded complex), the rates were low (see Figure 2.26 and Table 2.11). The same probe-quencher systems when allowed to diffuse freely, quenching occurred with diffusion controlled rates (see Figure 2.27 and Table 2.11). This result can be interpreted to mean that at an edge-to-edge distance of 9.4 Å quenching is slow, but at some other distance quenching occurred with a higher rate. A similar inference is obtained from a study of electron transfer in the **AA/5** system.

The **AA/5** system falls in the inverted region. Figure 2.20 shows the fluorescence decay profiles of **AA** (1×10^{-5} M) in the absence and presence of **5**. All the decays fit well into single exponential functions. The short lifetime component which characterizes electron transfer in the hydrogen-bonded system is absent in the decay profile at all quencher concentrations studied. Hence it was assumed that electron transfer took place only through the diffusional pathway here. The fact that biexponential decay is absent in the **AA/5** system suggests two possibilities: (1) Hydrogen-bonded complex is not formed in this case and (2) hydrogen-bonded complex is formed but the rate of electron transfer within the complex (k_{et}) is lower than k_0 and hence is non-observable. NMR studies suggested that hydrogen-bonded complex is indeed formed in this case. Thus, if biexponential decay is not observed, it must indeed be due to the inefficiency of the electron transfer process within the hydrogen-bonded complex compared to the intrinsic decay rate of **AA**. This result can be interpreted to mean that at an edge-to-edge distance of 9.4 Å, the PET process is not at all efficient, but at some other distances PET occurred with diffusion controlled rates. The data as such does not say whether this distance is lower or higher than 9.4 Å. From theoretical considerations (see Chapter 3 for details) we suggest that this distance may be greater than 9.4 Å. In order to seek some support for this, we have carried out a study of distance dependence of electron transfer in these systems and the details are reported in Chapter 3 of this thesis.

Electron transfer reactions we have studied span only a small free energy range and we can conclude that in the moderately negative free energy range absence of inverted region in PET can be attributed to diffusion. In the highly negative free energy region other factors may be important. For example, formation of products in the excited states is a good possibility. If this happens the actual free energy change would be smaller by the excitation energy of the product and will be insufficient to fall within the inverted region. This hypothesis appears quite reasonable because the excitation energies of the radical products are small and these states may be accessible at large driving forces. The formation of electronically excited molecular ions in electron transfer reactions can in principle be proved by the observation of their luminescence, but this is generally very weak and beyond the detection limit of most currently available instruments.

Another outcome of this study is the clear identification of systems that belong to the normal and inverted regions. Thus **PA/1, PA/2, PA/3** and **AA/1** fall in the normal region whereas **PA/4, PA/5** and **AA/4** fall in the inverted region. This has enabled us to study the distance and temperature dependence of electron transfer reactions in hydrogen-bonded systems in the normal and inverted regions. These studies are reported in Chapters 3 and 4 of this thesis.

2.5. Conclusions

We have studied the free energy dependence of electron transfer in a few donor-acceptor systems assembled through hydrogen bonding interactions in chloroform solution. Our study shows that when diffusion is prevented Marcus behavior is observed and when diffusion is allowed Rehm-Weller behavior is observed. Thus the non-observance of the inverted region in PET reactions is attributed to diffusion. The maximum in the Marcus plot for the hydrogen-bonded fraction was found to be shifted to a less negative free energy value in chloroform, and this is further confirmation of the Marcus type electron transfer taking place in the hydrogen-bonded fraction of the donor-acceptor systems.

2.6. Experimental section

2.6.1. Materials

Pyrene-1-acetic acid and anthracene-9-acetic acid were synthesized according to reported procedures.[71] All the quencher molecules used for the study, namely, 4-(*N,N*-dimethylamino)phenylacetic acid (**1**),[72] 2,5-dimethoxyphenylacetic acid (**2**),[73] 4-cyanophenylacetic acid (**3**),[74] 4-nitrophenylacetic acid (**4**)[75] and 2,4-dinitrophenylacetic acid (**5**)[76] were prepared according to literature procedures. All these were thoroughly purified and dried before use.

The chloroform and toluene used for the fluorescence lifetime measurements was rigorously dried and deaerated before use.

2.6.2. Measurements

The absorption spectra were recorded on a Shimadzu-3101PC UV-Vis-NIR scanning spectrophotometer. Fluorescence spectra were recorded on a SPEX Fluorolog F112X spectrofluorimeter. Fluorescence lifetimes were determined using Edinburgh Instruments FL900CD single photon counting system and the data were analysed by Edinburgh software. For the fluorescence measurements, probe concentrations were 1×10^{-5} M and quencher concentrations were in the range of $(1 - 4) \times 10^{-3}$ M.

2.7. References

1. Kavarnos, G. J. *Fundementals of Photoinduced Electron Transfer*; VCH: New York, 1993.

2. Marcus, R. A. *Int. J. Chem. Kinet.* **1981**, *13*, 865.

3. Sutin, N. *Acc. Chem. Res.* **1982**, *15*, 275.

4. Marcus, R. A.; Siders, P. *J. Phys. Chem.* **1982**, *86*, 622.

5. Siders, P.; Marcus, R. A. *J. Am. Chem. Soc.* **1981**, *103*, 741.

6. Marcus, R. A. *Faraday Discuss. Chem. Soc.* **1982**, *74*, 7.

7. Marcus, R. A.; Sutin, M. *Biochim. Biophys. Acta* **1985**, *811*, 266.

8. Marcus, R. A. *J. Chem. Phys.* **1956**, *24*, 966.

9. Marcus, R. A. *J. Chem. Phys.* **1956**, *24*, 979.

10. Marcus, R. A. *Faraday Discuss. Chem. Soc.* **1960**, *29*, 21.

11. Rehm, D.; Weller, A. *Ber. Bunsenges. Phys. Chem.* **1969**, *73*, 834.

12. Rehm, D.; Weller, A. *Isr. J. Chem.* **1970.** *8.* 259.

13. Bock, C. R.; Meyer, T. J.; Whitten, D. G. *J. Am. Chem. Soc.* **1975**, *97*, 2909.

14. Scheerer, R.; Gratzel, M. *J. Am. Chem. Soc.* **1977**, *99*, 867.

15. Breymann, U.; Dreeskamp, H.; Koch, E.; Zander, M. *Chem. Phys. Lett.* **1978**, *59*, 68.

16. Martens, F. M.; Verhoeven, J. W.; Gase. R. A.; Pandit, U. K.; Boer, T. J. *Tetrahedron*, **1978**, *34*, 443.

17. Indelli, M. T.; Scandola, F. *J. Am. Chem. Soc.* **1978**, *100*, 7732.

18. Nagle, J. K.; Dressick, W. J.; Meyer, T. J. *J. Am. Chem. Soc.* **1979.** *101*, 3993.

19. Beitz, J. V.; Miller, J. R. *J. Chem. Phys.* **1979**, *71*, 4579.

20. Miller, J. R.; Beitz, J. V.; Huddleston. R. K. *J. Am. Chem. Soc.* **1984**, *106*, 5057.

21. Miller, J. R.; Calcaterra, L. T.; Closs, G. L. *J. Am. Chem. Soc.* **1984**, *106*, 3047.

22. Closs, G. L.; Miller, J. R. *Science* **1988**, *240*, 440.

23. Wasielewski, M. R.; Niemczyk, M. P.; Svee, W. A.; Pewitt, E. B. *J. Am. Chem. Soc.* **1985**, *107*, 1080.

24. Irvine, M. P.; Harrison, R. J.; Beddard, G. S.; Leighton, P.; Sanders, J. K. M. *Chem. Phys.* **1986**, *104*, 315.

25. Ohno, T.; Yoshimura, A.; Mataga, N. *J. Phys. Chem.* **1986**, *90*, 3295.

26. Wasielewski, M. R.; Johnson, D. G.; Svee, W. A. in *Supramolecular*

Photochemistry; Balzani, V. Ed.; D. Reidel: Amsterdam. 1987; p 255.

27. Harrison. R. J.; Pearce, B.; Beddard, G. S.; Cowan, J. A.; Sanders, J. K. M. *Chem. Phys.* **1987**, *116*, 429.

28. Osuka, A.; Zhang, R. P.; Maruyama, K.; Yamazaki, I.; Nishimura, Y. *Bull. Chem. Soc. Jpn.* **1992**, *65*, 2807.

29. Heitele, H.; Pollinger, F.; Haberle, T.; Michel-Beyerle, M. E.; Staab, H. A. *J. Phys. Chem.* **1994**, *98*, 7402.

30. Osuka, A.; Noya, G.; Taniguchi, S.; Okada, T.; Nishimura, Y.; Yamazaki, I.; Mataga, N. *Chem. Eur. J.* **2000**, *6*, 33.

31. Gould, I. R.; Ege. D.; Mattes, S. L.; Farid, S. *J. Am. Chem. Soc.* **1987**, *109*, 3794.

32. Gould, I. R.; Farid, S. *J. Am. Chem. Soc.* **1988**, *110*, 1991.

33. Gould, I. R.; Farid, S. *J. Am. Chem. Soc.* **1988**, *110*, 7242.

34. Gould, I. R.; Farid, S. *J. Am. Chem. Soc.* **1988**, *110*, 7883.

35. Gould, I. R.; Farid, S. *J. Am. Chem. Soc.* **1990**, *112*, 4290.

36. Mataga, N.; Ashai, T.; Kanda, Y.; Okada, T.; Kakitani, T. *Chem. Phys.* **1988**, *127*, 249.

37. Ashai, T.; Mataga, N. *J. Phys. Chem.* **1989**, *93*, 6575.

38. Ashai, T.; Mataga, N.; Takahashi, Y.; Miyashi, T. *Chem. Phys. Lett.* **1990**, *171*, 309.

39. Segawa, H.; Takehara. C.; Honda. K.; Schimidzu, T.; Ashai, T.; Mataga, N. *J. Phys. Chem.* **1992**, *96*, 503.

40. Zon, C.; Miers, J. B.; Ballew, R. W.; Dlott, D. D.; Schuster, G. B. *J. Am. Chem. Soc.* **1991**, *113*, 7823.

41. Jayanthy. S. S.; Ramamurthy. P. *J. Phys. Chem.* **1997**, *101*, 2016.

42. Weller, A.; Zachariasse, K. *Chem. Phys. Lett.* **1971**, *10*, 590.

43. Efrima, S.; Bixon, M. *Chem. Phys. Lett.* **1974**, *25*, 34.

44. Joussot-Dubien, J.; Albrecht, A. C.; Gerischer, H.; Knox. R. S.; Marcus, R. A.; Schott, M.; Weller, A.; Willig. F. in *Light Induced Charge Separation in Biology and Chemistry*; Gerischer. H., Katz, J. J. Eds.; Verlag Chemie: New York, 197; p 129.

45. Suppan. P. *Top. Curr. Chem.* **1992**, *163*, 95.

46. Hug, G. L.; Marciniak, B. *J. Phys. Chem.* **1995**, *99*, 1478.

47. Prasad, E.; Gopidas, K. R. *J. Am. Chem. Soc.* **2000**, *122*, 3191.

48. Julliard, M. in *Photoinduced Electron Transfer, Part B*; Fox, M. A., Channon, M. Eds.; Elsevier: New York, 1998; p 216 and references cited therein.

49. Murakami, H.; Hohsaka, T.; Ashizuka, Y.; Sisido, M. *J. Am. Chem. Soc.* **1998**, *120*, 7520.

50. Zanini, G. P.; Montejano, H. A.; Previtall, C. M. *J. Chem. Soc. Faraday Trans.* **1995**, *91*, 1197.

51. Mataga, N. *Pure Appl. Chem.* **1984**, *56*, 1255.

52. Aoki, I.; Sakaki, S.; Shinikai, S. *J. Chem. Soc. Chem. Commun.* **1992**, 730.

53. Derissen, J. L. *J. Mol. Struct.* **1971**, *7*, 67.

54. Doan, V.; Köppe, R.; Kasai, P. H. *J. Am. Chem. Soc.* **1997**, *119*, 9810.

55. Turro, C.; Chang, C. K.; Leroi, G. E.; Cukier, R. I.; Nocera, D. G. *J. Am. Chem. Soc.* **1992**, *114*, 4013.

56. de Rege P. J. F.; Williams, S. A.; Therien, M. J. *Science* **1995**, *269*, 1409.

57. Roberts, J. A.; Kirby, J. P.; Nocera, D. G. *J. Am. Chem. Soc.* **1995**, *117*, 8051.

58. Kirby, J. P.; Roberts, J. A.; Nocera, D. G. *J. Am. Chem. Soc.* **1997**, *119*, 9230.

59. Siders, P.; Marcus, R. A. *J. Am. Chem. Soc.* **1981**, *103*, 748.

60. Kakitani, T.; Mataga, N. *Chem. Phys.* **1985**, *93*, 381.

61. Kakitani, T.; Mataga, N. *J. Phys. Chem.* **1986**, *90*, 993.

62. Kakitani, T.; Mataga, N. *J. Phys. Chem.* **1987**, *91*, 6277.

63. Heinziger, K.; Palinkas, G. *Stud. Phys. Theor. Chem.* **1985**, *38*, 313.

64. Tachiya, M.; Murata, S. *J. Phys. Chem.* **1992**, *96*, 8441.

65. Northup, S. H.; Hynes, J. T. *J. Chem. Phys.* **1980**, *73*, 2700.

66. Calef, D. F.; Wolynes, P. G. *J. Phys. Chem.* **1983**, *87*, 3387.

67. Zusman, L. D. *Chem. Phys.* **1980**, *49*, 295.

68. Sutin, N. *Prog. Inorg. Chem.* **1983**, *30*, 441.

69. Marcus, R. A. *Discuss. Faraday Soc.* **1960**, *29*, 129.

70. Greiner, G.; Pasquini, P.; Weiland, R.; Orthwein, H.; Rau, H. *J. Photochem. Photobiol. A: Chem.* **1990**, *51*, 179.

71. Klassen, S. E.; Daub, G. H.; Van der Jagt, D. L. *J. Org. Chem.* **1983**, *48*, 4361.

72. Romanelli, M. G.; Becker, E. I. in *Org. Syn. Vol. 47*; Emmons, W. D. Ed.;

John Wiley and Sons Inc.: London, 1967; p 69.

73. Abbott, L. D.; Smith, J. D. *J. Biol. Chem.* **1949**, *179*, 365.

74. Robertson, G. R. I   n *Org. Syn. Coll. Vol. 1*; Blatt, A. H. Ed.; John Wiley and Sons Inc.: London, 1958; p 52.

75. Robertson, G. R. in *Org. Syn. Coll. Vol. 1*; Blatt, A. H. Ed.; John Wiley and Sons Inc.: London, 1958; p 406.

76. Furniss, B. S., Hannaford, A. J., Smith, P. W. G., Tatchel, A. R. Eds.; *Vogel's Text Book of Practical Organic Chemistry;* E. L. B. S.: London, 1989; p 837.

CHAPTER 3

STUDY OF THE DISTANCE DEPENDENCE OF PHOTOINDUCED ELECTRON TRANSFER RATES IN HYDROGEN-BONDED DONOR-ACCEPTOR SYSTEMS

3.1. Abstract

In this chapter, a systematic study of the distance dependence of electron transfer in hydrogen-bonded donor-acceptor systems is reported. For the pyreneacetic acid/4-dimethylaminophenylacetic acid hydrogen-bonded system, which fall in the normal region, the rate constant showed an order of magnitude decrease as the distance increased from 12 to 17 Å. For the pyreneacetic acid/ 4-nitrophenylactetic acid hydrogen-bonded system, which belong to the inverted region, the rate constant remained almost invariant over the same distance. This study thus showed that the distance dependence of electron transfer is not the same in the normal and inverted regions. The observed distance dependencies were analysed using Marcus theory and the results are presented here.

3.2. Introduction

Of the several factors that affect the rates of electron transfer reactions the distance between the donor and acceptor is very important. Hence a variety of experimental approaches are being used to obtain electron transfer rates as a function of separation distance. In one of the earlier reports, Kuhn and Mobius

studied the electron transfer process between donors and acceptors separated by a fatty acid Langmuir Blodgett film.[1-3] In this case the distance was changed by changing the length of the fatty acid chain. It was found that an increase in the fatty acid layer thickness from 22 to 28 Å reduces the rate of electron transfer by an order of magnitude. Contemporary work by Miller and co-workers showed that electron transfer can occur in rigid organic glasses.[4] They were able to quantify the distance dependence of electron transfer from biphenyl anion to different acceptors in methyltetrahydrofuran glass at 77 K.[5] The results obtained however had two major setbacks: (1) the donor-acceptor distances were random and (2) there were possibilities of electron transfers to the second nearest and farthest acceptor molecules. Experimental systems were then designed to eliminate the problem of variable distances inherent in intermolecular electron transfer reactions by covalently linking the donors and acceptors. In covalently linked systems, intramolecular electron transfer may or may not use the intervening bridge molecular orbitals to accomplish effective electronic coupling between the donor and acceptor. When electron transfer proceeds directly from the edge of the donor to the edge of the acceptor, by a mechanism not involving the orbitals of the bridging group, it is referred to as 'through-space' pathway. If on the other hand, the orbitals of the bridging group assist in transferring the electron, the pathway is referred to as 'through-bond' pathway. The work described in this chapter will be restricted to those systems in which intramolecular electron transfer proceeds directly from the donor to the acceptor through the orbitals of the bridging groups.

In order to understand the significance of our distance dependence studies, a brief survey of the previous work in this area is required and this is attempted here.

It is generally observed that for photoinduced charge separation and thermal charge recombination reactions, the rate constants display exponential distance dependence[6]

$$k_{et} = A \exp(-\beta \times distance) \tag{3.1}$$

The equation is found to be valid irrespective of whether the distance is expressed as the number of bonds separating the donor and acceptor moieties or as the centre-to-centre distance 'd_c'. β is called the damping factor and its value primarily depends on the electronic structure and conducting nature of the bridging unit. Bridging units which allow facile transfer of electron from donor to acceptor moiety will have low (≤ 0.5) β values.

There are a large number of studies that address the distance dependence of electron transfer reactions.[8-44] These can be grouped into four categories based on the nature of the bridging group. In the first category we consider donors covalently linked to acceptors by rigid spacers. This type of linking offers the advantage of maintaining the donor and acceptor at a fixed distance independent of conformational motion. The most influential experimental study in this category was made by Closs *et al.*[16] They studied intramolecular electron transfer from 4-biphenyl radical anion donor to 2-naphthyl acceptor in the rigid systems shown in Chart 3.1. They found that the rate constant of electron transfer decreased

exponentially from 4.2×10^9 s^{-1} to 1.5×10^6 s^{-1} as the number of intervening bonds increased from 5 to 10. In another study, Johnson *et al.* showed that the rate of hole transfer from the biphenyl cation radical to naphthalene across the same spacers depicted in **1 - 3** yields almost the same distance dependence as the electron transfer.[17] Dervan *et al.* investigated the distance dependence of electron transfer in the porphyrin-quinone systems **4 - 6** (Chart 3.2), where the donor-acceptor distance changed from 6 to 14 Å.[18] It was observed that the rate constant for electron transfer decreased from 7.7×10^9 s^{-1} for **4** to 2×10^7 s^{-1} for **6**. Rigid bridging groups such as phenyl,[19,20] norbornyl,[21-24] polyspirocyclobutyl[25] etc. have also been employed in distance dependence studies. In most of the cases an exponential rate dependence on distance was observed.

Chart 3.1

4

5

6
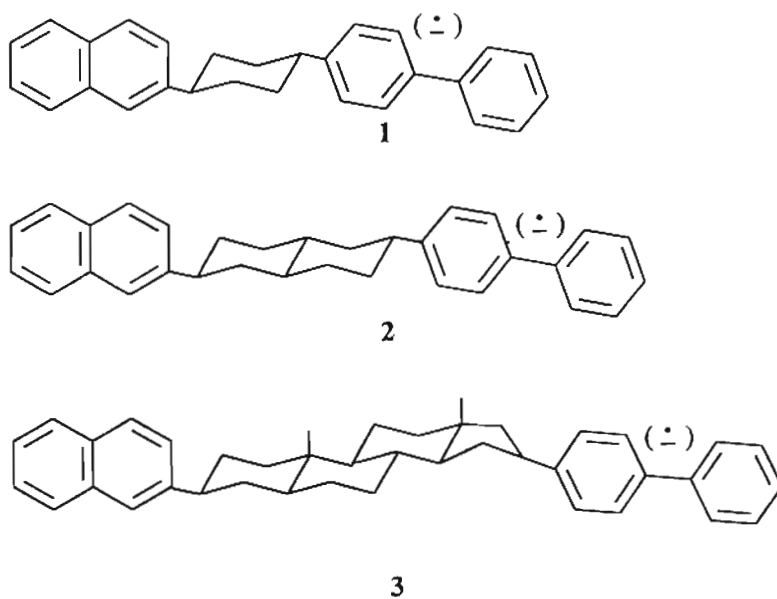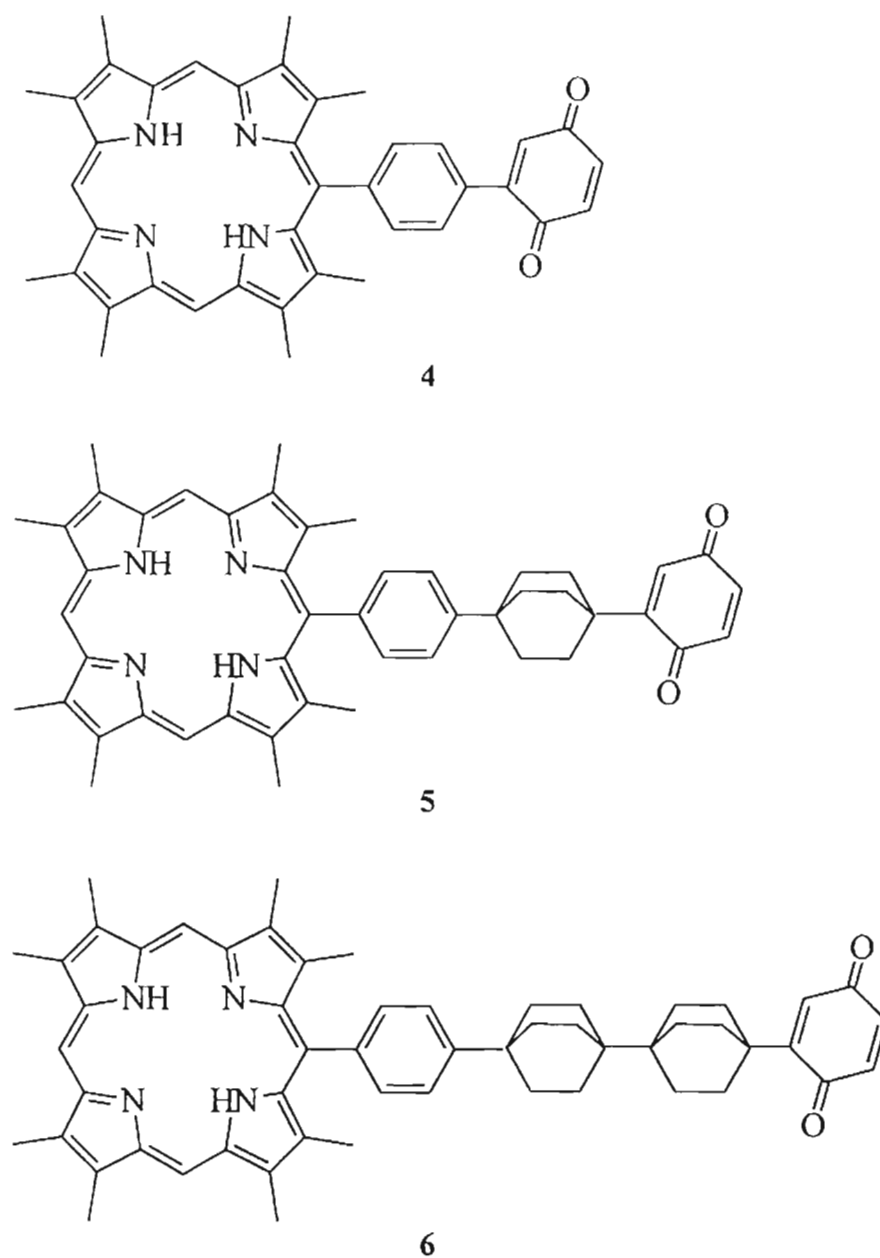
Chart 3.2

Studies using donor-acceptor systems linked by rigid spacers have shown unequivocally that the nature and configuration of the bridge plays an important role in mediating electron transfer. Often, electron transfer appears to be mediated by a super exchange mechanism involving the anti-bonding orbitals of the bridge.

Therefore aromatic and unsaturated bridges are expected to be more effective in mediating electron transfer than their saturated counter parts. Accordingly, electron transfer studies on model systems linked by conjugated bridges showed only a weak distance dependence. In this context it is worth mentioning a recent study by Davis *et al.*[26] These authors have synthesized a series of structurally well-defined molecules that incorporate tetracene as the donor and pyromellitimide as the acceptor, linked by *p*-phenylenevinylene oligomers of various lengths (Chart 3.3). PET in this series exhibited very weak distance dependence ($\beta < 0.04$ Å^{-1}) for donor-acceptor separations as large as 40 Å with rate constants remaining in the range of 10^{11} s^{-1}.
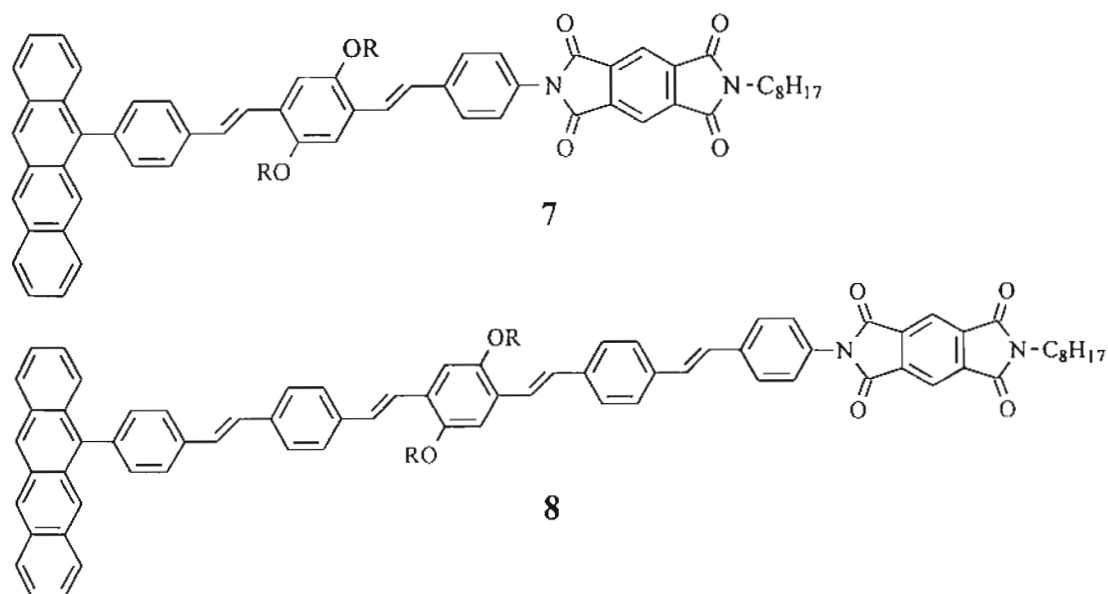
Chart 3.3

In the second category we include systems where the donor and acceptor are linked by flexible spacers. These studies are complicated due to a distribution of rate constants corresponding to different conformations of the molecules.[27-28] In

some cases this difficulty can be eliminated by using complexing agents like cyclodextrin, which can form rotaxane type complexes that keep the molecules in an extended conformation as shown in Scheme 3.1. In this context, a study by Mallouk and co-workers is worth mentioning. They have studied the electron transfer process in a series of dyads consisting of $Ru(bpy)_3^{2+}$ donor covalently linked to a paraquat acceptor *via* a methylene chain of variable length (**9,** n = 2 - 8, Chart 3.4).[29] Rate constants of PET in these systems decreased exponentially as n varied from 1 - 5, but remained constant for n = 7 - 8. The high rate constants for n = 7 - 8 systems were attributed to the flexible nature of the linker which can bring the donor and acceptor moieties in close proximity and promote through-space electron transfer. But when the n = 7 - 8 systems are complexed with cyclodextrin, the k_{et} values followed the same exponential decrease as observed for n = 1 - 5 and this was attributed to extended conformations of the type shown in Scheme 3.1. In another study the authors have investigated the PET process in **9** (n = 2 - 8) encapsulated in zeolite cavities and observed exponential decrease of the rate constant with distance.[30]

Scheme 3.1

9
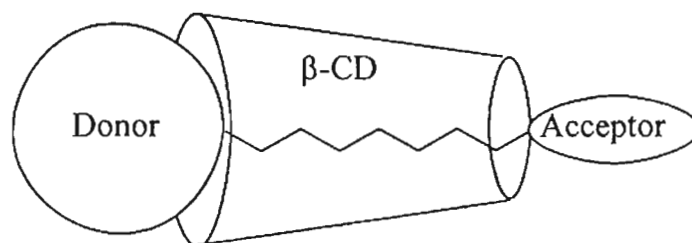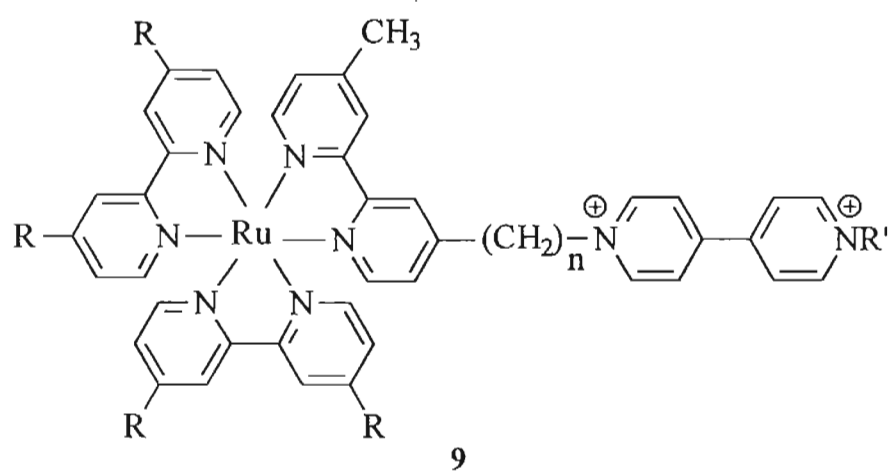
R = H, CH$_3$
R' = CH$_3$, CH$_2$CN
n = 1 - 5, 7, 8

Chart 3.4

In the third category we include systems in which donor and acceptor sites are separated by a protein fragment of varying length. Oligoprolines are the most commonly used bridging units.[31-35] Schanze and Sauer, for example, studied PET processes in Ru(bpy)$_3^{2+}$/oligo-L-proline/p-benzoquinone systems and found that the rate constant decreased from 1 x 10^9 s^{-1} to 4 x 10^5 s^{-1} as the number of oligoproline bridging units increased from 1 to 5.[33,34] Isied *et al.* studied PET among metal complexes linked *via* oligoproline units, where the donor-acceptor distance varied in the range 1.4 to 29.3 Å.[35] All these systems have been designed to gain a better understanding of the electron transfer pathways in proteins. Results obtained from these studies suggest that proteins are not good electrical conductors. Even in the most efficient protein systems the electron transfer rate

constant dropped by four orders of magnitude as the distance between the donor and acceptor increased by 10 Å.

The fourth category deals with electron transfer studies in DNA. DNA's double helix ladder connected by base pair rungs creates a neat stack of π electrons. One can then ask whether the DNA double helix facilitates charge transfer over long distances and whether the base-pair stack can act as a conduit for chemistry at a distance. In order to answer these questions, a large number of experiments have been carried out, but the matter appears highly controversial at present.[36-44]

Results obtained by Barton and co-workers suggested that DNA can act as a 'molecular wire' and promote extremely rapid electron transfer. They have attached intercalating metallocomplexes to either end of a DNA duplex. At one end a luminescing ruthenium complex acted as an electron donor and at the other end a rhodium complex acted as the acceptor.[36,37] From the quenching of the luminescence of the ruthenium complex it appeared that despite a 40 Å distance between the donor and the acceptor very rapid electron transfer occurred. A β value of < 0.2 Å^{-1} was obtained in this study. Studies by Meade and others, on the other hand, suggested that DNA acted as an insulator. Meade and co-workers have measured the rate of electron transfer through an eight base strand of DNA and concluded that DNA acted much like proteins.[39] Theoretical studies by Beratan *et al.* suggest that the energy gaps between the donors and DNA bridges are too large to facilitate fast distance independent electron migration.[40] Thus the

distance dependence of electron transfer in DNA is a very controversial and very active research area.

It is very clear from the above discussion that a vast amount of work has been carried out to understand the distance dependence of electron transfer reactions. However, distance dependence of electron transfer in hydrogen-bonded donor-acceptor systems has not been addressed so far. Electron transfer reactions involving donors and acceptors held together by hydrogen bonding interactions are common in biological systems. The 'pathway model' for biological electron transport is based on the assumption that covalent bonds, hydrogen bonds, ionic contacts, van der Waals contacts etc. modulate the electronic coupling between the donor and acceptor.[45-53] Thus a study of the distance dependence of electron transfer in hydrogen-bonded donor-acceptor systems is also important and in this chapter we describe such a study. There are additional reasons to undertake the distance dependence study described in this chapter. Most of the distance dependence studies described earlier in this chapter pertain to the normal region. Theoretical calculations of electron transfer rate constants as a function of both driving force and distance showed that in the normal region the rates are strongly distance dependent while in the inverted region it should depend only very weakly on distance (vide infra).[54-58] Despite its great importance and significance, especially in the design of supramolecular devices based on PET, distance dependence of electron transfer in the inverted region has not been studied in detail.[29] This we believe is attributed to the fact that there is a general absence of

systems in the inverted region that can be studied by fluorescence quenching methods. During the course of our studies we have observed that pyreneacetic acid/4-nitrophenylacetic acid and pyreneacetic acid/2,4-dinitrophenylacetic acid hydrogen-bonded donor-acceptor systems belonged to the inverted region and electron transfer in these systems can be studied by fluorescence quenching techniques (see Chapter 2). This observation has prompted us to undertake a study that will address the distance dependence of electron transfer in the inverted region. While discussing the reasons for the absence of inverted region in bimolecular PET reactions in Chapter 2, we have briefly touched upon the work of Rau and co-workers. They suggested that inverted region is not observed in bimolecular PET reactions because of the peculiar distance dependence of electron transfer in the inverted region.[59] We thought that this suggestion can also be examined by undertaking a study of distance dependence in the inverted region. With these objectives in mind a study of the distance dependence of electron transfer in hydrogen-bonded systems belonging to the normal and inverted region was undertaken and the results are presented in this chapter.

For the distance dependence studies in hydrogen-bonded systems we have assembled the donors and acceptors across a hydrogen-bonded carboxylic acid interface as shown in Scheme 3.2. The distance between the donor and acceptor was changed by changing the values of 'm' and 'n'. In hydrogen-bonded systems of this type, where the CH_2 groups are absent, the edge-to-edge distance between the donor and acceptor is 6.9 Å.[60,61]
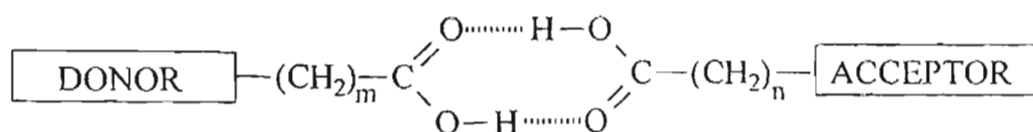
Scheme 3.2

In accordance with literature practice, we assumed that the separation distance increases by 1.27 Å for every CH_2 group.[29] Thus the edge-to-edge distance between the donors and acceptors in our systems can be calculated using the following equation

$$d = [6.9 + (m + n) \times 1.27] \text{ Å} \tag{3.2}$$

It should be noted that the centre-to-centre distance d_c will be ~ 2.5 Å larger than the edge-to-edge distance for the systems under study. Although the methylene chain is flexible, for small values of 'm' and 'n' we expect the complex to assume near linear configurations.

Structures of the molecules used in this study are shown in Chart 3.5. Numbers shown in the brackets along with the structures indicate the number of CH_2 groups in them. Pyrene-1-acetic acid (**PA(1)**) and its homologues, namely, pyrene-1-propanoic acid (**PA(2)**) and pyrene-1-butanoic acid (**PA(3)**) were used as probes. We have seen in Chapter 2 that, in the pyreneacetic acid/4-dimethylamino-phenylacetic acid (**PA(1)/10(1)**) system, the pyrene moiety acts as the acceptor and dimethylaniline unit acts as the donor, and this system falls in the normal region. So, for distance dependence studies in the normal region we have used different combinations of **PA(1-3)/10(1-3)** systems. (m + n) values can be

PROBES
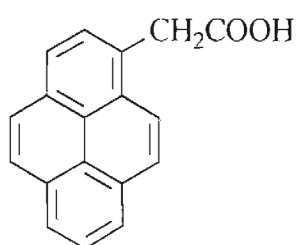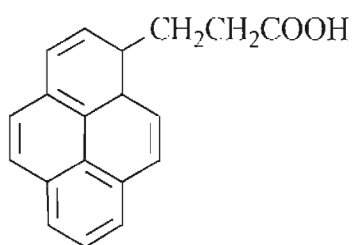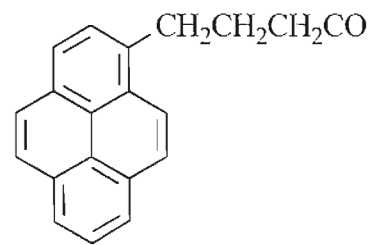
PA(1)   **PA**(2)   **PA**(3)

QUENCHERS
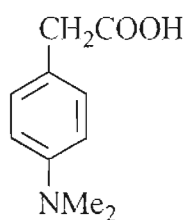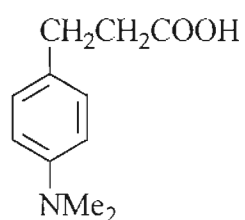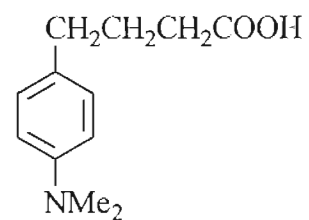
10(1)   **10**(2)   **10**(3)
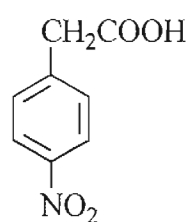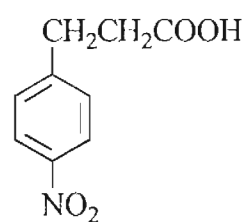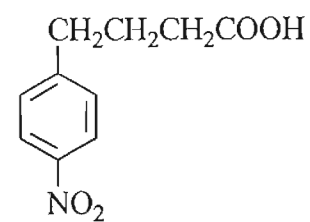
11(1)   **11**(2)   **11**(3)

Chart 3.5

varied from 2 to 6 with these combinations. This corresponds to a change of the centre-to-centre distance from 12 to 17 Å. Similarly it was shown in Chapter 2 that the pyreneacetic acid/4-nitrophenylacetic acid (**PA(1)/11(1)**) system falls in the inverted region (pyrene chromophore is the donor and nitrophenyl group is the acceptor in this case). So for the distance dependence studies in the inverted region we have used combinations of **PA(1-3)/11(1-3)** systems, which allowed us to vary the donor-acceptor distance, d_c in the range 12 - 17 Å.

A major difficulty we have encountered in these studies is the weakening of the hydrogen bond association with increase in chain length. For the **PA(1-3)/10(1-3)** systems in dichloromethane solution, the short lifetime component of the decay, which can be taken as the signature of the hydrogen-bonded complex, could not be observed when $(m + n) > 5$. For the **PA(1-3)/11(1-3)** systems, bimolecular decays could not be observed for $(m + n) > 3$ in dichloromethane. However, biexponential decays could be observed for this systems in toluene solution for $(m + n) \leq 6$. Thus, in this chapter we report electron transfer studies in the **PA(1-3)/10(1-3)** systems in dichloromethane solution for $(m + n) \leq 5$ and in **PA(1-3)/11(1-3)** systems in toluene solution for $(m + n) \leq 6$.

3.3. Results

3.3.1. Photophysical and redox properties of probes and quenchers

Absorption and emission spectra of **PA**(3) in dichloromethane are given in Figure 3.1. The spectra are almost identical to those of **PA**(1) reported in Chapter 2 of this thesis. The fluorescence lifetimes of **PA**(1-3) were measured in two solvents and the values obtained are presented in Table 3.1. Oxidation and reduction potentials of **PA**(1-3) in acetonitrile were measured and these values are also presented in Table 3.1. It can be noticed from the table that the photophysical and redox properties of the pyrene chromophore is unaffected by the hydrogen bonding appendages present in **PA**(1-3).
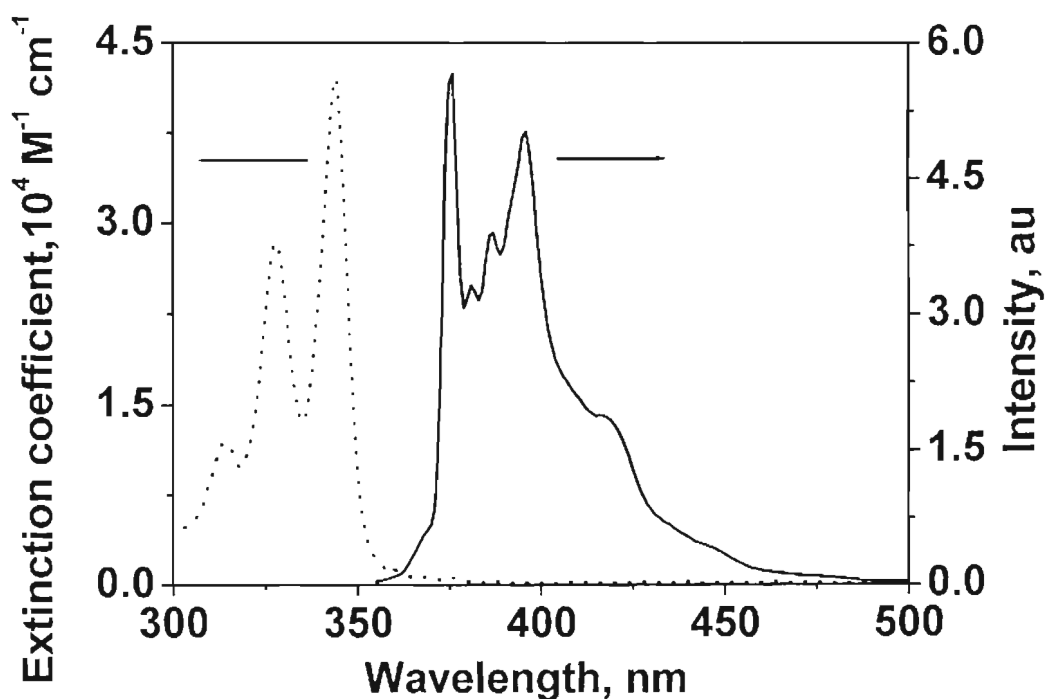
Figure 3.1. Absorption (dotted line) and emission spectra (solid line) of PA(3) in dichloromethane. For emission spectrum, excitation was at 345 nm.

Photophysical properties of the quenchers have no relevance to our studies. It is however, necessary to obtain the oxidation potentials of **10**(1-3) and reduction potentials of **11**(1-3). These were obtained in acetonitrile solution using cyclic voltammetry and the values are presented in Table 3.1. Here again, it can be noted that the redox potentials are not at all influenced by the length of the alkyl chain. Electron transfer rate constants for the various hydrogen-bonded systems were obtained by fluorescence lifetime quenching experiments. In the absence of the quenchers, fluorescence decays of the probes were exponential from which the intrinsic lifetimes (τ_0) were obtained.

Table 3.1. The fluorescence lifetimes (τ_0) of PA and redox potentials (E_{ox} and E_{red} *vs.* SCE) of PA, 10 and 11.

Chromophore	τ_0 ns (dichloromethane)	τ_0 ns (toluene)	E_{ox} V	E_{red} V
PA(1)	100 ± 10	150 ± 5	1.08	-2.12
PA(2)	90 ± 12	130 ± 5	1.10	-2.18
PA(3)	85 ± 10	130 ± 7	1.12	-2.13
10(1)	-	-	0.85	-
10(2)	-	-	0.98	-
10(3)			0.99	
11(1)	-	-	-	-1.23
11(2)	-	-	-	-1.17
11(3)	-	-	-	-1.17

In the presence of a quencher carboxylic acid, the fluorescence decays become biexponential and can be described by

$$I_{(t)} = \chi_{(P-Q)} \exp(-t/\tau_1) + \chi_{(P)} \exp(-t/\tau_2)$$ (3.3)

Where $\chi_{(P-Q)}$ is the fraction present as hydrogen-bonded complex and $\chi_{(P)}$ is the fraction of free probe molecules. τ_1 and τ_2 are the two lifetime components. The electron transfer rate constant with the hydrogen-bonded complex can be obtained from equation 3.4.

$$k_{et} = 1/\tau_1 - 1/\tau_0$$ (3.4)

3.3.2. Lifetime quenching studies in PA(1-3)/10(1-3) systems

PA/10 system falls in the normal region and as mentioned previously these systems were studied for (m + n) = 2 - 5 in dichloromethane solution. For (m + n) = 2, m = 1 and n = 1, but for other values of (m + n) we can use different combinations. For example, to get (m + n) = 3 we can either use the **PA(1)/10(2)** system or **PA(2)/10(1)** system. We have in fact studied all the possible combinations and compared the values.

For all the **PA(1-3)** systems, fluorescence decay profiles were recorded in the absence and presence of different combinations of **10(1-3)**. Representative examples of decay profiles are given in Figures 3.2 - 3.5. For all the cases studied, decays were analysed using equation 3.3 to obtain values of τ_1, τ_2, $\chi_{(P-Q)}$ and $\chi_{(P)}$. These values along with the χ^2 values for the fits are given in Tables 3.2 - 3.9.
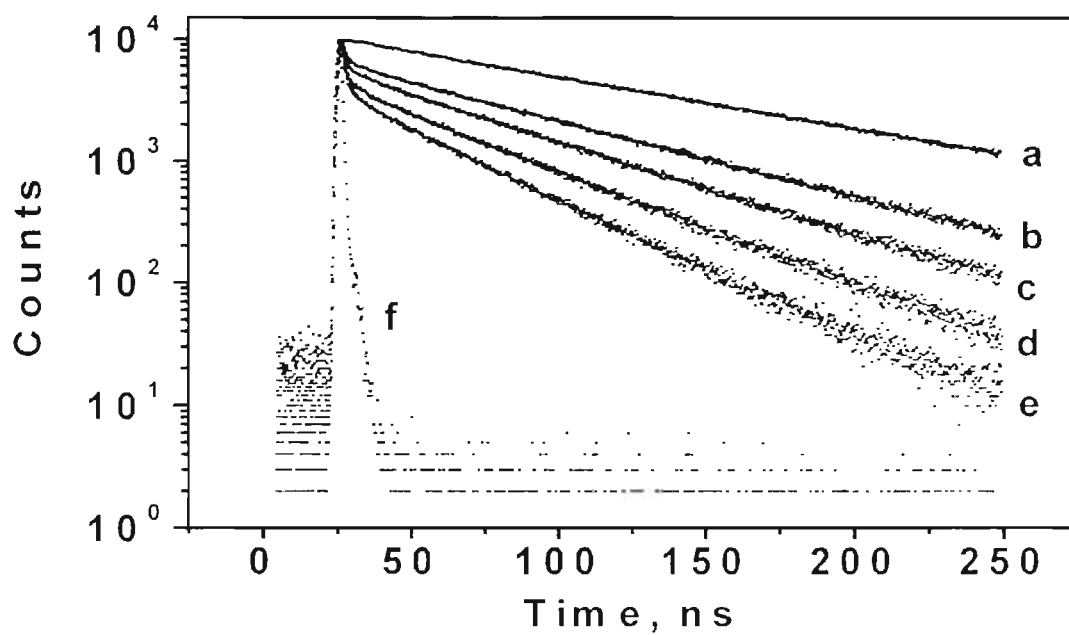
Figure 3.2. The fluorescence decay profiles of PA(1) in the absence (a) and in presence of (b - e) 10(1) (1 - 4 mM). (f) is the lamp profile.
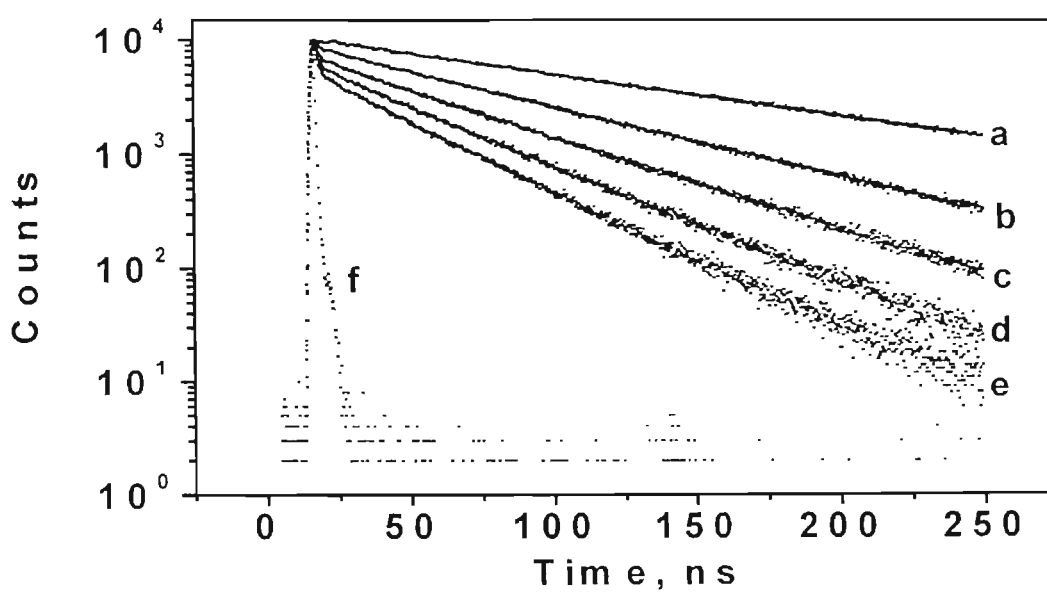
Figure 3.3. The fluorescence decay profiles of PA(1) in the absence (a) and in presence of (b - e) 10(2) (1 - 4 mM). (f) is the lamp profile.

Figure 3.4. The fluorescence decay profiles of PA(2) in the absence (a) and in presence of (b - e) 10(2) (1 - 4 mM). (f) is the lamp profile.

Figure 3.5. The fluorescence decay profiles of PA(3) in presence of (a - d) 10(2) (1 - 4 mM). (e) is the lamp profile.

Table 3.2. Fluorescence lifetimes (τ_1 and τ_2), fractional contributions (χ_{P-Q} and χ_P) and χ^2 values obtained for the fluorescence quenching of PA(1) by 10(1). [PA(1)] was 1 x 10^{-5} M.

[10(1)], M	τ_1, ns	$\chi_{(P-Q)}$, %	τ_2, ns	$\chi_{(P)}$, %	χ^2
0	-	-	101.0	100.00	1.0
1 x 10^{-3}	1.10	08.51	67.0	91.49	1.2
2 x 10^{-3}	1.10	36.36	54.0	63.64	1.1
3 x 10^{-3}	1.10	44.73	44.0	55.27	1.1
4 x 10^{-3}	0.90	80.77	35.3	19.23	1.2

Table 3.3. Fluorescence lifetimes (τ_1 and τ_2), fractional contributions (χ_{P-Q} and χ_P) and χ^2 values obtained for the fluorescence quenching of PA(1) by 10(2). [PA(1)] was 1 x 10^{-5} M.

[10(2)], M	τ_1, ns	$\chi_{(P-Q)}$, %	τ_2, ns	$\chi_{(P)}$, %	χ^2
0	-	-	105	100	1.2
1 x 10^{-3}	1.90	5.00	94.05	95.00	1.1
2 x 10^{-3}	1.90	24.32	72.20	75.68	1.2
3 x 10^{-3}	1.85	44.65	47.55	55.35	1.1
4 x 10^{-3}	1.80	65.72	28.02	34.28	1.3

Table 3.4. Fluorescence lifetimes (τ_1 and τ_2), fractional contributions (χ_{P-Q} and χ_P) and χ^2 values obtained for the fluorescence quenching of PA(2) by 10(1). [PA(2)] was 1 x 10^{-5} M.

[10(1)], M	τ_1, ns	$\chi_{(P-Q)}$, %	τ_2, ns	$\chi_{(P)}$, %	χ^2
0	-	-	98	100	1.1
1 x 10^{-3}	1.90	5.30	92.50	94.70	1.1
2 x 10^{-3}	1.86	23.50	75.06	76.50	1.0
3 x 10^{-3}	1.92	38.32	52.89	61.68	1.2
4 x 10^{-3}	1.92	50.20	30.15	49.80	1.1

Table 3.5. Fluorescence lifetimes (τ_1 and τ_2), fractional contributions (χ_{P-Q} and χ_P) and χ^2 values obtained for the fluorescence quenching of PA(1) by 10(3). [PA(1)] was 1 x 10^{-5} M.

[10(3)], M	τ_1, ns	$\chi_{(P-Q)}$, %	τ_2, ns	$\chi_{(P)}$, %	χ^2
0	-	-	103	100	1.1
1 x 10^{-3}	5.40	1.50	82.15	98.50	1.1
2 x 10^{-3}	5.40	6.50	65.05	93.50	1.1
3 x 10^{-3}	5.38	13.65	42.98	86.35	1.2
4 x 10^{-3}	5.39	20.16	25.63	79.84	1.2

Table 3.6. Fluorescence lifetimes (τ_1 and τ_2), fractional contributions (χ_{P-Q} and χ_P) and χ^2 values obtained for the fluorescence quenching of PA(2) by 10(2). [PA(2)] was 1×10^{-5} M.

[10(2)], M	τ_1, ns	$\chi_{(P-Q)}$, %	τ_2, ns	$\chi_{(P)}$, %	χ^2
0	-	-	95.00	100	1.1
1×10^{-3}	5.8	3.2	82.06	96.8	1.2
2×10^{-3}	5.7	10.8	62.40	89.8	1.1
3×10^{-3}	5.7	22.5	42.05	77.5	1.2
4×10^{-3}	5.8	30.2	23.8	69.8	1.1

Table 3.7. Fluorescence lifetimes (τ_1 and τ_2), fractional contributions (χ_{P-Q} and χ_P) and χ^2 values obtained for the fluorescence quenching of PA(3) by 10(1). [PA(3)] was 1×10^{-5} M.

[10(1)], M	τ_1, ns	$\chi_{(P-Q)}$, %	τ_2, ns	$\chi_{(P)}$, %	χ^2
0	-	-	82	100	1.1
1×10^{-3}	5.60	1.60	62.35	98.40	1.1
2×10^{-3}	5.57	7.90	49.90	92.10	1.2
3×10^{-3}	5.60	15.35	35.63	84.65	1.2
4×10^{-3}	5.60	22.02	20.80	77.98	1.1

Table 3.8. Fluorescence lifetimes (τ_1 and τ_2), fractional contributions (χ_{P-Q} and χ_P) and χ^2 values obtained for the fluorescence quenching of PA(2) by 10(3). [PA(2)] was 1 x 10^{-5} M.

[10(3)], M	τ_1, ns	$\chi_{(P-Q)}$, %	τ_2, ns	$\chi_{(P)}$, %	χ^2
0	-	-	90	100	1.1
1 x 10^{-3}	10.00	2.8	82.3	97.2	1.2
2 x 10^{-3}	10.65	8.2	67.9	91.8	1.2
3 x 10^{-3}	10.65	15.0	52.3	85.0	1.2
4 x 10^{-3}	10.63	20.2	44.0	79.8	1.1

Table 3.9. Fluorescence lifetimes (τ_1 and τ_2), fractional contributions (χ_{P-Q} and χ_P) and χ^2 values obtained for the fluorescence quenching of PA(3) by 10(2). [PA(3)] was 1 x 10^{-5} M.

[10(2)], M	τ_1, ns	$\chi_{(P-Q)}$, %	τ_2, ns	$\chi_{(P)}$, %	χ^2
0	-	-	90	100	1.1
1 x 10^{-3}	10.60	2.29	76.30	97.91	1.1
2 x 10^{-3}	10.60	6.50	59.82	34.50	1.2
3 x 10^{-3}	10.60	13.87	48.37	86.13	1.1
4 x 10^{-3}	10.65	19.30	32.06	80.70	1.2

Analysis of the various parameters in Tables 3.2 - 3.9 leads to the following observations: (1) For a given system, the short lifetime component τ_1 remained independent of quencher concentration. This is in accordance with observations made by others for hydrogen-bonded donor-acceptor systems and confirmed that τ_1 arises due to electron transfer quenching within the hydrogen-bonded complex.[62-65] (2) Systems for which same (m + n) values can be obtained using different combinations of m and n, τ_1 values obtained were similar. This indicates that the rate of electron transfer within the complex depends only on the values of (m + n) and not on individual values of m and n. (3) At the same quencher concentration $\chi_{(P-Q)}$ values tend to decrease as (m + n) increases. This indicates weakening of the hydrogen bonds as the flexibility of the systems increases. The association constant can be obtained from a plot of $\chi_{(P-Q)}/\chi_{(P)}$ *vs.* [Quencher]. We have found out from such plots that the association constant for the **PA(1)/10(3)** system is approximately 3 times lower than that of **PA(1)/10(1)** system. This aspect, in fact, is very clear from the decay profiles. For example, the biexponential nature of the decay is very obvious in the **PA(1)/10(1)** system (Figure 3.2) even at low concentration of **10(1)**, but is not very observable for the **PA(3)/10(2)** system (Figure 3.5) even at the highest concentration of **10(2)**. (4) The τ_1 values increase with increase in distance (*ie.* increase in (m + n)). This suggests that the rate of electron transfer within the hydrogen-bonded assembly decrease with increase in separation of donor and acceptor. The electron transfer

rate constants k_{et} for the various systems were calculated using equation 3.4 and the results are presented later in Table 3.18.

χ^2 values presented in Tables 3.2 - 3.9 are all $\leq$ 1.3. This indicated that the fits are good in all cases. We have recorded the fluorescence decay profiles of PA(3)/10(3) system also. Fitting the decays in this case to biexponential functions yielded χ^2 > 1.4. This is attributed to the absence of hydrogen bond formation in this case. Because of this, the results obtained for this system are not presented here. It should also be mentioned here that, in the distance dependence studies of electron transfer in hydrogen-bonded systems reported in this chapter, we are interested only in the τ_1 values. τ_2, $\chi_{(P-Q)}$ and $\chi_{(P)}$ values are not used for any quantitative purposes.

3.3.3. Lifetime quenching studies in PA(1-3)/11(1-3) systems

For this system in dichloromethane solution good biexponential decay profiles were observed only for (m + n) $\leq$ 3. Hence we studied the system in toluene where biexponential decays could be observed up to (m + n) = 6. In order to determine the electron transfer rate constants, fluorescence decay profiles of PA(1-3) were recorded in toluene in the absence and presence of different concentration of 11(1-3). In the case of systems for which (m + n) > 2, different combinations of PA(1-3)/11(1-3) were studied. Representative examples of decay profiles for these systems are given in Figures 3.6 - 3.9. For all the cases studied, decays were analysed using equation 3.3. The values are given in Table 3.10 - 3.17.
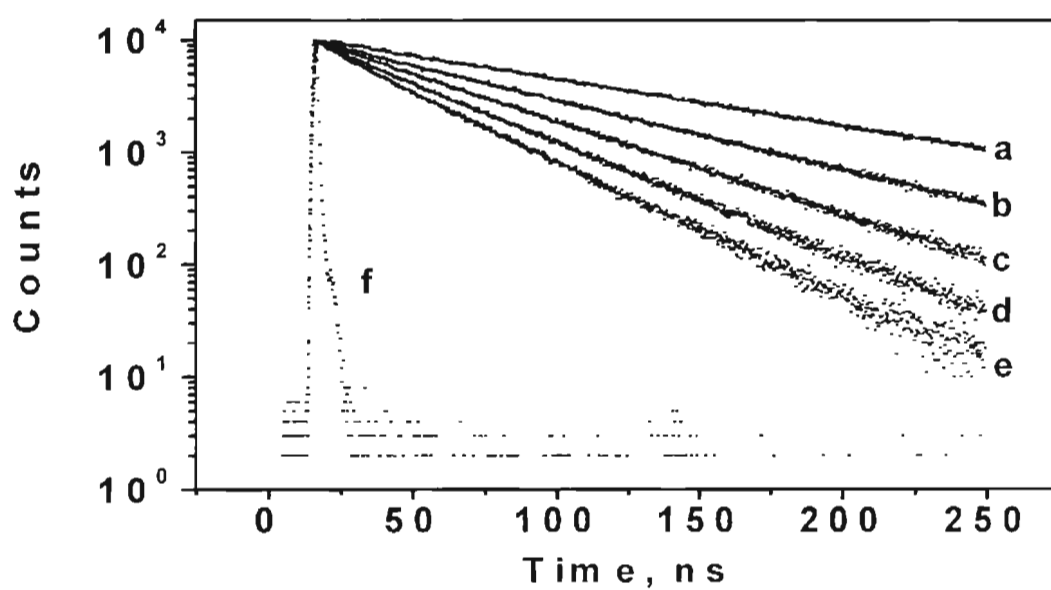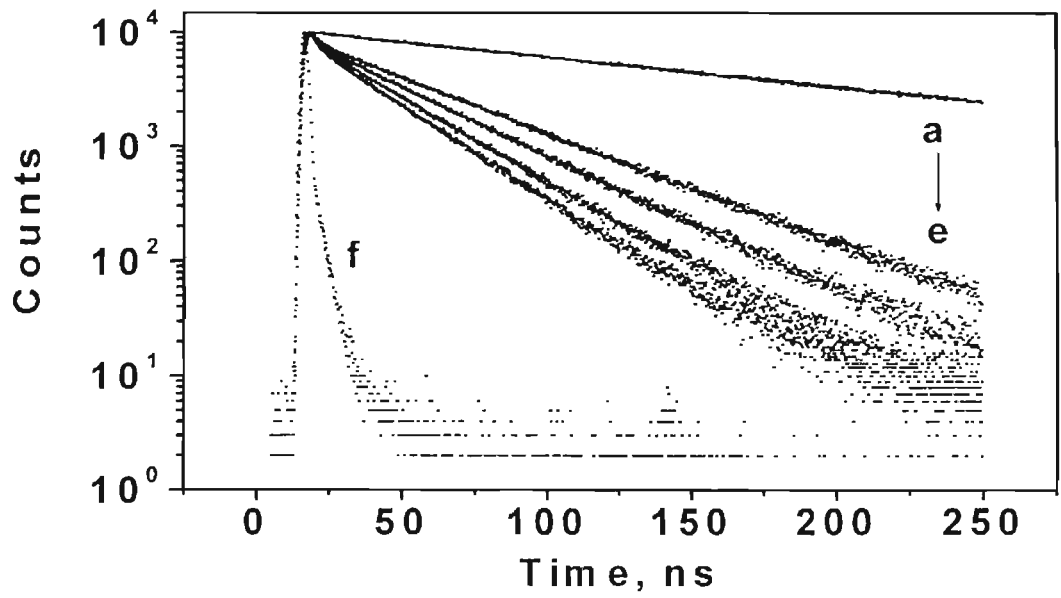
Figure 3.6. The fluorescence decay profiles of PA(1) (a) in the absence; (b - e) in presence of 11(2) (1 - 4 mM); (f) is the lamp profile.
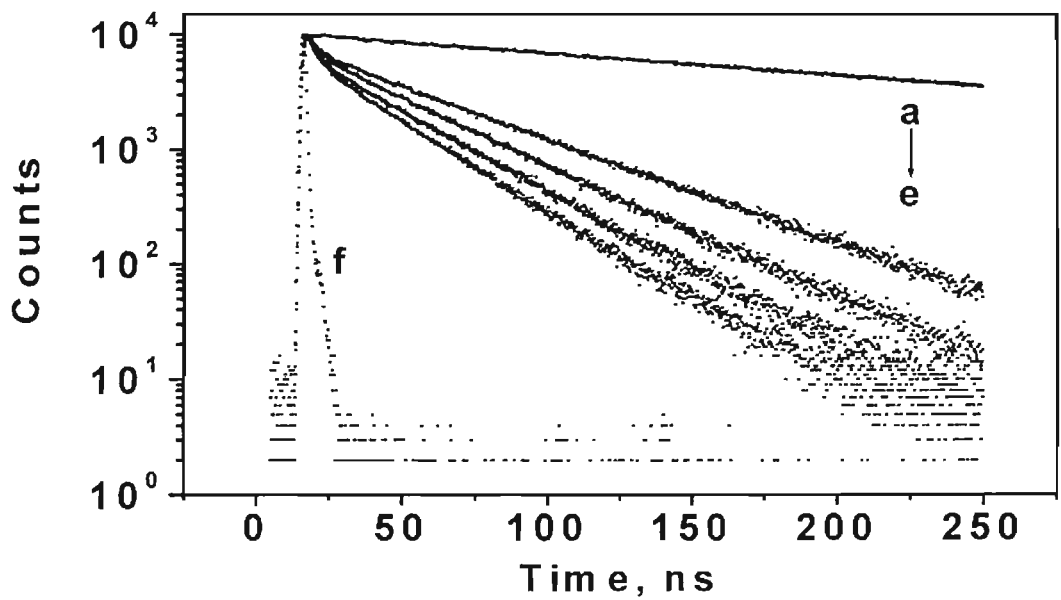
Figure 3.7. The fluorescence decay profiles of PA(2) (a) in the absence; (b - e) in presence of 11(2) (1 - 4 mM); (f) is the lamp profile.
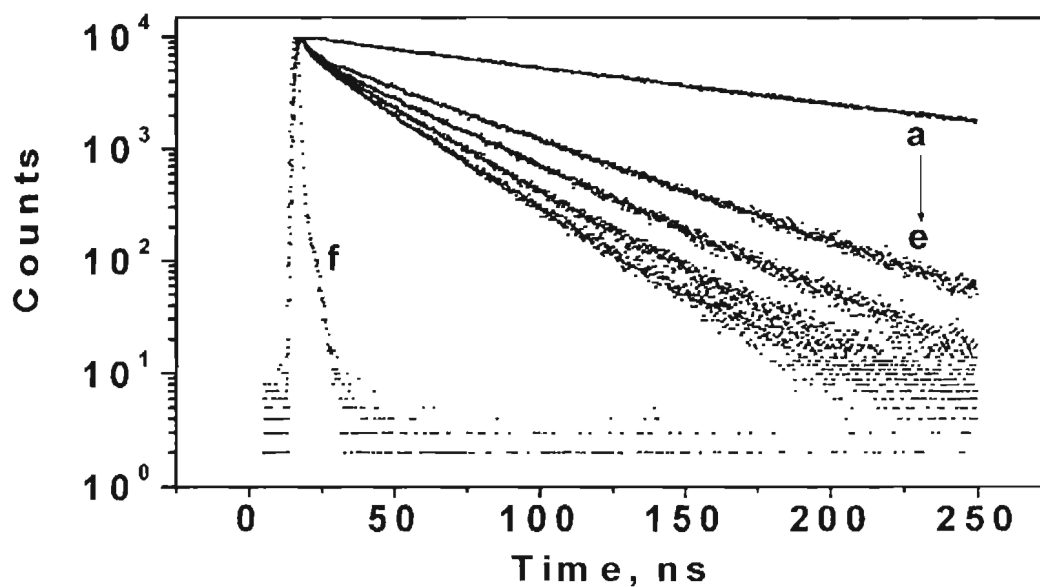
Figure 3.8. The fluorescence decay profiles of PA(2) (a) in the absence; (b - e) in presence of 11(3) (1 - 4 mM); (f) is the lamp profile.
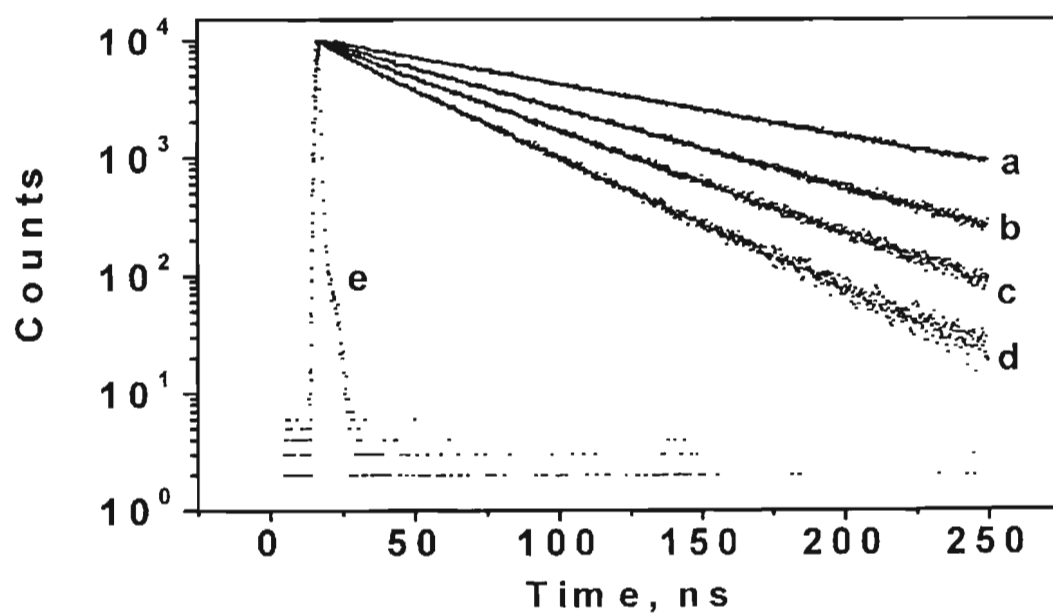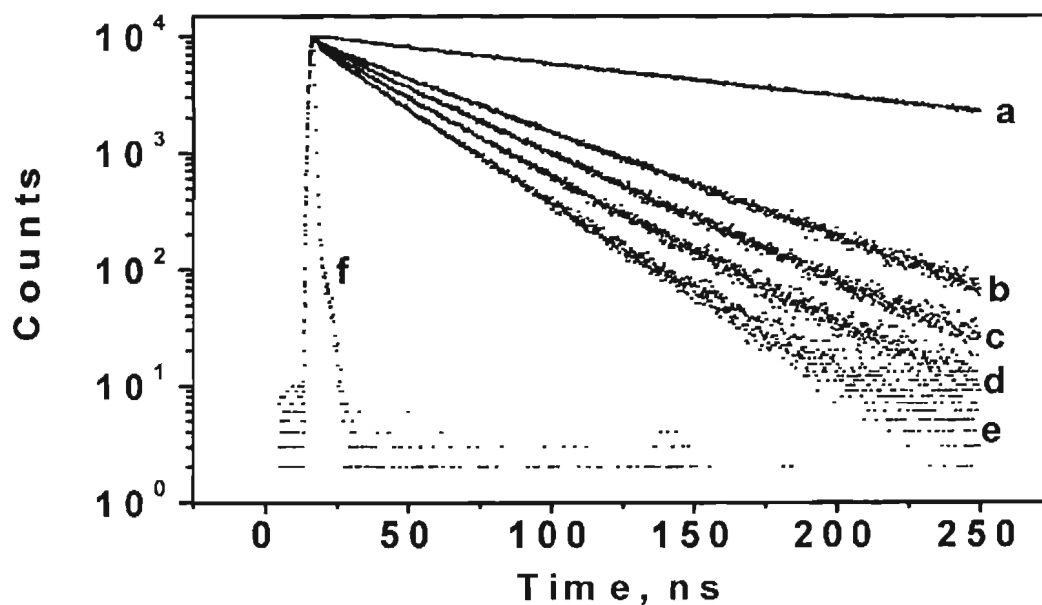

Figure 3.9. The fluorescence decay profiles of PA(3) (a) in the absence; (b - e) in presence of 11(3) (1 - 4 mM); (f) is the lamp profile.

Table 3.10. Fluorescence lifetimes (τ_1 and τ_2), fractional contributions (χ_{P-Q} and χ_P) and χ^2 values obtained for the fluorescence quenching of PA(1) by 11(2). [PA(1)] was 1 x 10^{-5} M.

[11(2)], M	τ_1, ns	$\chi_{(P-Q)}$, %	τ_2, ns	$\chi_{(P)}$, %	χ^2
0	-	-	153	100	1.1
1 x 10^{-3}	2.2	3.88	41.92	96.12	1.1
2 x 10^{-3}	2.2	5.07	34.65	94.93	1.0
3 x 10^{-3}	2.2	7.03	29.17	92.97	1.1
4 x 10^{-3}	2.0	8.17	25.09	91.83	1.1

Table 3.11. Fluorescence lifetimes (τ_1 and τ_2), fractional contributions (χ_{P-Q} and χ_P) and χ^2 values obtained for the fluorescence quenching of PA(2) by 11(1). [PA(2)] was 1 x 10^{-5} M.

[11(1)], M	τ_1, ns	$\chi_{(P-Q)}$, %	τ_2, ns	$\chi_{(P)}$, %	χ^2
0	-	-	130	100	1.1
1 x 10^{-3}	2.13	3.50	53.65	96.50	1.1
2 x 10^{-3}	2.15	4.75	32.01	95.25	1.0
3 x 10^{-3}	2.15	6.92	25.65	93.08	1.1
4 x 10^{-3}	2.10	8.00	19.80	92.00	1.2

Table 3.12. Fluorescence lifetimes (τ_1 and τ_2), fractional contributions (χ_{P-Q} and χ_P) and χ^2 values obtained for the fluorescence quenching of PA(1) by 11(3). [PA(1)] was 1×10^{-5} M.

[11(3)], M	τ_1, ns	$\chi_{(P-Q)}$, %	τ_2, ns	$\chi_{(P)}$, %	χ^2
0	-	-	150	100	1.1
1×10^{-3}	2.95	3.01	56.03	96.99	1.1
2×10^{-3}	2.93	5.62	45.23	94.38	1.0
3×10^{-3}	2.95	6.92	36.93	93.08	1.2
4×10^{-3}	2.90	7.01	21.06	92.99	1.1

Table 3.13. Fluorescence lifetimes (τ_1 and τ_2), fractional contributions (χ_{P-Q} and χ_P) and χ^2 values obtained for the fluorescence quenching of PA(2) by 11(2). [PA(2)] was 1×10^{-5} M.

[11(2)], M	τ_1, ns	$\chi_{(P-Q)}$, %	τ_2, ns	$\chi_{(P)}$, %	χ^2
0	-	-	125.0	100	1.2
1×10^{-3}	3.0	3.52	46.5	96.48	1.1
2×10^{-3}	2.9	4.55	36.0	95.45	1.1
3×10^{-3}	2.9	6.89	30.5	93.11	1.2
4×10^{-3}	2.9	8.03	26.5	91.97	1.1

Table 3.14. Fluorescence lifetimes (τ_1 and τ_2), fractional contributions (χ_{P-Q} and χ_P) and χ^2 values obtained for the fluorescence quenching of PA(3) by 11(1). [PA(3)] was 1×10^{-5} M.

[11(1)], M	τ_1, ns	$\chi_{(P-Q)}$, %	τ_2, ns	$\chi_{(P)}$, %	χ^2
0	-	-	126	100	1.1
1×10^{-3}	2.90	3.00	58.01	97.00	1.2
2×10^{-3}	2.92	4.08	44.32	95.92	1.2
3×10^{-3}	2.92	5.32	35.01	94.68	1.1
4×10^{-3}	2.93	6.85	22.03	93.15	1.2

Table 3.15. Fluorescence lifetimes (τ_1 and τ_2), fractional contributions (χ_{P-Q} and χ_P) and χ^2 values obtained for the fluorescence quenching of PA(2) by 11(3). [PA(2)] was 1×10^{-5} M.

[11(2)], M	τ_1, ns	$\chi_{(P-Q)}$, %	τ_2, ns	$\chi_{(P)}$, %	χ^2
0	-	-	125	100	1.1
1×10^{-3}	3.2	2.75	50.01	97.25	1.2
2×10^{-3}	3.2	3.99	36.92	96.01	1.1
3×10^{-3}	3.2	5.02	28.45	94.98	1.1
4×10^{-3}	2.9	6.25	25.44	93.75	1.1

Table 3.16. Fluorescence lifetimes (τ_1 and τ_2), fractional contributions (χ_{P-Q} and χ_P) and χ^2 values obtained for the fluorescence quenching of PA(3) by 11(2). [PA(3)] was 1 x 10^{-5} M.

[11(2)], M	τ_1, ns	$\chi_{(P-Q)}$, %	τ_2, ns	$\chi_{(P)}$, %	χ^2
0	-	-	130	100	1.0
1 x 10^{-3}	3.12	2.55	52.16	97.45	1.1
2 x 10^{-3}	3.10	3.90	43.12	96.10	1.2
3 x 10^{-3}	3.10	4.65	38.06	95.35	1.2
4 x 10^{-3}	3.10	6.32	26.05	93.68	1.0

Table 3.17. Fluorescence lifetimes (τ_1 and τ_2), fractional contributions (χ_{P-Q} and χ_P) and χ^2 values obtained for the fluorescence quenching of PA(3) by 11(3). [PA(3)] was 1 x 10^{-5} M.

[11(3)], M	τ_1, ns	$\chi_{(P-Q)}$, %	τ_2, ns	$\chi_{(P)}$, %	χ^2
0	-	-	124	100	1.2
1 x 10^{-3}	3.5	2.32	55.15	97.68	1.1
2 x 10^{-3}	3.4	3.55	48.10	96.45	1.1
3 x 10^{-3}	3.4	4.62	30.12	95.38	1.2
4 x 10^{-3}	3.4	5.06	27.25	94.94	1.1

As seen in the tables, χ^2 values obtained are ≤ 1.2, indicating that the fits are good in all cases. A comparison of the data presented in Tables 3.10 - 3.17 to those obtained for the **PA(1-3)/10(1-3)** systems indicated two major differences: (1) τ_1 values for the **PA/11** systems showed only marginal variation with distance and (2) $\chi_{(P-Q)}$ values also did not change appreciably with distance. The latter aspect indicated that in toluene solution the association constant is not influenced by the flexibility of the systems. In this case also we are interested only in the τ_1 values and the other three parameters are not used for any quantitative purposes.

3.3.4. Distance dependence of electron transfer in PA/10 and PA/11 systems

In order to study the distance dependence of electron transfer in hydrogen-bonded donor-acceptor systems in the normal and inverted regions, we have selected the **PA/10** and **PA/11** systems. The distance between the redox sites was varied by introducing CH_2 groups between the chromophores and the hydrogen bonding appendage. The rate constants for electron transfer were extracted from the fluorescence decays using equations 3.3 and 3.4. The rate constants thus obtained for the two systems are presented in Table 3.18 along with the calculated donor-acceptor distance.

Table 3.18. Dependence of electron transfer rate constant (k_{et}) on distance (d_c) for PA/10 and PA/11 systems.

Chromophore	m+ n	d_c, Å	k_{et}, 10^8 s^{-1}
PA/10	2	11.94	9.0 ± 0.18
	3	13.21	5.3 ± 0.19
	4	14.48	1.7 ± 0.07
	5	15.75	0.83 ± 0.03
PA/11	2	11.94	3.9 ± 0.10
	3	13.21	4.4 ± 0.17
	4	14.48	3.4 ± 0.13
	5	15.75	3.2 ± 0.15
	6	17.02	2.9 ± 0.12

For the **PA/10** system, which belonged to the normal region, the rate constant for electron transfer decreased from 9.0×10^8 s^{-1} to 8.3×10^7 s^{-1} as the centre-to-centre distance increased from 12 to 16 Å. For the **PA/11** system, which falls in the inverted region, a very different type of distance dependence was observed. In this case the rate constant showed a small initial increase followed by a small decrease. Our results thus suggested that, for a hydrogen-bonded system in the normal region rate constant decreased appreciably with distance, but for a hydrogen-bonded system in the inverted region, the rate constant showed only a

feeble dependence on distance. In the following section we try to analyse our results in the light of electron transfer theories.

3.4. Discussion

In this chapter we have carried out a study of the distance dependence of electron transfer reactions in hydrogen-bonded donor-acceptor systems. For this purpose we have assembled donor and acceptor moieties at the ends of a carboxylic acid dimer type hydrogen-bonded bridge and varied the distance by introducing CH_2 groups. The study has been undertaken for the following reasons: (1) Distance dependence of electron transfer in hydrogen-bonded systems involving small-molecule donor-acceptor systems was not studied earlier; (2) these systems provide an opportunity to study the distance dependence of electron transfer in the inverted region by fluorescence methods and (3) it may throw some light into the suggestion that the inverted region can be masked by the distance dependence of rate constants in the inverted free energy regime. We are aware that the systems we are dealing with are flexible and several conformations of the molecules can be present in the medium. The centre-to-centre distances, $'d_c'$ presented in Table 3.18 were calculated assuming linear configurations and d_c will be somewhat smaller for other conformations. This may cast some doubts about the validity of our conclusions. Our intention, however, is only to compare the behaviours of the normal and inverted regions. We expect the same kind of flexibility and the same kind of conformations for the systems in the normal and

inverted regions. Because of this we believe that the flexibility of the molecules do not influence our conclusions very much. In the following section we try to build up the necessary theoretical background to understand the problem at hand. We will then use this information to analyse our results of the distance dependence studies.

According to the Marcus theory for non-adiabatic electron transfer, the rate constant for electron transfer is given by[66-71]

$$k_{et} = (2\pi/\hbar) \; H_{el}^2 \; (4\pi\lambda k_B T)^{-1/2} \; \exp \; [-(\lambda + \Delta G^\circ)^2/4\lambda k_B T] \qquad (3.5)$$

where, $\hbar$ is the Planck's constant divided by 2π, λ is the reorganization energy, k_B is the Boltzmann constant, T is the temperature and H_{el} is the coupling matrix element, λ is known as the reorganization energy and ΔG° is the free energy change associated with the reaction. In order to evaluate the effect of distance on $k_{et,}$ we need to understand the distance dependencies of each of the terms present in the Marcus equation.

Of the several terms present in equation 3.5, the terms that show a dependence on donor-acceptor distance are H_{el}, λ and ΔG°. The distance dependence of H_{el} is given by

$$H_{el}^2 = (H_{el}^0)^2 \; \exp \; [-\beta(d-d_0)] \qquad (3.6)$$

where H_{el}° is the coupling element at the contact distance d_0 and β was defined earlier in equation 3.1. The value of β depends on the nature and conductivity of the bridging unit. Equation 3.1 in fact arises from equation 3.6. Figure 3.10 shows

the expected variation of k_{et} with distance calculated using equation 3.1 for three

different values of β. Values of A = 1 x 10^{13} s^{-1} and d_0 = 7 Å were used for this

calculation. Notice that k_{et} decreases rapidly with distance when β is high (curve

c), but for a low value of β (curve a), the dependence of k_{et} on distance is very

shallow. Bridging units of very small β values are termed 'molecular wires'.
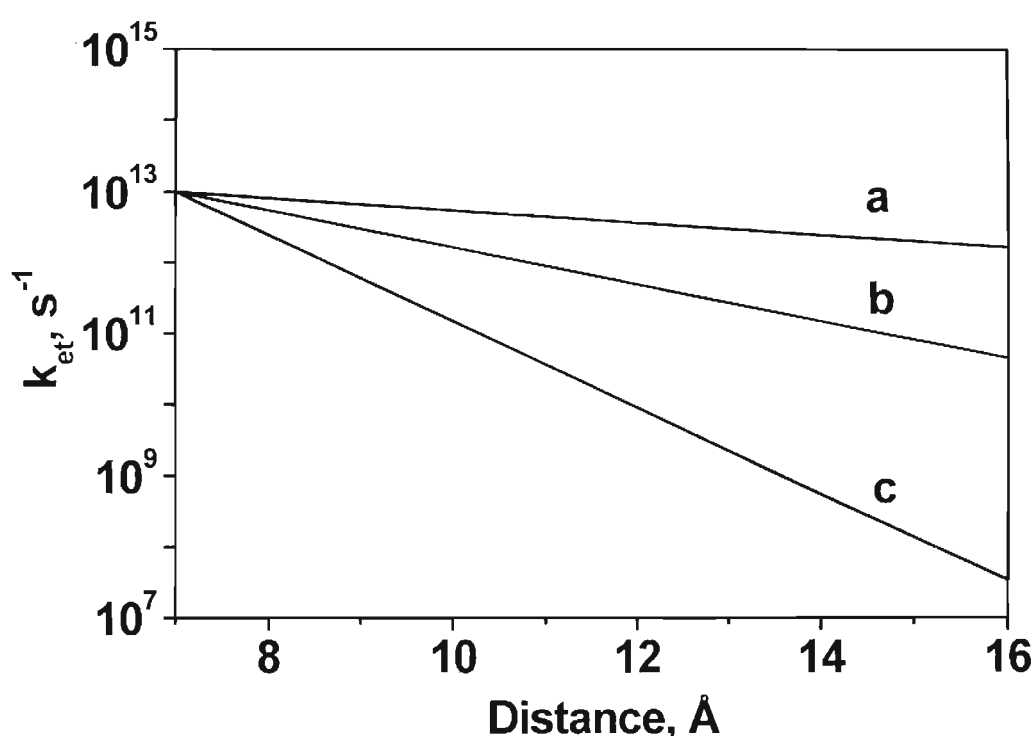
Figure 3.10. Dependence of k_{et} on distance, calculated using equation 3.1 for three different β values. (a) 0.2 (b) 0.6 and (c) 1.4 Å^{-1}.

The reorganization energy λ is the sum of the inner shell (λ_i) and outer shell

(λ_o) reorganization energies. λ_i is solvent and temperature independent. For rigid

aromatic molecules λ_i is small and a value of 0.2 eV is usually assumed.[75,76] λ_o is

given by[72,73]

$$\lambda_o = \Delta e^2 \left(\frac{1}{2r_D} + \frac{1}{2r_A} - \frac{1}{d_c} \right) \left(\frac{1}{\varepsilon_{op}} - \frac{1}{\varepsilon_s} \right) \qquad (3.7)$$

The value of λ_o thus depends on the radii of the donor (r_D) and acceptor (r_A), centre-to-centre distance (d_c) between the donor and acceptor and the optical (ε_{op}) and static (ε_s) dielectric constants of the solvent. In Figure 3.11 we have plotted calculated values of λ_o as a function of d_c in three different solvents (acetonitrile, dichloromethane and toluene) for $r_D = 6$ Å, $r_A = 4$ Å (curves a - c) and also for $r_D = 4$ Å and $r_A = 3$ Å (curves a' - c'). The following points are obvious from Figure 3.11. (1) For any donor-acceptor system, λ_o increases with solvent polarity (2) λ_o increases as the molecular size decreases (3) distance dependence of λ_o is significant in polar solvents, but is very insignificant in non-polar solvents.
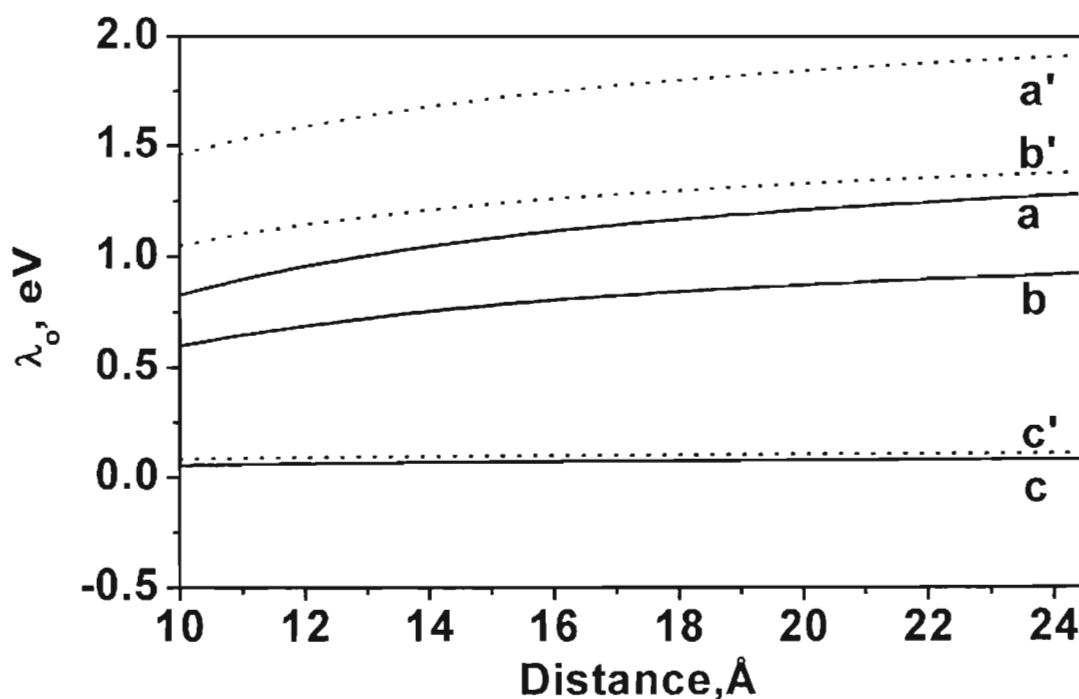
Figure 3.11. Variation of λ_o with distance for donor-acceptor system in (a,a') acetonitrile, (b,b') dichloromethane and (c,c') toluene. For (a-c), $r_D = 6$ Å and $r_A = 4$ Å, for (a'-c') $r_D = 4$ Å and $r_A = 3$ Å.

The free energy change of electron transfer, $\Delta G°$ is given by the Weller equation 3.8.[74]

$$\Delta G^0 = E_{ox} - E_{red} - E_{00} - \frac{e^2}{2}\left(\frac{1}{r_D} + \frac{1}{r_A}\right)\left(\frac{1}{37} - \frac{1}{\varepsilon}\right) - \frac{e^2}{\varepsilon\, d_c} \qquad (3.8.)$$

It can be noted from equation 3.8 that $\Delta G°$ also depends on the radii of the donor and acceptor, the centre-to-centre distance and dielectric properties of the solvent. In Figure 3.12 we have plotted the calculated distance dependence of $\Delta G°$ for the three solvents for $r_D = 6$ Å, $r_A = 4$ Å (curves a - c) and also for $r_D = 4$ Å and $r_A = 3$ Å (curves a' - c'). Values of $E_{0,0} = 3.6$ eV, $E_{ox} = 1.08$ V and $E_{red} = -1.25$ eV were used for the calculations and these values correspond to the pyrene-nitrobenzene donor-acceptor system. The following points can be noticed from Figure 3.12. (1) $\Delta G°$ values are larger (less negative) in smaller molecules; (2) $\Delta G°$ values are more negative for more polar solvents, and (3) distance dependence of $\Delta G°$ is very insignificant in polar solvents, but highly significant in non-polar solvents.

Let us now look at the distance dependencies of electron transfer reactions in the normal and inverted regions. First, let us consider electron transfer in a polar solvent such as acetonitrile. For this purpose we consider small molecule donor-acceptor systems ($r_D = 4$ Å, $r_A = 3$ Å) separated by saturated bridges ($\beta = 1.4$ Å^{-1}). We assume that $H_{el}° = 100$ cm^{-1} for this system at $d_o = 7$ Å. Our analysis has shown that H_{el} should decrease and λ_o should increase rapidly with distance for this system ($\Delta G°$ is relatively independent of distance in acetonitrile). The distance
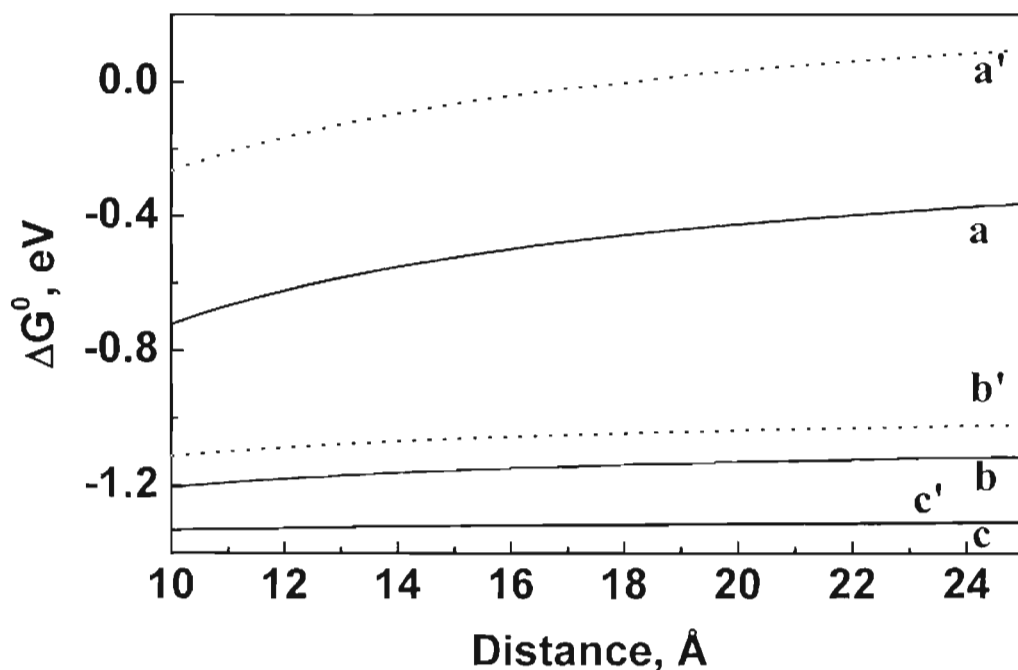
Figure 3.12. Dependence of ΔG° on distance calculated using equation (3.8) with $E_{ox} = 1.08$ V, $E_{red} = -1.25$ V, $E_{00} = 3.6$ eV for (a) acetonitrile, (b) dichloromethane and (c) toluene were $r_D = 6$ Å and $r_A = 4$ Å and for (a') acetonitrile, (b') dichloromethane and (c') toluene were $r_D = 4$ Å and $r_A = 3$ Å.

dependence of electron transfer rate constant can be calculated by substituting the distance dependent values of H_{el}, ΔG° and λ_o in equation 3.5. We have done such calculations for two different $(\Delta G^{\circ})_o$ values ($(\Delta G^{\circ})_o$ refers to ΔG° value at contact distance) and the results obtained are plotted in Figure 3.13. Curves a and b in Figure 3.13 correspond to $(\Delta G^{\circ})_o$ values of -0.5 and -3.0 eV, respectively. For these systems $(\lambda_o)_o = 1.6$ eV ($(\lambda_o)_o$ is the value of λ_o at contact distance). This means that curve a represents a system in the normal region and the curve b represents a system in the inverted region. It can be seen from Figure 3.13 that, for

the system in the normal region, the rate constant is maximum at contact distance (= 7Å) and decreases exponentially with distance. But for a system belonging to the inverted region (curve b) the rate constant shows a substantial initial increase, reaches a maximum at $d_c \approx 10.2$ Å and then decreases. This analysis implies that for a system belonging to the normal region, the electron transfer process will be fastest at contact distance, but for a system belonging to the inverted region, the electron transfer process will be fastest at a distance larger than contact distance.
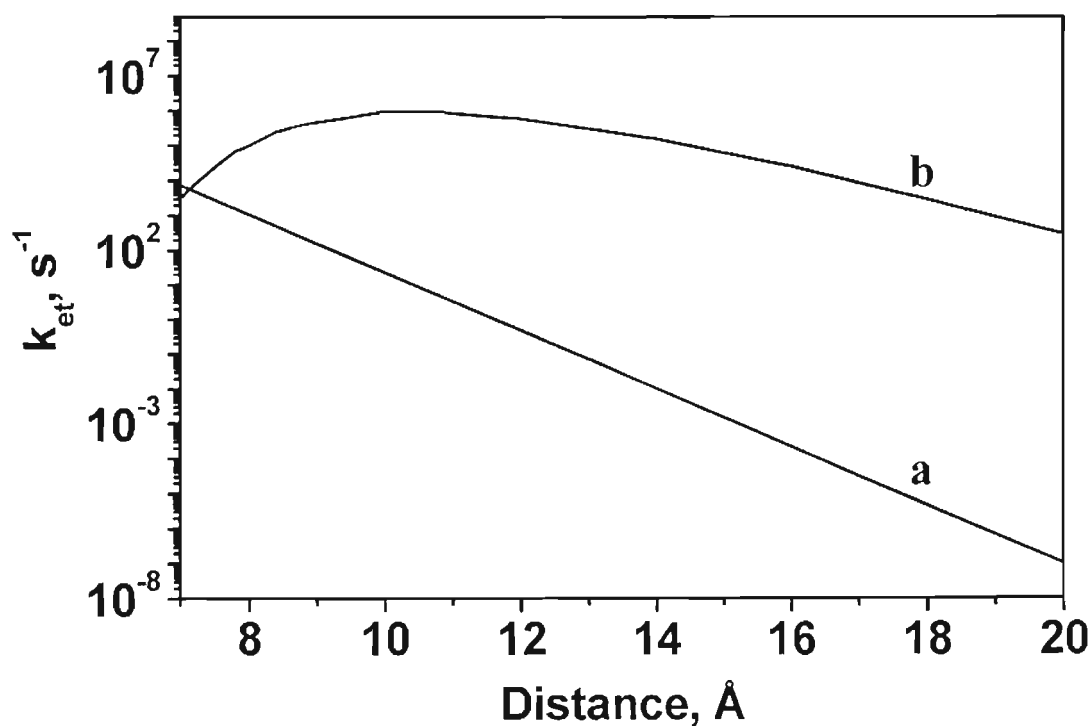
Figure 3.13. Calculated rate *vs.* distance curves in acetonitrile for (a) normal ($\Delta G° = -0.5$ eV) and (b) inverted regions ($\Delta G° = -3.0$ eV). Parameters used were $H_{el}^0 = 100$ cm^{-1}, $\beta = 1.4$ Å^{-1}, $\lambda_i = 0.2$ eV, $r_D = 4$ Å, $r_A = 3$ Å.

Notice in Figure 3.13 that curves a and b have similar k_{et} values at contact distance. But at larger separations, k_{et} for the system in the inverted region is several orders of magnitude larger compared to that for the system in the normal region. It should also be mentioned that the shape and position of maximum k_{et} for curve b depend very much on the r_D and r_A values. With increasing r_D and r_A values, the curve gets somewhat flattened and position of maximum k_{et} shifts to larger distances.

A similar kind of effect is predicted for electron transfer in non-polar solvents also. In this case variation of λ_o with distance is negligible, but this is compensated by the large distance dependence of $\Delta G°$ (Figure 3.12). In Figure 3.14 we have presented the calculated distance dependence of electron transfer rate constants in toluene for three $(\Delta G°)_o$ values. Parameters used for the calculations were $H_{el}° = 60$ cm^{-1}, $\beta = 1.1$ Å^{-1}, $r_D = 6$ Å and $r_A = 4$ Å (we have selected these values because we expected similar values for the hydrogen-bonded donor-acceptor systems we have studied). Curve a is for a system in the normal region and it has its maximum rate at contact distance. Curves b and c are for systems belonging to the inverted region and for these systems the rate maximum occur at distances much larger than the contact distance. A comparison of curves b and c leads to the following observations. For a system belonging to the inverted region close to the top of the Marcus plot, the distance dependence of k_{et} is shallow (curve b). In this case the rate constant showed a small increase as the

distance changed from 10 - 12 Å and there after showed a marginal decrease with increase in distance. This treatment, in fact, predicted almost identical rate constants for the system at 10 and 16 Å. For a system belonging to the deep inverted region (curve c), the behaviour is somewhat different. Here the rate is very low ($< 10^4$ s^{-1}) at contact distance and shows a large increase with distance to reach the maximum k_{et} at $\sim$ 15 Å. In fact, the rate constant increased by two orders of magnitude as the distance increased from 10 - 15 Å. With further increase in distance the rate constant decreased very slowly.
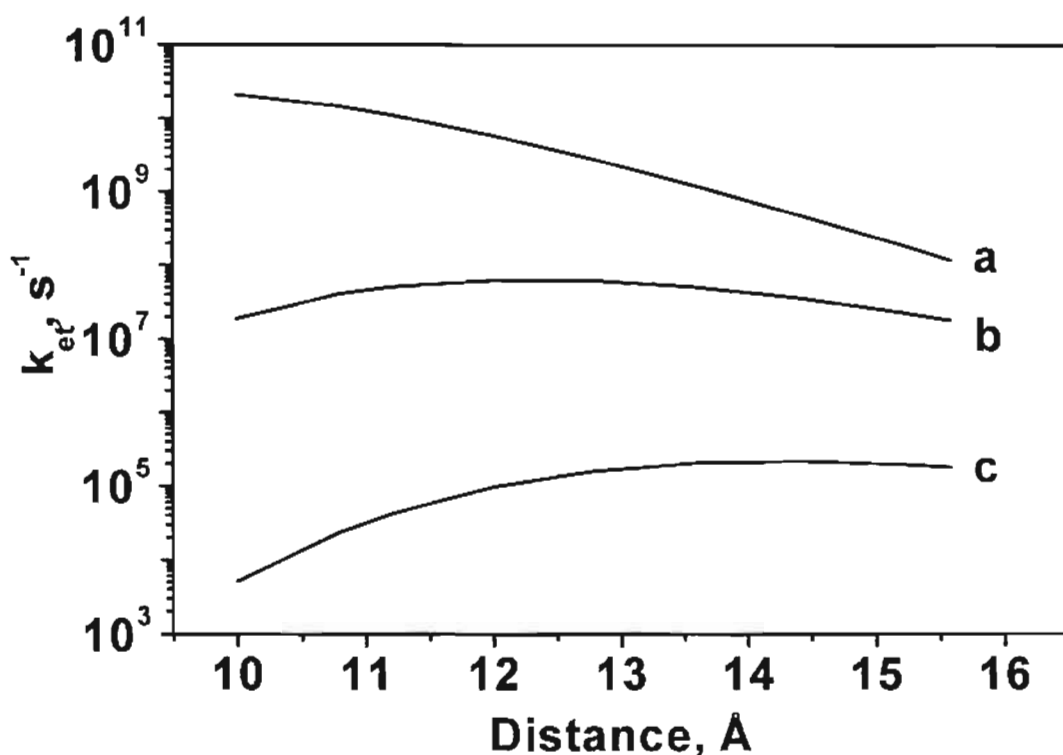
Figure 3.14. Calculated rate *vs.* distance curves in toluene for (a) ($\Delta G)_o$ = -0.45 eV, (b) ($\Delta G)_o$ = -0.75 eV and (c) ($\Delta G)_o$ = -0.95 eV. Other parameters were, H_{el}^0 = 60 cm^{-1}, β = 1.1 Å^{-1}, λ_i = 0.2 eV, r_D = 6 Å, r_A = 4 Å.

Theoretical treatments like this have prompted several authors to predict that: (1) for systems in the normal region the rate decreases exponentially with distance; (2) for the inverted region rate maximum occurs at $d > d_0$ and (3) for systems in the inverted region the rates at larger separations are several orders of magnitude larger than those for systems in the normal region.[54-58] The first of these predictions has been verified beyond doubt for several donor-acceptor systems. The latter two predictions, to the best of our knowledge, have not been experimenatlly verified so far. In fact, almost all the studies that address the distance dependence of electron transfer reactions deals with systems that belonged to the normal region. To the best of our knowledge, there is only one experimental study that specifically addressed the distance dependence problem in the inverted region.[29] In this study the authors failed to observe an increase in rate with distance. They have observed a weak exponential distance dependence of the rate constant ($\beta = 0.66$ Å^{-1}) and used an alternate model for λ_0 to explain their results.

The absence of distance dependence studies in the inverted region, in our opinion, can be attributed to the lack of systems in the inverted region that can be studied by fluorescence methods. The inverted region is observed only rarely.[75,76] Even for those donor-acceptor dyads for which the inverted region is observed, the bell shaped function actually consists of two distinct parts: (1) photoinduced forward process, which is restricted to the normal region and (2) the thermal back electron transfer which is restricted to the inverted region.[77-83] The latter process.

cannot be studied by fluorescence methods. Some of the hydrogen-bonded systems we have studied belonged to the inverted region and the distance dependence in these systems could be studied by fluorescence methods. This was one of the reasons to undertake this study. In the following section we try to analyze the distance dependencies we have observed in our hydrogen-bonded systems using the Marcus theory.

Rate constants obtained for the **PA**(1-3)/**10**(1-3) systems (▼) are shown against the corresponding distances in Figure 3.15. In order to fit the data to the Marcus equation the following approach was used. λ_o and ΔG^o values for the systems were calculated using equation 3.7 and 3.8 respectively, with the following values: $E_{ox} = 0.85$ V, $E_{red} = -2.1$ V, $E_{0.0} = 3.6$ eV, $r_A = 6$ Å and $r_D = 4$ Å.
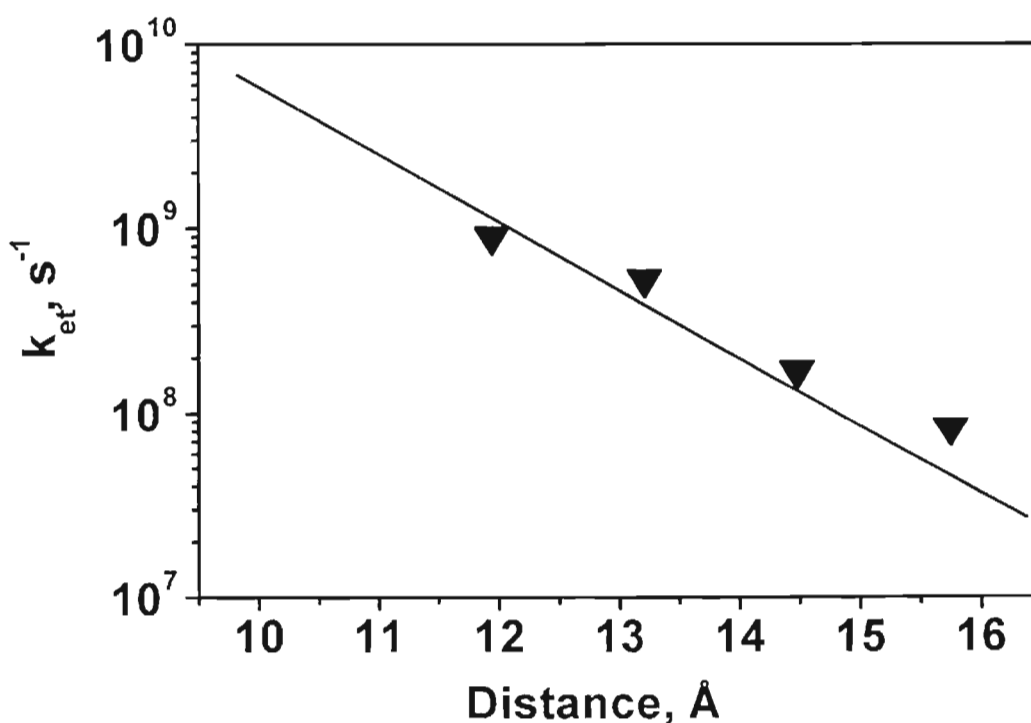
Figure 3.15. Distance dependence of rate constants (k_{et}) for the PA/10 system in dichloromethane. The solid line is a fit using $H_{el}^0 = 10$ cm^{-1}, $\beta = 0.6$ Å^{-1}, $\lambda_i = 0.2$ eV, $r_A = 6$ Å and $r_D = 4$ Å.

λ_i is assumed to be 0.2 eV. k_{et} values were then calculated using different combinations of H_{el}^0 and β values. The best fit corresponded to $H_{el}^0 = 10$ cm^{-1} and $\beta = 0.6$ Å^{-1} and this is shown in Figure 3.15. It can be judged from Figure 3.15 that the fit is very good.

Observed rate constants for the inverted region (**PA(1-3)/11(1-3)**) system, shown as triangles in Figuer 3.16, showed a small increase followed by a decrease. For these systems $E_{ox} = 1.08$ eV and $E_{red} = -1.25$ eV. The rate constants were calculated as described above and the best fit obtained is shown in Figure 3.16. For the best fit $H_{el}^0 = 20$ cm^{-1} and $\beta = 0.6$ Å^{-1}. It can be seen from Figure 3.16 that
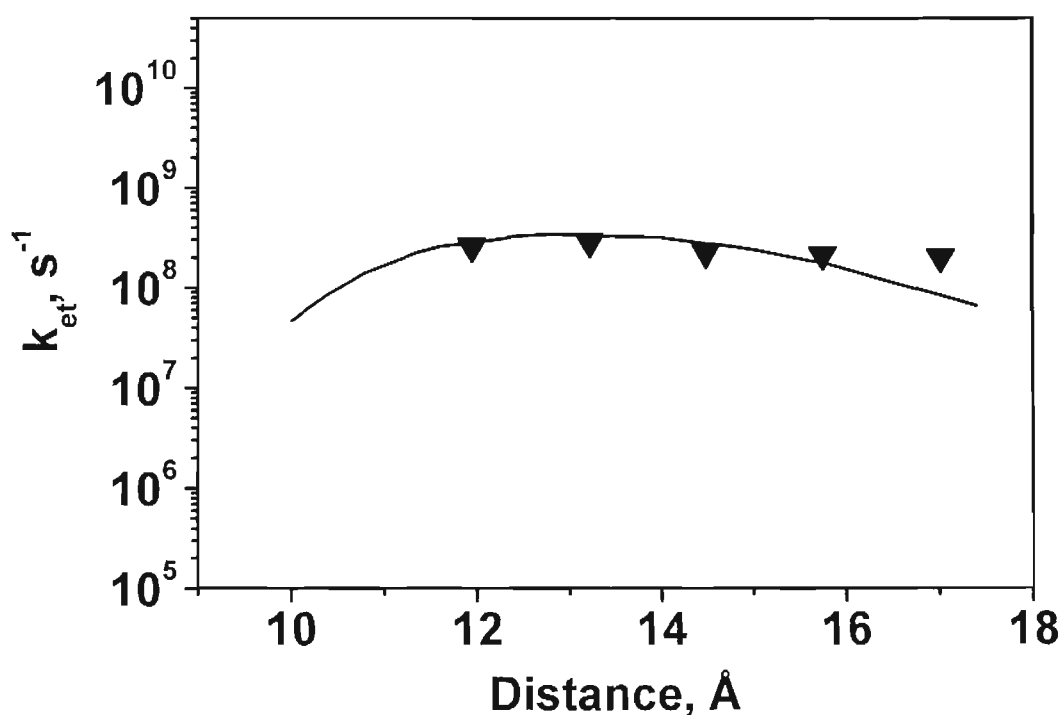
Figure 3.16. Distance dependence of rate constants (k_{et}) for the PA/11 system in toluene. The solid line is a fit using $H_{el}^0 = 20$ cm^{-1}, $\beta = 0.6$ Å^{-1}, $\lambda_i = 0.2$ eV, $r_A = 4$ Å and $r_D = 6$ Å for the PA/11 system.

the first four points fit reasonably well to Marcus equation. The value at the largest separation shows some positive deviation from the theoretical curve. We attribute this to the flexibility of the system. Flexibility leads to several conformations and some of them may have very close arrangements of the donor and acceptor. This allows through-space interactions also to contribute thereby raising the overall rate constant compared to the predicted value. Such effects are reported earlier in electron transfer and triplet energy transfer reactions in flexible systems.[84,29]

Our analysis has shown that the distance dependence of electron transfer in hydrogen-bonded systems belonging to the normal and inverted regions can be adequately explained by the Marcus model. The β values we have obtained are much smaller than those obtained for electron transfer reactions mediated by saturated bridges or protein networks. Since there are no other studies of distance dependence in hydrogen-bonded systems, it will be highly premature to draw any conclusion about the low β values observed.

The distance dependence study mentioned above has given us an opportunity to examine the suggestion of Rau and co-workers that the absence of inverted region in bimolecular PET reactions can be related to the distance dependence of electron transfer rates.[59] The basis of their suggestion is the following. In the case of freely moving molecules there will be several quencher molecules at different distances around a given probe. According to the Marcus theory rate maximum occurs at $\Delta G^\circ = -\lambda$. For a system in the inverted region

$\Delta G° < -\lambda$ at contact distance. But we have seen that λ_o increases with distance in a polar solvent. The authors claim that, because of the increase in λ_o with distance, $\Delta G° = -\lambda$ can be attained at larger distances and the rate constant will be maximum at this distance and electron transfer will occur at this distance. Thus, for systems having large driving forces, at very short distances (in particular at van der Waals contact), the free energy could bring the system within the inverted region, but electron transfer would take place at some larger distance where $\Delta G° - -\lambda$ and rate is maximum. This has the effect of truncating the observed rate to the maximum value possible in a solvent, which will be equal to k_{diff} for the solvent. The inverted region will not be observed for bimolecular reactions if this situation actually exists.

Our distance dependence studies do not support this suggestion. In the familiar two-sphere model in which equation 3.7 is based, each redox site is represented by a sphere in a dielectric continuum. In this case λ_o (or for that matter $\Delta G°$) becomes independent of separation distance at large d_c. In the case of two identical spheres, λ_o changes only by about a factor of 2 when the distance changes from contact distance to infinite separation. This means that in the deep inverted region ($\Delta G° < -2$ eV), the condition that $\Delta G° = -\lambda$ can never be achieved at larger distances. Electron transfer rates in the deep inverted region will be very low ($< 10^4$ s^{-1}, see Figure 3.14) and the enhanced rates at larger distances will be much smaller than diffusion controlled rates. Two alternatives can be suggested

for not observing the inverted region in this free energy regime. The first is to suggest that the masking is due to formation of products in the excited state or presence of other reaction pathways (see Chapter 2). The second is to consider other models for λ_o and ΔG^o. In this context it is to be mentioned that Sutin and co-workers have already suggested a model in which λ_o is much more distance dependent than that in the two-sphere model.[54] In this case the two redox sites are considered to be embedded in an ellipsoidal or spherical cavity immersed in a dielectric continuum. In this case the variation of λ_o with distance is proportional to d^n where $n > 1$ when the separations are large and one or both of the redox sites are symmetrically located either on the long axis of the ellipsoidal cavity or on the diameter of a spherical cavity. With such a model the condition of $\Delta G^o = -\lambda$ may be obtained at larger separations even in the deep inverted region. More experiments are needed to verify these alternatives.

3.5. Conclusions

We have studied the distance dependence of electron transfer reactions in two hydrogen-bonded systems, one of which falls in the normal region and the other belongs to the inverted region. For the system in the normal region the rate constant decreased exponentially with distance. For the system in the inverted region, the rate constant showed a small initial increase followed by a decrease. The overall variation of the rate constant was very small in this case. An analysis of the results showed that the distance dependencies in hydrogen-bonded systems

in the normal and inverted regions can be adequately explained by the Marcus theory. We have examined the suggestion of Rau and co-workers that the inverted region is not generally observed in bimolecular PET reactions due to the distance dependence of electron transfer. Our study and the theroretical considerations suggested that this suggestion is invalid.

3.6. Experimental section

3.6.1. Materials

All the probes and quencher molecules used for this study were prepared by known procedures.[85-88] These were thoroughly purified and dried before use. The dichloromethane and toluene used for fluorescence lifetime measurements were rigorously dried and deaerated before use. Spectroscopic grade acetonitrile was used for the cyclic voltammetric studies.

3.6.2. Measurements

The absorption spectra were recorded on a Shimadzu-3101PC UV-Vis-NIR scanning spectrophotometer. Fluorescence spectra were recorded on a SPEX Fluorolog F112X spectrofluorimeter. Fluorescence lifetimes were determined using Edinburgh Instruments FL900CD single photon counting system and the data were analysed by Edinburgh software. For the fluorescence measurements probe concentrations were 1×10^{-5} M and quencher concentrations were in the range of $(1-4) \times 10^{-3}$ M. Cyclic voltammograms were recorded using a

BAS CV50W voltammetric analyser. Solutions of the aromatic compounds (1×10^{-3} M) in acetonitrile containing 0.1 M tetra-*n*-butylammonium tetrafluoroborate as supporting electrolyte, were thoroughly deaerated before use. A glassy carbon electrode was used as the working electrode and a platinum wire was used as the counter electrode.

3.7. References

1. Mann, B.; Kuhn, H. *J. Appl. Phys.* **1971**, *42*, 4398.

2. Kuhn, H. *J. Photochem.* **1979**, *10*, 111.

3. Mobius, D. *Acc. Chem. Res.* **1981**, *14*, 63.

4. Miller, J. R. *J. Chem. Phys.* **1972**, *56*, 5173.

5. Miller, J. R.; Beitz, J. V.; Huddleston, R. K. *J. Am. Chem. Soc.* **1984**, *106*, 5057.

6. Verhoeven, J. W. in *Electron Transfer - From Isolated Molecules to Biomolecules, Part I*; Jortner, J., Bixon, M., Prigogine, I., Rice, S. A. Eds.; John Wiley and Sons, Inc.: London, 1999; p 603.

7. Heiler, D.; McLendon, G.; Rogalskyj, P. *J. Am. Chem. Soc.* **1987**, *109*, 7540.

8. McLendon, G. *Acc. Chem. Res.* **1988**, *21*, 160.

9. Schmidt, J. A.; McIntosh, A. R.; Weedon, A. C.; Bolton, J. R.; Connolly, J. S.; Hurley, J. K.; Wasielewski, M. R. *J. Am. Chem. Soc.* **1988**, *110*, 1733.

10. Wasielewski, M. R.; Johnson, D. G.; Svec, W. A.; Kersey, K. M.; Minsek, D. W. *J. Am. Chem. Soc.* **1988**, *110*, 7219.

11. Wasielewski, M. R.; Niemczyk, M. P.; Johnson, D. G.; Svec, W. A.; Minsek, D. W. *Tetrahedron*, **1989**, *45*, 4785.

12. Helms, A.; Heiler, D.; McLendon, G. *J. Am. Chem. Soc.* **1991**, *113*, 4325.

13. Helms, A.; Heiler, D.; McLendon, G. *J. Am. Chem. Soc.* **1992**, *114*, 6227.

14. Ryu, C. K.; Wang, R.; Schmehl, R. H.; Ferrere, S.; Ludwikow, M.; Merkert, J. W.; Headford, C. L.; Elliott, C. M. *J. Am. Chem. Soc.* **1992**, *114*, 430.

15. Portela, C. F.; Brunckova, J.; Richards, J. I.; Schöllhorn, B.; Iamamoto, Y.; Magde, D.; Traylor, T. G.; Perrin, C. L. *J. Phys. Chem. A*: **1999**, *103*, 10540.

16. Closs, G. L.; Calcaterra, L. T.; Green, N. J.; Penfeild, K. W.; Miller, J. R. *J. Phys. Chem.* **1986**, *90*, 3673.

17. Johnson, M. D.; Miller, J. R.; Green, N. S.; Closs, G. L. *J. Phys. Chem.* **1989**, *93*, 1173.

18. Leland, B. A.; Joran, A. R.; Felker, P. M.; Hopfeild, J. J.; Zewail, A. H.; Dervan, P. B. *J. Phys. Chem.* **1985**, *89*, 5571.

19. Heitele, H.; Michel-Beyerle, M. E. *J. Am. Chem. Soc.* **1985**, *107*, 8286.

20. Finckh, P.; Heitele, H.; Michel-Beyerle, M. E. *Chem. Phys.* **1989**, *138*, 1.

21. Hush, N. S.; Paddon-Row, M. N.; Cotsaris, E.; Oevering, H.; Verhoeven, J. W.; Heppener, M. *Chem. Phys. Lett.* **1985**, *117*, 8.

22. Oevering, H.; Paddon-Row, M. N.; Heppener, M.; Oliver, A. M.; Cotsaris, E.; Verhoeven, J. W.; Hush, N. S. *J. Am. Chem. Soc.* **1987**, *109*, 3258.

23. Oevering, H.; Verhoeven, J. W.; Paddon-Row, M. N.; Cotsaris, E.; Hush, N. S. *Chem. Phys. Lett.* **1988**, *150*, 179.

24. Jordan, K. D.; Paddon-Row, M. N. *Chem. Rev.* **1992**, *92*, 395.

25. Knapp, S.; Murali Dhar T. G.; Albaneze, J.; Gentemann. S.; Potenza, J. A.; Holten, D.; Schugar, H. J. *J. Am. Chem. Soc.* **1991**, *113*, 4010.

26. Davis, W. B.; Svec, W. A.; Ratner, M. A.; Wasielewski, M. R. *Nature* **1998**, *396*, 60.

27. Siemiarczuk, A.; McIntosh, A. R.; Ho, T. F.; Stillman, M. J.; Roach, K. J.; Weedon, A. C.; Bolton, J. R.; Connolly, J. S. *J. Am. Chem. Soc.* **1983**, *105*, 7224.

28. Mataga, N.; Karen, A.; Okada, T.; Nishitani, S.; Kurata, N.; Sakada, Y.; Misumi, S. *J. Phys. Chem.* **1984**, *88*, 5138.

29. Yonemoto, E. H.; Saupe, G. B.; Schmehl, R. H.; Hubig, S. M.; Riley, R. L.; Iverson, B. L.; Mallouk, T. E. *J. Am. Chem. Soc.* **1994**, *116*, 4786.

30. Yonemoto, E. H.; Kim, Y. I.; Schmehl, R. H.; Hubig, S. M.; Riley, R. L.; Iverson, B. L.; Mallouk, T. E. *J. Am. Chem. Soc.* **1994**, *116*, 10557.

31. Cabana, L.; Schanze, K. in *Electron Transfer in Biology and the Solid State, Inorganic Compounds with unusual Properties*; Johnson, M. K., King, R. V., Kurtz, D. M.; Kutal, G., Norton, M. L., Scott, R. A., Eds.; American Chemical Society: Washington, DC, 1990; p 101.

32. Isied, S. S. in *Electron Transfer in Inorganic, Organic and Biological Systems*; Bolton, J. R., Mataga, N., McLendon, G. Eds.; American Chemical Society: Washington, DC, 1991; Chapter 15.

33. Schanze, K.; Sauer, K. *J. Am. Chem. Soc.* **1988**, *110*, 1180.

34. Schanze, K.; Cabana, L. A. *J. Phys. Chem.* **1990**, *94*, 2740.

35. Isied, S. S.; Ogawa, M. Y.; Wishart, J. F. *Chem. Rev.* **1992**, *92*, 381.

36. Murphy, C. J.; Arkin, M. R.; Jenkins, Y.; Ghatlia, N. D.; Bossmann, S. H.; Turro, N. J.; Barton, J. K. *Science* **1993**, *262*, 1025.

37. Murphy, C. J.; Arkin, M. R.; Jenkins, Y.; Ghatlia, N. D.; Bossmann, S. H.; Turro, N. J.; Barton, J. K. *Proc. Natl. Acad. Sci. USA* **1994**, *91*, 5319.

38. Brun, A. M.; Harriman, A. *J. Am. Chem. Soc.* **1994**, *116*, 10383.

39. Meade, T. J.; Kayyem, J. F. *Angew. Chem. Int. Ed. Engl.* **1995**, *34*, 352.

40. Priyadarshy, S.; Risser, S. M.; Beratan, D. N. *J. Phys. Chem.* **1996**, *100*, 17678.

41. Gasper, S. M.; Shuster, G. B. *J. Am. Chem. Soc.* **1997**, *119*, 12762.

42. Fukui, K.; Tanaka, K. *Angew. Chem. Int. Ed. Engl.* **1998**, *37*, 158.

43. Kelley, S. O.; Jackson, N. M.; Hill, M. G.; Barton, J. K. *Angew. Chem. Int. Ed. Engl.* **1999**, *38*, 941.

44. Shuster, G. B. *Acc. Chem. Res.* **2000**, *33*, 253.

45. Bowler, B. E.; Meade, T. J.; Mayo, S. L.; Richards, J. H.; Gray, H. B. *J. Am. Chem. Soc.* **1989**, *111*, 8757.

46. Meade, T. J.; Gray, H. B.; Winkler, J. R. *J. Am. Chem. Soc.* **1989**, *111*, 4353.

47. Therien, M. J.; Selman, M.; Gray, H. B.; Chang, I.-J.; Winkler, J. R. *J. Am. Chem. Soc.* **1990**, *112*, 2420.

48. Onuchic, J. N.; Beratan, D. N. *J. Chem. Phys.* **1990**, *92*, 722.

49. Beratan, D. N.; Onuchic, J. N. *Adv. Chem. Ser.* **1991**, *228*, 71.

50. Beratan, D. N.; Betts, J. N.; Onuchic, J. N. *Science* **1991**, *252*, 1285.

51. Winkler, J. R.; Gray, H. B. *Chem. Rev.* **1992**, *92*, 369.

52. Betts, J. N.; Beratan, D. N.; Onuchic, J. N. *J. Am. Chem. Soc.* **1992**, *114*, 4043.

53. Beratan, D. N.; Betts, J. N.; Onuchic, J. N. *J. Phys. Chem.* **1992**, *96*, 2852.

54. Sutin, N. in *Supramolecular Photochemistry*; Balzani, V. Ed.; Riedel: Amsterdam, 1987; p 73.

55. Brunschwig, B. S.; Ehrenson, S.; Sutin, N. *J. Am. Chem. Soc.* **1984**, *106*, 6858.

56. Angel, S. A.; Peters, K. S. *J. Phys. Chem.* **1991**, *95*, 3606.

57. Murata, S.; Tachiya, M. *J. Phys. Chem.* **1996**, *100*, 4064.

58. Georgievskii, Y.; Burshtein, A. I.; Chernbrod, B. M. *J. Chem. Phys.* **1996**, *105*, 3108.

59. Greiner, G.; Pasquini, P.; Weiland, R.; Orthwein, H.; Rau, H. *J. Photochem. Photobiol. A: Chem.* **1990**, *51*, 179.

60. Derissen, J. L. *J. Mol. Struct.* **1971**, *7*, 67.

61. Doan, V.; Köppe, R.; Kasai, P. H. *J. Am. Chem. Soc.* **1997**, *119*, 9810.

62. Turro, C.; Chang, C. K.; Leroi, G. E.; Cukier, R. I.; Nocera, D. G. *J. Am. Chem. Soc.* **1992**, *114*, 4013.

63. Sessler, J. L.; Wang, B.; Harriman, A. *J. Am. Chem. Soc.* **1993**, *115*, 10418.

64. Berman, A.; Izraeli, E. S.; Levanon, H.; Wang, B.; Sessler, J. L. *J. Am. Chem. Soc.* **1995**, *117*, 8252.

65. Sessler, J. L.; Brown, C. T.; O'Connor, D.; Springs, S. L.; Wang, R.; Sathiosatham, M.; Hirose, T. *J. Org. Chem.* **1998**, *63*, 7370.

66. Marcus, R. A. *Int. J. Chem. Kinet.* **1981**, *13*, 865.

67. Marcus, R. A.; Siders, P. *J. Phys. Chem.* **1982**, *86*, 622.

68. Siders, P.; Marcus, R. A. *J. Am. Chem. Soc.* **1981**, *103*, 741.

69. Marcus, R. A. *Faraday Discuss. Chem. Soc.* **1982**, *74*, 7.

70. Marcus, R. A.; Sutin, M. *Biochim. Biophys. Acta* **1985**, *811*, 266.

71. Sutin, N. *Acc. Chem. Res.* **1982**, *15*, 275.

72. Marcus, R. A. *J. Chem. Phys.* **1956**, *24*, 966.

73. Marcus, R. A. *Annu. Rev. Phys. Chem.* **1964**, *15*, 155.

74. Kavarnos, G. J. *Fundamentals of Photoinduced Electron Transfer*; VCH: New York, 1993.

75. Turro, C.; Zaleski, J. M.; Karabatsos, Y. M.; Nocera, D. G. *J. Am. Chem. Soc.* **1996**, *118*, 6060.

76. Thanasekaran, P.; Rajendran, T.; Rajagopal, S.; Srinivasan, C.; Ramaraj, R.; Ramamurthy, P.; Venkatachalapathy, B. *J. Phys. Chem. A* **1997**, *101*, 8195.

77. Closs, G. L.; Miller, J. R. *Science* **1988**, *240*, 440.

78. Wasielewski, M. R.; Niemczyk, M. P.; Svec, W. A.; Pewitt, E. B. *J. Am. Chem. Soc.* **1985**, *107*, 1080.

79. Wasielewski, M. R.; Johnson, D. G.; Svec, W. A. in *Supramolecular Photochemistry*, Balzani, V. Ed.; D. Riedel: Amsterdam, 1987; p 255.

80. Mataga, N.; Ashai, T.; Kanda, Y.; Okada, T.; Kakitani, T. *Chem. Phys.* **1988**, *127*, 249.

81. Gould, I. R.; Ege, D.; Moser, J. E.; Farid, S. *J. Am. Chem. Soc.* **1990**, *112*, 4290.

82. Fox, L. S.; Kozik, M.; Winkler, J. R.; Gray, H. B. *Science* **1990**, *247*, 1069.

83. Zou, C.; Miers, J. B.; Ballew, R. M.; Dlott, D. D.; Schuster, G. B. *J. Am. Chem. Soc.* **1991**, *113*, 7823.

84. Klan, P.; Wagner, P. J. *J. Am. Chem. Soc.* **1998**, *120*, 2198.

85. Klassen, S. E.; Daub, G. H.; Vanderjagt, D. L. *J. Org. Chem.* **1983**, *48*, 4361.

86. Bachmann, W. E.; Carmack, M. *J. Am. Chem. Soc.* **1941**, *63*, 2494.

87. Romanelli, M. G.; Becker, E. I. in *Org. Syn. Vol. 47*; Emmons, W. D. Ed.; John Wiley and Sons Inc.: London, 1967; p 69.

88. Robertson, G. R. in *Org. Syn. Coll. Vol. 1*; Blatt, A. H. Ed.; John Wiley and Sons Inc.: London, 1958; p 406.

CHAPTER 4

STUDY OF THE TEMPERATURE DEPENDENCE OF PHOTOINDUCED ELECTRON TRANSFER RATES IN HYDROGEN-BONDED DONOR-ACCEPTOR SYSTEMS

4.1. Abstract

We have studied the dependence of electron transfer rates upon temperature in the range of 298 K to 220 K for three donor-acceptor systems, which are assembled at fixed distance by hydrogen bonding interactions involving carboxylic acid groups. One of these systems falls in the normal region and the remaining two systems belong to the inverted region. Analysis of the results showed that the Marcus treatment provides a reasonably good estimate of the temperature dependence of electron transfer rates for the system in the normal region. For systems in the inverted region, electron transfer rates were nearly independent of temperature and could not be explained by the Marcus equation. These however, could be adequately described by the golden rule expression, which takes into account the nuclear tunneling *via* one or more high frequency vibrational modes.

4.2. Introduction

Study of the temperature dependence of reaction rates provides useful information about reaction mechanism. The most commonly observed temperature dependence of reaction rates is the Arrhenius type of dependence, where the rate of the reaction increases by a factor of 2 - 3 for every 10 °C rise in temperature. In

these cases a plot of log k *vs.* 1/T will be linear with a negative slope. Non-Arrhenius types of temperature dependence have also been observed in several cases. These usually indicate multistep reactions or reactions which change their mechanism with temperature. Non-Arrhenius behaviour can also be indicative of two competing reactions with different activation energies. From a linear log k *vs.* 1/T plot. the activation parameters (E_a, $\Delta H^{\#}$ and $\Delta S^{\#}$) of the reaction can be obtained. These parameters can be used to provide a full description of the kinetic data and also for a mechanistic interpretation of the reaction.

In order to understand the mechanistic aspects and also to evaluate the various theories of electron transfer, temperature dependence of several photoinduced electron transfer reactions were studied.[1] For example, Baggot and Pilling studied the temperature dependence of the quenching of the singlet excited states of pyrene and naphthalene by substituted benzonitriles using the single photon counting technique.[2] For these donor-acceptor systems, temperature dependence of the quenching rate constants depended very much on the free energy changes associated with the electron transfer processes. The results were not in tune with simple outer sphere electron transfer theories and the authors have invoked the formation of an exciplex prior to electron transfer to explain the observations. Temperature dependence of the fluorescence quenching rate constant for the pyrene/1,2,4-trimethoxybenzene system was also studied.[1] This study indicated that a mechanism involving mixed excimer formation operates even in strongly polar solvents.

Ruthenium polypyridyl complexes can act as electron donors or acceptors in the excited state. Temperature dependence of the fluorescence quenching of several Ru(II) complexes by quenchers such as metal ions, viologen acceptors and amine donors were investigated in detail.[3] Some of these systems gave linear Arrhenius plots while others showed anomalous behaviours. For example, quenching of the luminescence of Ruthenium(II)-2,2'-bipyridine-4,4'-disulfonic acid by Cu(II) resulted in a non-linear Arrhenius plot.[4] This is explained to be due to two parallel electron transfer processes taking place in this system. The first of these is the normal outer sphere electron transfer from *Ru(II) to Cu(II). The second is an inner sphere electron transfer process, which involves penetration of the ligand $SO_3^{\ominus}$ substituent into the inner co-ordination sphere of the Cu(II) ion. It was observed in these studies that the temperature dependence of the luminescence quenching rate constant in solution can be fitted into the Marcus theory or Rehm-Weller correlation only after making several assumptions.

Effect of temperature on the electron transfer rate constants in covalently linked donor-acceptor systems have been investigated by several groups.[5-17] For example, Heitele *et al.* have measured the temperature dependence of intramolecular electron transfer in **1** (Chart 4.1), where an anthracene acceptor is linked to a dimethylaniline donor through a covalent spacer.[8] The temperature dependence of the rate constant in this system depended on the solvent used. In a related study the temperature dependence of the electron transfer rate in **2** (Chart 4.1) was investigated in propionitrile and propylene glycol.[5] The temperature

dependence in propylene glycol was markedly stronger than that in propionitrile. This difference was attributed to the influence of dielectric relaxation dynamics on electron transfer. It was proposed that as the dielectric relaxation time increases, a smooth transition from a non-adiabatic to a solvent controlled adiabatic behaviour is taking place in **2**.
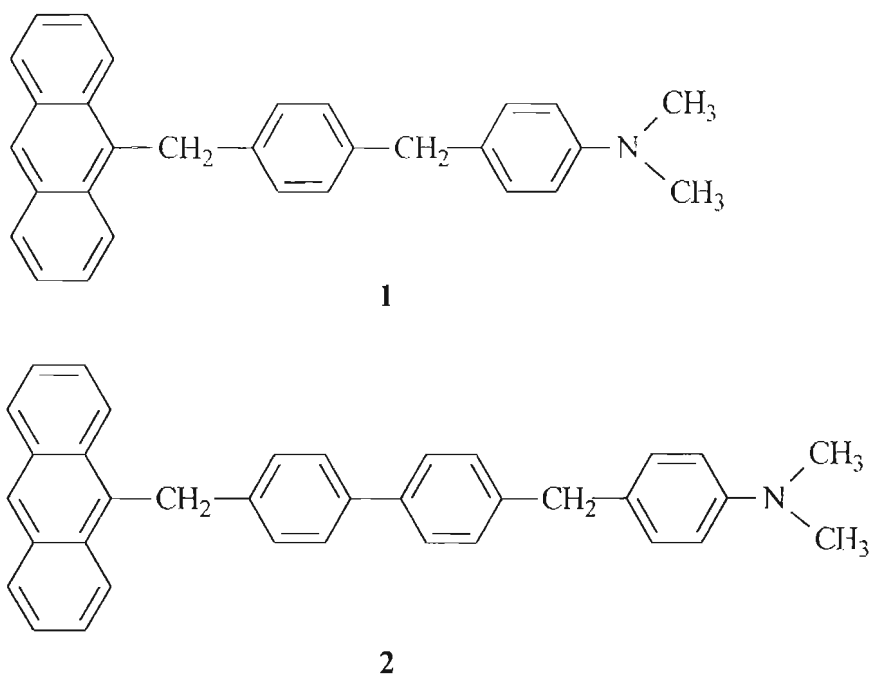
Chart 4.1

Temperature dependence of the electron transfer rate constants for donor-acceptor systems belonging to the normal and inverted regions were investigated by Liang *et al.* using the covalently linked system **3** (Chart 4.2).[7] In **3**, the biphenyl radical anion is the donor and A stands for different acceptor moieties. When A is a weak acceptor like naphthalene, the system falls in the normal region and Arrhenius type of temperature dependence was observed. Where A is a strong

acceptor group such as 2-benzoquinonyl or 5-chloro-2-benzoquinonyl, free energy changes for electron transfers were less than -2 eV and these belonged to the inverted region. The rate constants for these systems were found to be independent of temperature in the range of -94 to +100 °C.[10] Kroon *et al.* have studied the temperature dependence of electron transfer rate constants in covalently linked dimethoxynaphthalene/dicyanovinyl systems.[13] They also obtained Arrhenius type of behaviour in the normal region and temperature independent rate constants in the inverted region. Chen *et al.*, on the other hand, obtained temperature dependent rate constants in the inverted region.[14] They have employed the metal complex Re(I)(CO)$_3$(bpy-PTZ)Cl (**4**, Chart 4.3). **4** is a covalently linked dyad in which excitation leads to transfer of an electron from the phenothiazine moiety to the metal complex. The back electron transfer process, which regenerates **4** in the ground state, falls in the inverted region. The back electron transfer rate constant increased with increase in temperature and the authors have explained this by invoking the energy gap law.

Moser and Grätzel obtained temperature independent rate constants for heterogeneous electron transfer reactions in the inverted region.[18] In this study, dyes adsorbed onto colloidal TiO$_2$ particles were excited by a laser pulse, which resulted in the injection of electrons from the dye to the conduction band of TiO$_2$.

electron transfer

3

Chart 4.2

4
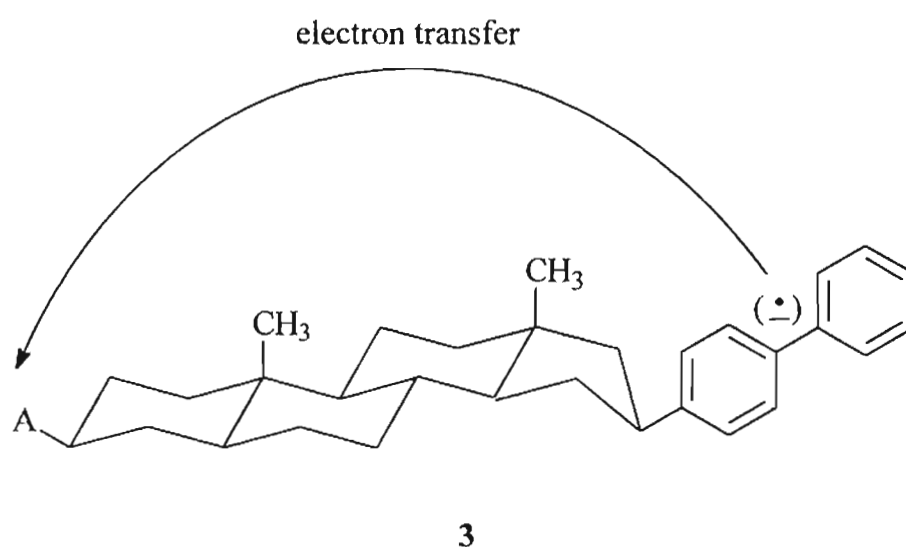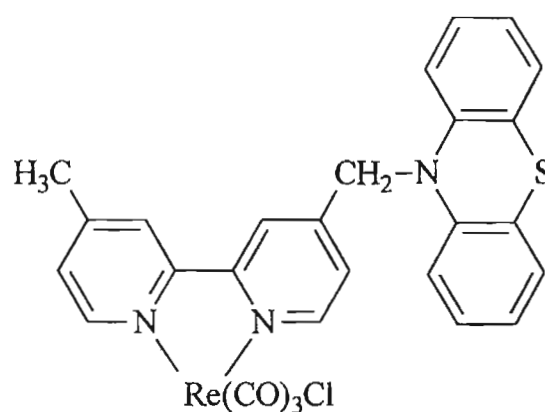
Chart 4.3

The back electron transfer process from the conduction band of the colloidal TiO_2 to the dye cation radicals belonged to the inverted region. Rate constants of these processes were found to be independent of temperature over a wide range (-200 to +30 °C). The results were interpreted in terms of a quantum mechanical model for non-adiabatic electron transfer reactions.

Temperature dependence of electron transfer reactions in several photosynthetic reaction centres have been investigated in detail.[19-30] For example Devault and Chance have studied the temperature dependence of the photoinduced oxidation of cytochromes in the photosynthetic bacterium *Chromatium.*[19] For this system, the rate constant decreased three fold as the temperature is lowered from 298 K to 100 K and remained constant below 100 K. Temperature dependence of the rate of electron transfer between bacteriopheophytin and the first quinone in isolated reaction centres of *Rhodopseudomonas sphaeroides* was investigated by Schenck *et al.* In this system the electron transfer rate increased three fold as the temperature decreased from 300 to 25 K and showed a sharp decrease at temperatures below 25 K.[20] Recently, Schmid and Labahn have studied the temperature dependence of charge recombination in a few mutated reaction centres from *Rhodobacter Sphaeroides* and found that the rate progressively decreased from 293 to 225 K and became essentially temperature independent below 225 K.[23] There are a large number of similar studies in related systems and some of these exhibited temperature independent electron transfer rates.[25-30]

The temperature dependence of electron transfer in bacterial reaction centres has been difficult to reconcile with the Marcus electron transfer model, which treats the vibrational degrees of freedom classically. According to the classical Marcus description, electron transfer can be described as a thermally activated process and this is expected to lead to an Arrhenius type of rate dependence on temperature. Hence the semiclassical model which takes into

account quantum vibrational effects was used to interpret the temperature effects observed in the naturally occurring systems. While both classical and semiclassical Marcus theory predict an inverted region at high driving force, the temperature dependence on electron transfer is different according to the two models. According to classical Marcus theory the rate of electron transfer is strongly activation controlled both in the normal and inverted regions. According to the semiclassical model, there exist a wide range of free energy change ($\Delta G°$) where the reaction is essentially activationless. This activationless region can lead to a tunneling mechanism, which explains the temperature insensitive behaviour seen in the naturally occurring systems. In order to gain further insight into nuclear tunneling and temperature independent behaviour observed in photosynthetic systems, detailed work in the inverted region is necessary. In this context, we have investigated the temperature dependence of electron transfer in hydrogen-bonded donor-acceptor systems both in the normal and inverted regions and the results are presented in this chapter. Temperature dependence of PET in hydrogen-bonded donor-acceptor systems has not been studied earlier. Hence this is the first study of this type.

For the present study we have used pyreneacetic acid (**PA**) as the probe molecule. The quenchers used were 4-dimethylaminophenylacetic acid (**5**), 4-nitrophenylacetic acid (**6**) and 2,4-dinitrophenylacetic acid (**7**). Structures of these molecules are shown in Chart 4.4.

PROBES

PA

QUENCHERS

5	**6**	**7**
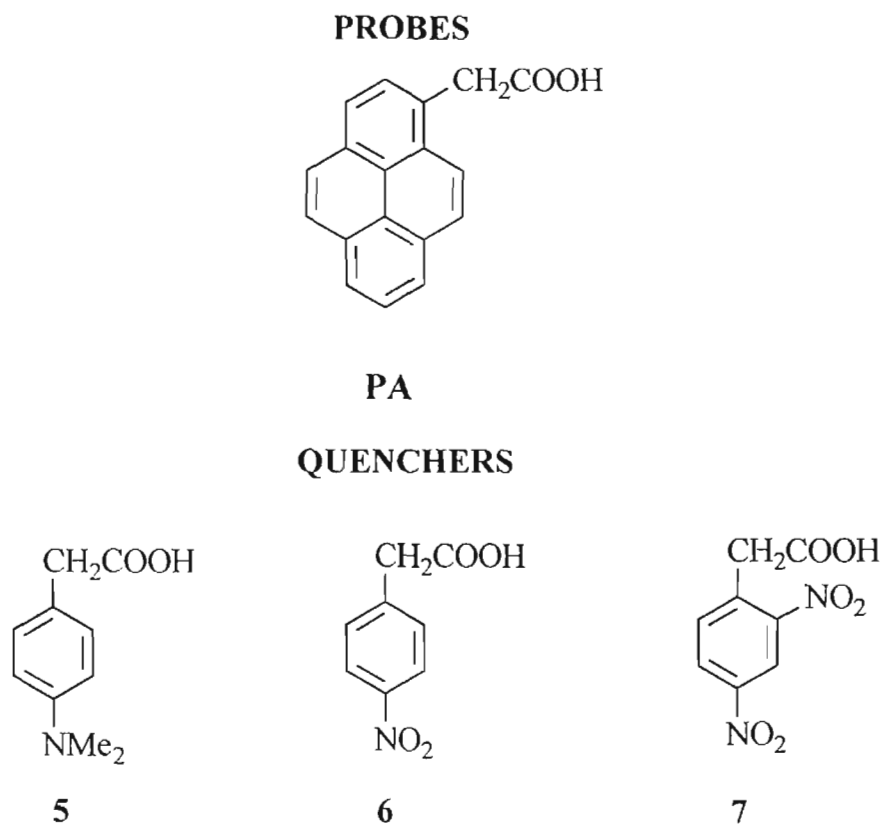
Chart 4.4

As discussed in earlier chapters, presence of carboxylic acid groups in the probe and quenchers enable them to form hydrogen-bonded complexes. In the case of **PA/5** system, electron transfer occurs from the dimethylaminophenyl moiety to the excited pyrene chromophore and the free energy change associated with this electron transfer reaction is -0.50 eV in dichloromethane. The free energy changes for the **PA/6** and **PA/7** systems are -1.16 and -1.40 eV, respectively, and in these cases the nitroaromatics act as acceptors and **PA** acts as the excited state donor. We have shown earlier (see Chapter 2) that the **PA/5** system lies in the normal region and the **PA/6** and **PA/7** systems lie in the inverted region. In this study we

have investigated the temperature dependence of electron transfer in these systems in the range of 220 - 298 K in dichloromethane solution.

4.3. Results

4.3.1. Absorption and emission properties of PA

Photophysical properties of **PA** at room temperature were discussed in earlier chapters of this thesis. In this study we have recorded the absorption and emission spectra of **PA** at different temperatures. Changing the temperature had no effect on the absorption spectrum. The fluorescence profile remained the same at all temperatures but the fluorescence intensity increased considerably at lower temperatures. The fluorescence lifetime (τ_0) also showed an increase with decrease in temperature. Figure 4.1 gives the fluorescence decay profiles of **PA** at two temperatures. Exponential decays were obtained at all temperatures studied and the (τ_0) values obtained are presented in Table 4.1.

Upon addition of millimolar quantities of a quencher, the hydrogen-bonded complex is formed. The fluorescence decays become biexponential (see Chapter 2 for details) which can be expressed by equation 4.1

$$I_{(t)} = \chi_{(P-Q)} \exp(-t/\tau_1) + \chi_{(P)} \exp(-t/\tau_2) \tag{4.1}$$

where, $\chi_{(P-Q)}$ and $\chi_{(P)}$ are the mole fractions of the associated and unassociated probe molecules and τ_1 and τ_2 are the two lifetime components. The electron transfer rate within the hydrogen-bonded complex can be obtained using equation

$$k_{et} = 1/\tau_1 - 1/\tau_0 \tag{4.2}$$
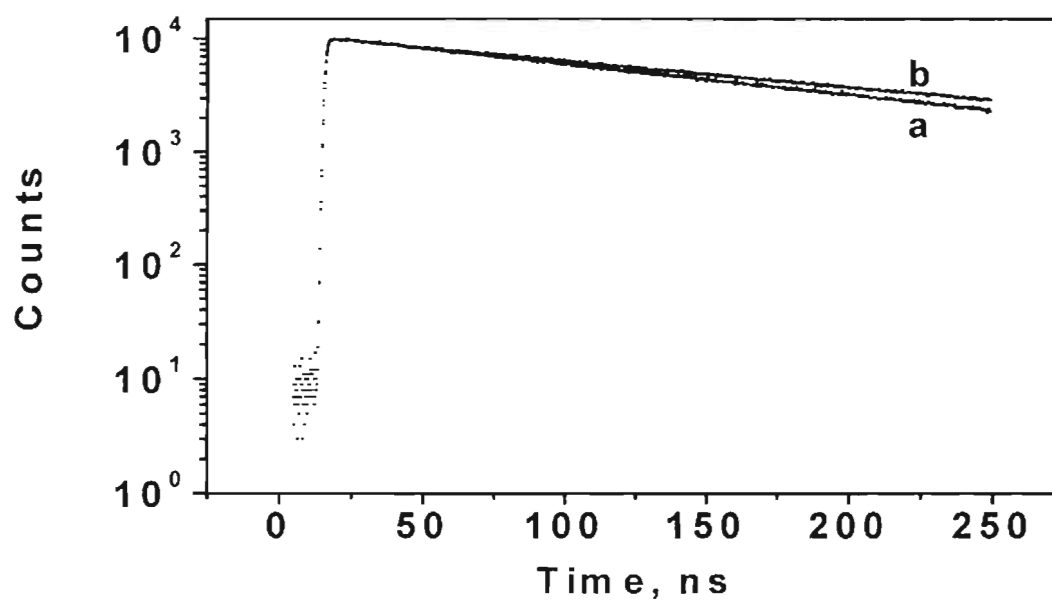
Figure 4.1. The fluorescence decay profiles of PA at (a) 298 K and (b) 220 K.

Table 4.1. Fluorescence lifetimes (τ_0) for PA in dichloromethane at different temperatures. [PA] was 1×10^{-5} M. χ^2 values for the fits are also given.

Temperature, K	τ_0, ns	χ^2
298	135 ± 5	1.0
280	150 ± 5	1.0
270	164 ± 6	1.1
260	172 ± 5	1.0
250	174 ± 4	1.0
240	176 ± 4	1.0
230	180 ± 3	1.1
220	182 ± 3	1.1

4.3.2. Fluorescence lifetime quenching studies of PA/5 system at different temperatures

For the **PA/5** system fluorescence decays were obtained at eight different temperatures in the 220 - 298 K range. At each temperature, fluorescence decays were obtained for three different quencher concentrations. Representative examples of decay profiles are presented in Figures 4.2 - 4.5. In all these cases decays were distinctly biexponential. These were fitted to biexponential functions and the values of various parameters obtained for the three different quencher concentrations are presented in Tables 4.2 - 4.4.
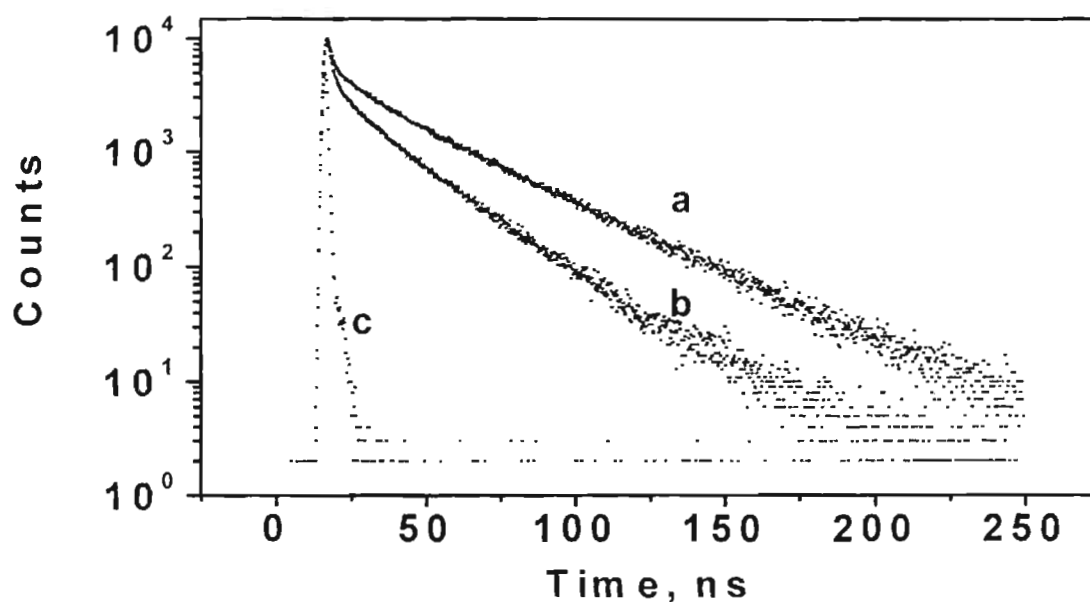
Figure 4.2. The fluorescence decay profiles of PA/5 at 280 K. (a) [PA] = 1 x 10^{-5} M, [5] = 1.5 x 10^{-3} M; (b) [PA] = 1 x 10^{-5} M, [5] = 2.0 x 10^{-3} M. (c) lamp profile.
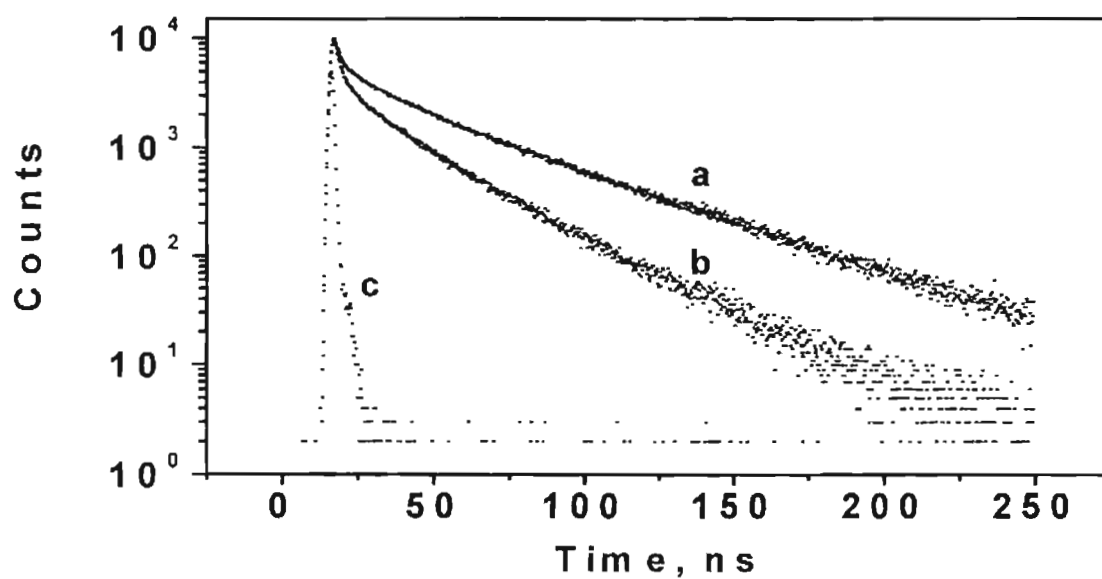
Figure 4.3. The fluorescence decay profiles of PA/5 at 260 K. (a) [PA] = 1 x 10^{-5} M, [5] = 1.5 x 10^{-3} M; (b) [PA] = 1 x 10^{-5} M, [5] = 2.0 x 10^{-3} M. (c) lamp profile.
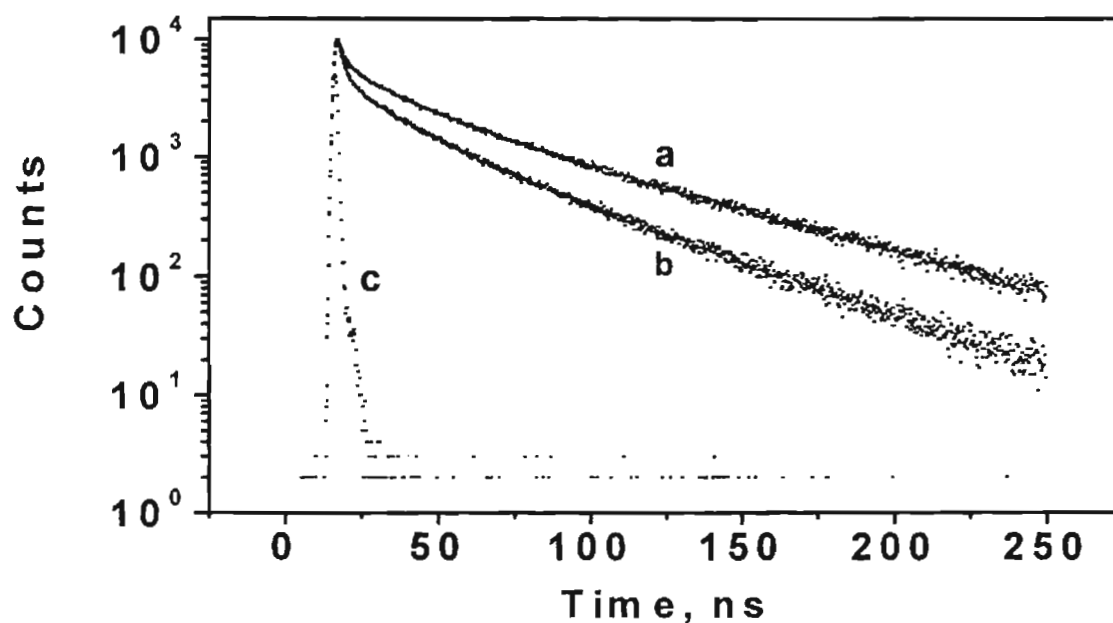
Figure 4.4. The fluorescence decay profiles of PA/5 at 240 K. (a) [PA] = 1 x 10^{-5} M, [5] = 1.5 x 10^{-3} M; (b) [PA] = 1 x 10^{-5} M, [5] = 2.0 x 10^{-3} M. (c) lamp profile.
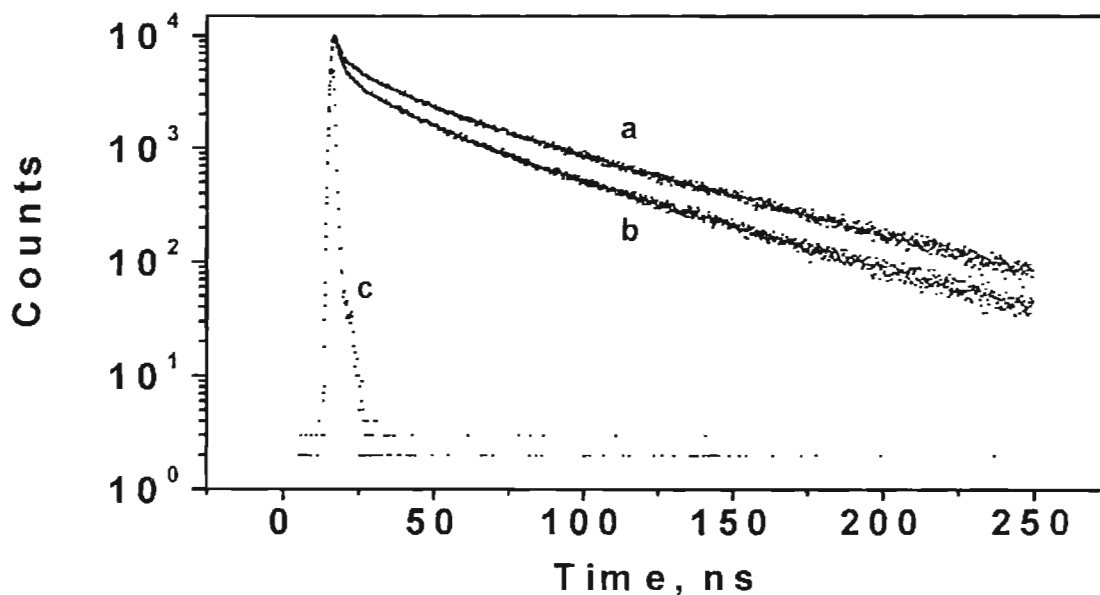
Figure 4.5. The fluorescence decay profiles of PA/5 at 220 K. (a) [PA] = 1 x 10^{-5} M, [5] = 1.5 x 10^{-3} M; (b) [PA] = 1 x 10^{-5} M, [5] = 2.0 x 10^{-3} M. (c) lamp profile.

Table 4.2. Fluorescence lifetimes (τ_1 and τ_2), fractional contributions (χ_{P-Q} and χ_P) and χ^2 values obtained for the fluorescence quenching of PA by 5 at different temperatures. [PA] was 1 x 10^{-5} M and [5] was 1 x 10^{-3} M.

Temperature, K	τ_1, ns	χ_{P-Q} %	τ_2, ns	χ_P %	χ^2
298	1.10	9.02	72.01	90.98	1.0
280	1.17	9.90	80.23	90.10	1.3
270	1.20	10.15	82.16	89.85	1.1
260	1.24	11.25	86.04	88.75	1.2
250	1.35	12.05	89.32	87.95	1.0
240	1.39	14.67	92.05	85.33	1.2
230	1.50	15.17	93.16	84.83	1.3
220	1.65	18.03	93.65	81.97	1.3

Table 4.3. Fluorescence lifetimes (τ_1 and τ_2), fractional contributions (χ_{P-Q} and χ_P) and χ^2 values obtained for the fluorescence quenching of PA by 5 at different temperatures. [PA] was 1×10^{-5} M and [5] was 1.5×10^{-3} M.

Temperature, K	τ_1, ns	χ_{P-Q}, %	τ_2, ns	χ_P, %	χ^2
298	1.10	14.05	68.70	85.95	1.1
280	1.16	15.82	70.65	84.18	1.1
270	1.20	15.42	73.80	84.58	1.2
260	1.22	18.06	75.06	81.94	1.1
250	1.38	17.65	78.58	82.35	1.4
240	1.41	19.23	80.64	80.77	1.3
230	1.52	21.26	81.65	78.74	1.4
220	1.62	23.85	83.01	76.15	1.3

Table 4.4. Fluorescence lifetimes (τ_1 and τ_2), fractional contributions (χ_{P-Q} and χ_P) and χ^2 values obtained for the fluorescence quenching of PA by 5 at different temperatures. [PA] was 1×10^{-5} M and [5] was 2.0×10^{-3} M.

Temperature	τ_1, ns	χ_{P-Q}, %	τ_2, ns	χ_P, %	χ^2
298	1.10	26.70	53.62	73.30	1.1
280	1.16	27.56	54.65	72.44	1.1
270	1.20	29.63	56.30	70.37	1.2
260	1.22	30.30	59.65	69.70	1.1
250	1.38	30.68	62.15	69.32	1.4
240	1.41	32.19	65.68	67.81	1.4
230	1.51	34.59	68.56	65.41	1.4
220	1.62	35.01	70.89	64.99	1.4

A comparison of the various parameters presented in Tables 4.2 - 4.4 leads to the following observations. (1) At a given temperature τ_1 values are independent of quencher concentration and τ_2 values decrease with increase in quencher concentrations. This suggests that hydrogen-bonded complexes are present at all the temperatures studied and confirms that τ_1 arises due to quenching in the hydrogen-bonded complex and τ_2 is due to diffusion mediated quenching. (2) τ_1 increases with decrease in temperature. This suggests that the rate constant for electron transfer within the hydrogen-bonded complex (k_{et}) decrease as the temperature is lowered. k_{et} values were calculated using equation 4.2 and these are presented later in Table 4.9 along with k_{et} values for other systems. (3) τ_2 values also increase with decrease in temperature. This suggests that the diffusional quenching is also slowed down at lower temperatures. The bimolecular quenching rate constants at the different temperatures can be obtained by plotting τ_0 / τ_2 vs. [Q] in the usual Stern Völmer method. By using three different quencher concentrations, we have constructed this plot and found that the quenching rate constant at 220 K is 2.2 times slower than that at room temperature. This is attributed to restricted collisional motion between molecules at the lower temperature. However, there is some error in this calculation, and this will be described later in this section. (4) At a given temperature $\chi_{(P-Q)}$, which is the mole fraction of the hydrogen-bonded complex, increases with increase in quencher concentration as expected. It can also be noted that for a given quencher

concentration, $\chi_{(P-Q)}$ increases with decrease in temperature. This suggests that the association constant for complex formation is larger at lower temperatures. The association constant K_a obtained from a plot of $\chi_{(P-Q)}/\chi_{(P)}$ vs. [5] at 220 K was found to be 2.05 times larger than that obtained at room temperature. (5) The χ^2 values for the fits are given in the last column in Tables 4.2 - 4.4. χ^2 values below 1.3 are considered good. In Tables 4.3 and 4.4 we can see that some of the χ^2 values are greater than 1.3. This is attributed to the precipitation of a small amount of the quencher **5** during the experiment. The single photon counting experiment usually takes 2 - 3 hours for data collection and during this period a small amount of **5** can precipitate out if the quencher concentration is high (> 1 mM) and the temperature is very low. Thus the quencher concentration varies slightly during the experiment and this leads to some errors in the values of τ_2, $\chi_{(P-Q)}$ and $\chi_{(P)}$. This in turn leads to slightly higher values of χ^2. It should be noted here that in the temperature dependence study described in this chapter we are concerned only with the τ_1 values. τ_2, $\chi_{(P-Q)}$ and $\chi_{(P)}$ values are not used for any quantitative analysis in this chapter. τ_1 values, as mentioned earlier, are independent of quencher concentration and hence will not be affected by precipitation of small amounts of **5** during the experiment. Thus, we believe that the k_{et} values reported in this chapter are largely free from these kinds of errors.

4.3.3. Fluorescence lifetime quenching studies of PA/6 system at different temperatures

In order to study the temperature dependence of electron transfer in the PA/6 system. fluorescence decays of **PA** in the presence of **6** were obtained at different temperatures. In this case also we have noticed that precipitation of small amounts of the quencher occurs at low temperatures when the quencher concentration is > 1 mM. Hence at temperatures below 250 K decay profiles were recorded only at 1 mM concentration of **6**. Representative examples of decay profiles are shown in Figures 4.6 - 4.9. As can be seen in these figures the decays were clearly biexponential. These were fitted to biexponential functions and values of the parameters thus obtained are presented in Tables 4.5 - 4.7.
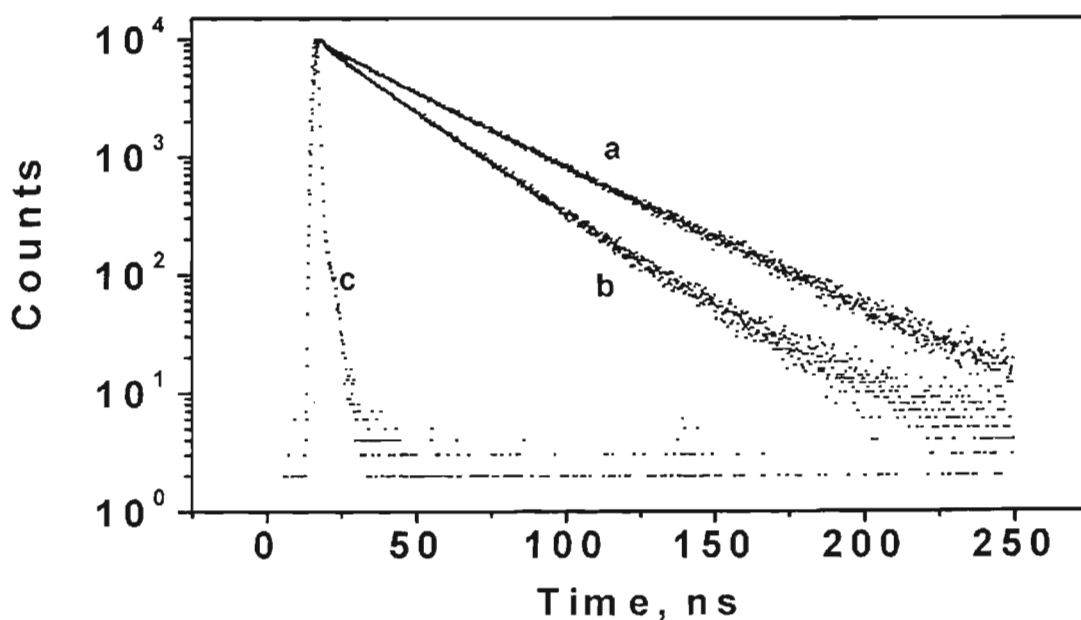
Figure 4.6. The fluorescence decay profiles of PA/6 at 280 K. (a) [PA] = 1 x 10⁻⁵ M, [6] = 1.5 x 10⁻³ M; (b) [PA] = 1 x 10⁻⁵ M, [6] = 2.0 x 10⁻³ M. (c) lamp profile.
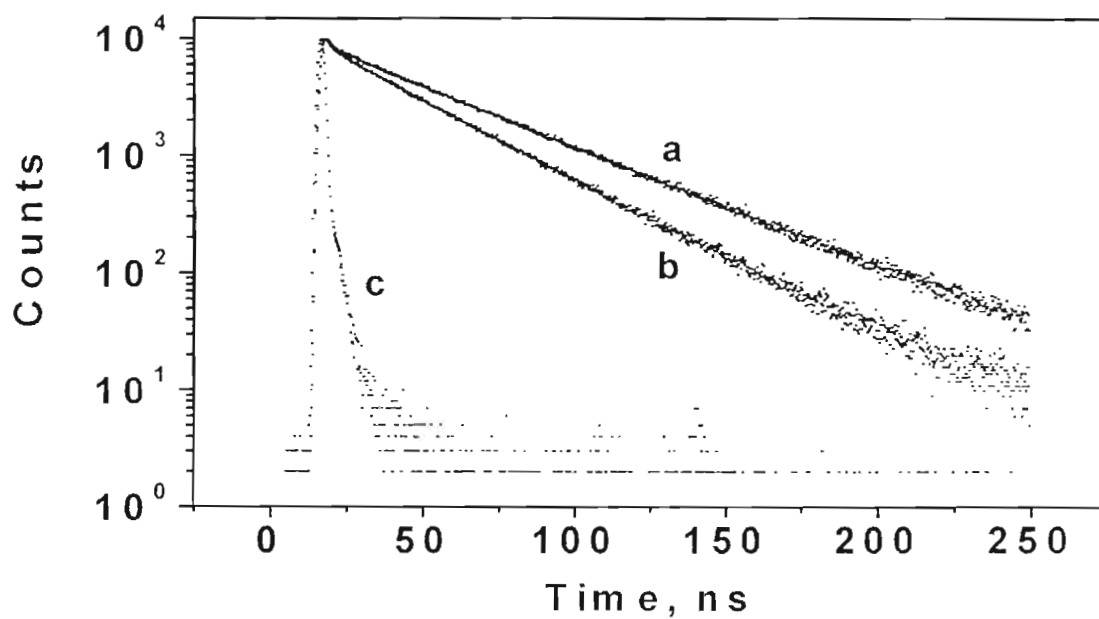
Figure 4.7. The fluorescence decay profiles of PA/6 at 270 K. (a) [PA] = 1 x 10^{-5} M, [6] = 1.5 x 10^{-3} M; (b) [PA] = 1 x 10^{-5} M, [6] = 2.0 x 10^{-3} M. (c) lamp profile.
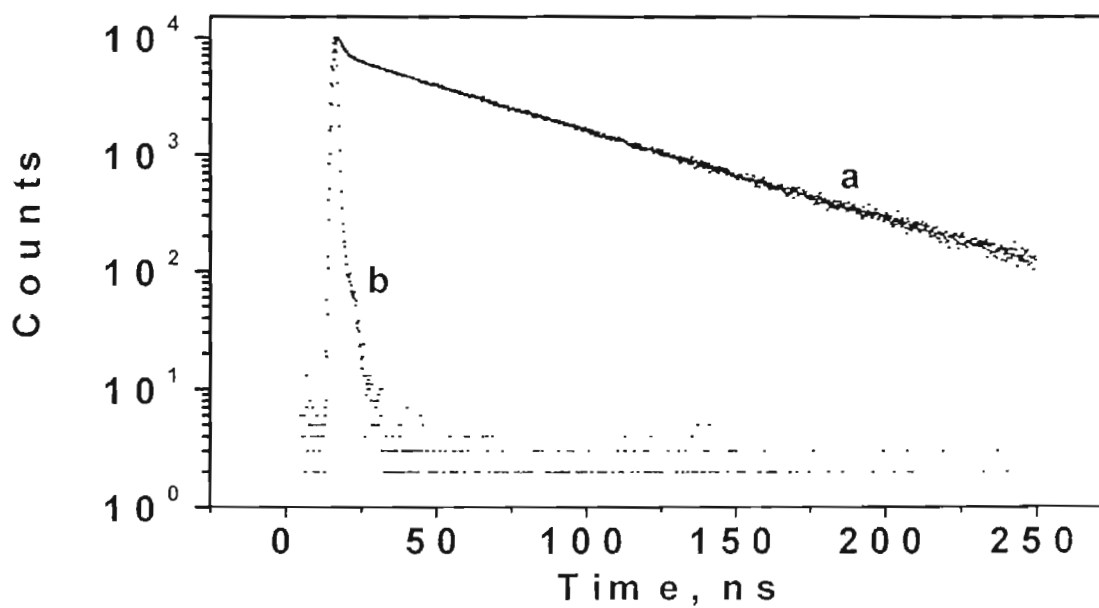
Figure 4.8. The fluorescence decay profiles of PA/6 at 240 K. (a) [PA] = 1 x 10^{-5} M, [6] = 1.5 x 10^{-3} M; (b) lamp profile.
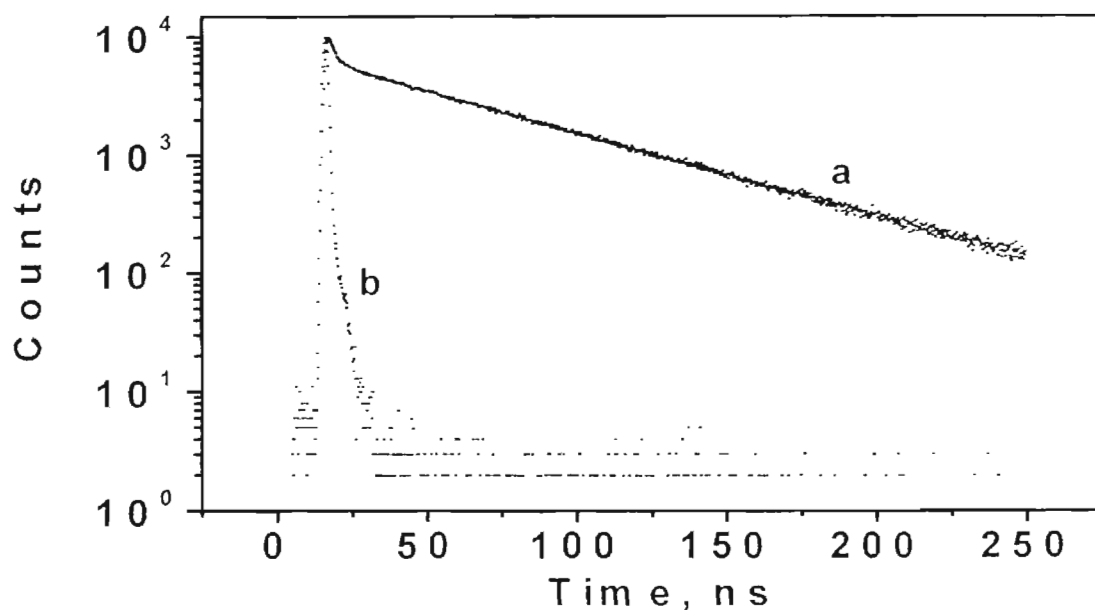
Figure 4.9. The fluorescence decay profiles of PA/6 at 220 K. (a) [PA] = 1 x 10^{-5} M, [6] = 1.5 x 10^{-3} M. (b) lamp profile.

Table 4.5. Fluorescence lifetimes (τ_1 and τ_2), fractional contributions (χ_{P-Q} and χ_P) and χ^2 values obtained for the fluorescence quenching of PA by 6 at different temperatures. [PA] was 1 x 10^{-5} M and [6] was 1 x 10^{-3} M.

Temperature, K	τ_1, ns	χ_{P-Q}, %	τ_2, ns	χ_P, %	χ^2
298	2.10	1.98	47.80	98.02	1.2
280	2.20	2.06	52.65	97.94	1.1
270	2.00	3.62	53.70	96.38	1.0
260	2.03	4.93	56.08	95.07	1.2
250	1.95	5.06	59.87	94.94	1.0
240	1.90	6.52	65.07	93.48	1.0
230	1.98	9.28	68.81	90.72	1.3
220	1.92	10.12	72.02	89.88	1.1

Table 4.6. Fluorescence lifetimes (τ_1 and τ_2), fractional contributions (χ_{P-Q} and χ_P) and χ^2 values obtained for the fluorescence quenching of PA by 6 at different temperatures. [PA] was 1 x 10^{-5} M and [6] was 1.5 x 10^{-3} M.

Temperature	τ_1, ns	χ_{P-Q}, %	τ_2, ns	χ_P, %	χ^2
298	2.12	3.50	26.72	96.44	1.1
280	2.23	5.62	32.50	94.38	1.2
270	2.00	8.15	37.63	91.85	1.1
260	2.02	12.05	39.82	87.95	1.0
250	1.96	14.50	46.02	85.50	1.1

Table 4.7. Fluorescence lifetimes (τ_1 and τ_2), fractional contributions (χ_{P-Q} and χ_P) and χ^2 values obtained for the fluorescence quenching of PA by 6 at different temperature. [PA] was 1x10^{-5} M and [6] was 2 x 10^{-3} M.

Temperature, K	τ_1, ns	χ_{P-Q}, %	τ_2, ns	χ_P, %	χ^2
298	2.10	5.82	19.89	94.18	1.2
280	2.20	7.85	21.36	92.15	1.1
270	2.12	10.23	25.06	97.88	1.1
260	2.03	12.58	34.63	87.42	1.1
250	1.94	13.06	39.83	86.94	1.2

Analysis of the data in Tables 4.5 - 4.7 shows that most of the observations made in the case of **PA/5** are true in the case of **PA/6** also. In the temperature range of 250 - 298 K, where three different quencher concentrations were studied, τ_1 values were found to be independent of quencher concentration. It can be seen from

Table 4.5 that, in the temperature range of 220 - 298 K, τ_1 varied only marginally. From the τ_1 values, k_{et} values were calculated using equation 4.2 and these are presented later in Table 4.9.

Tables 4.5 - 4.7 showed that $\chi_{(P-Q)}$ increases with decrease in temperature. This aspect can be easily inferred from a visual comparison of Figures 4.6 - 4.9. The short lifetime component for the **PA/6** system ([**6**] = 1 mM) is not very distinct at 298 K (Figure 4.6) but is clearly observable at 220 K (Figure 4.9). This clearly demonstrates that the association constant for hydrogen bond formation increases as the temperature is lowered.

4.3.4. Fluorescence lifetime quenching studies of PA/7 system at different temperatures

In the **PA/7** system, pyrene acts as the donor moiety and dinitrophenyl group acts as the acceptor moiety. The free energy change for this system lies in the deep inverted region and hence the rate constant for electron transfer is very low. It was also observed that the decay profiles in this case did not appear clearly biexponential due to the relatively large values of τ_1 (see Chapter 2). In order to study the temperature dependence of electron transfer rate constant in the **PA/7** system, fluorescence decays of **PA** in the presence of **7** were obtained at different temperatures. Since the solubility of **7** was low compared to that of **6**, these experiments were carried out at only one low concentration of **7**. Typical decay profiles are given in Figures 4.10 and 4.11. The decays at all temperatures were fitted to equation 4.1 and the parameters obtained are collected in Table 4.8.
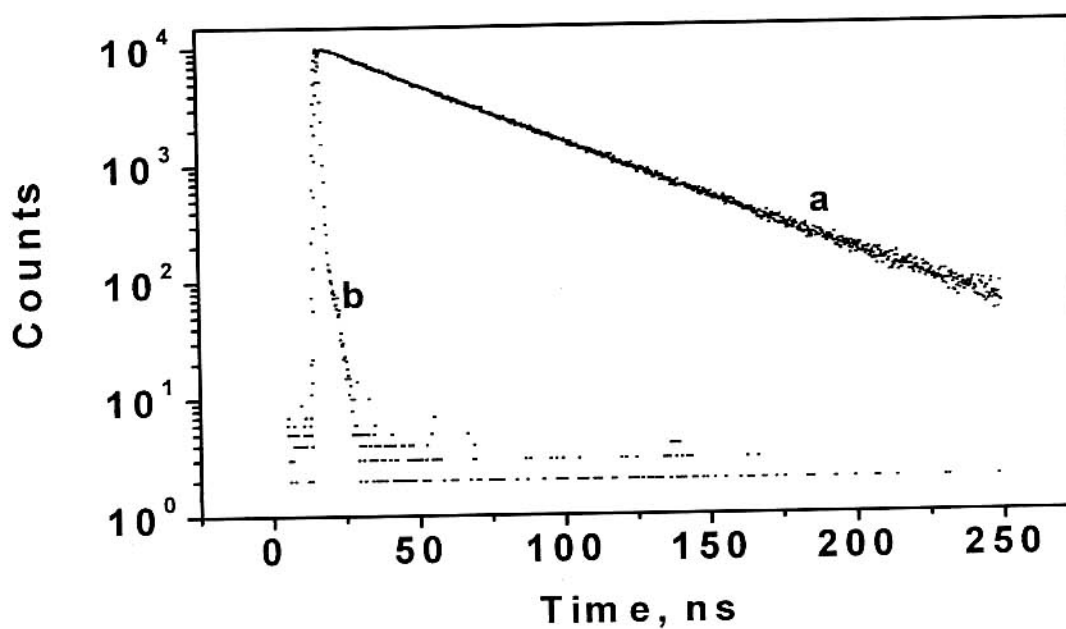
Figure 4.10. The fluorescence decay profiles of PA (1 x 10^{-5} M) in the presence of 7 (1 x 10^{-3}M) in dichloromethane at 280 K. (b) is the lamp profile.
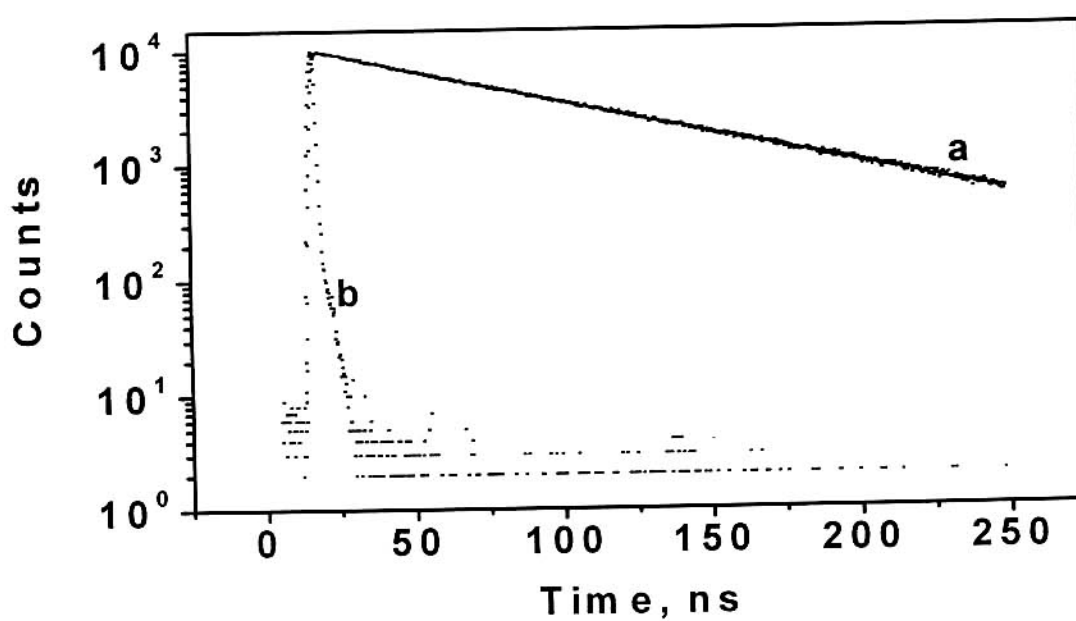
Figure 4.11. The fluorescence decay profiles of PA (1 x 10^{-5} M) in the presence of 7 (1 x 10^{-3}M) in dichloromethane at 220 K. (b) is the lamp profile.

Table 4.8. Fluorescence lifetimes (τ_1 and τ_2), fractional contributions (χ_{P-Q} and χ_P) and χ^2 values obtained for the fluorescence quenching of PA by 7 at different temperature. [PA] was 1 x 10^{-5} M and [7] was 1 x 10^{-3} M.

Temperature, K	τ_1, ns	χ_{P-Q}, %	τ_2, ns	χ_P, %	χ^2
298	19.20	1.41	45.60	98.59	1.1
280	20.72	1.56	66.26	98.44	1.0
270	20.40	1.98	70.65	98.02	1.1
260	21.88	2.20	74.19	97.80	1.1
250	20.47	2.47	76.60	97.53	1.0
240	18.39	3.00	80.78	97.00	1.0
230	18.90	3.74	81.40	96.26	1.2
220	20.12	3.82	82.80	96.18	1.0

Notice that the χ^2 values for the fits are ≤ 1.2, which indicate that the fit is very good in all cases. An inspection of the table shows that τ_1 is independent of temperature within experimental error. From the τ_1 values electron transfer rate constants (k_{et}) for hydrogen-bonded **PA/7** were calculated and these are presented in Table 4.9.

4.3.5. Temperature dependence of electron transfer rate constants for hydrogen-bonded systems

As mentioned in the previous sections, we have collected the fluorescence decays of the **PA/5**, **PA/6** and **PA/7** systems at several temperatures in the 220 - 298 K range. The observed decays were fitted to biexponential functions.

The short lifetime component (τ_1) obtained in each case was attributed to electron transfer within the hydrogen-bonded complex. From the τ_1 values rate constants for electron transfer within the hydrogen-bonded complex (k_{et}) were calculated using equation 4.2 and the values obtained for the three systems at various temperatures are presented below in Table 4.9.

Table 4.9. Electron transfer rate constants (k_{et}) for hydrogen-bonded donor-acceptor systems PA/5, PA/6 and PA/7 at various temperatures.

Temperature, K	k_{et}, 10^7 s^{-1}		
	PA/5	PA/6	PA/7
298	90.15 ± 7.6	46.88 ± 2.3	4.45 ± 0.60
280	84.80 ± 8.5	44.78 ± 2.0	4.16 ± 0.45
270	82.71 ± 8.2	49.38 ± 1.9	4.28 ± 0.47
260	80.07 ± 7.8	48.64 ± 1.8	3.99 ± 0.37
250	73.50 ± 5.9	50.71 ± 1.8	4.31 ± 0.48
240	71.37 ± 5.5	52.06 ± 1.4	4.84 ± 0.50
230	66.04 ± 2.6	49.95 ± 1.0	4.73 ± 0.51
220	60.05 ± 1.9	51.53 ± 1.0	4.41 ± 0.44

An inspection of Table 4.9 reveals the following facts. For the **PA/5** system, which lies in the normal region, the rate constant for electron transfer increased from 6.0 x 10^8 s^{-1} at 220 K to 9.02 x 10^8 s^{-1} at 298 K. This is an Arrhenius type of behaviour. For the **PA/6** system, which falls in the inverted

region, the rate constant exhibited an oscillatory behaviour. It is perhaps more appropriate to consider that k_{et} is independent of temperature for this system. For the **PA/7** system, which falls in the deep inverted region, rate constant is again found to be independent of temperature. Thus our study shows that, for hydrogen-bonded donor-acceptor systems, electron transfer rate constants in the normal region follows Arrhenius type of behaviour but in the inverted region rates are independent of temperature. In the following section we have tried to analyse this result using classical and semiclassical electron transfer theories.

4.4. Discussion

According to the classical Marcus description, electron transfer can be described as a thermally activated process where the Gibbs activation energy ($\Delta G^{\#}$) is given by equation 4.3,[31]

$$\Delta G^{\#} = (\Delta G^{\circ} + \lambda)^2 / 4\lambda \qquad (4.3)$$

In equation 4.3, λ is the total reorganization energy and is given by

$$\lambda = \lambda_i + \lambda_o \qquad (4.4)$$

where, λ_i is the inner-sphere reorganization energy and λ_o is the outer-sphere reorganization energy. The rate constant for electron transfer is then given by [32-36]

$$k_{et} = (2\pi/\hbar) \, H_{el}^2 \, (4\pi\lambda k_B T)^{-1/2} \exp [-(\lambda + \Delta G^{\circ})^2/4\lambda k_B T] \qquad (4.5)$$

where, $\hbar$ is the Planck's constant divided by 2π, H_{el} is the electronic matrix element coupling the reactant and product states and k_B is the Boltzmann constant. In this equation the temperature term appears both in the pre-exponential and exponential parts. In the pre-exponential factor the temperature term appears as its square root and hence its effect on the rate constant will be small. Thus, the major effects due to the temperature comes from the exponential term. But the exponential term depends on the values of $\Delta G°$ and λ and vanishes when $\Delta G° = -\lambda$. Thus, temperature dependence studies of electron transfer reactions are meaningful only if the $\Delta G°$ values are also addressed, because the slopes of the Arrhenius plots will vary depending on the $\Delta G°$ value. In summary, equation 4.5 predicts that when $\Delta G° = -\lambda$, rates of electron transfer reactions will be nearly temperature independent, but when $\Delta G° \neq -\lambda$, an activation barrier will be present and this will result in an Arrhenius type of rate dependence on temperature.

Electron transfer rate constants for the **PA/5** system were found to increase with increase in temperature. We have attempted to fit the data to equation 4.5 using calculated values of λ, $\Delta G°$ and H_{el}. For electron transfer between aromatic donor-acceptor systems λ_i is small and a value of 0.2 eV is assumed in several cases[10,37,38] and we have also used this value. λ_o was calculated using equation 4.6.[39,40]

$$\lambda_o = \Delta e^2 \left(\frac{1}{2r_p} + \frac{1}{2r_q} - \frac{1}{d_c} \right) \left(\frac{1}{\varepsilon_{op}} - \frac{1}{\varepsilon_s} \right) \qquad (4.6)$$

In equation 4.6, r_P and r_Q are the radii of the probe and quencher molecules, d_c is the centre-to-centre distance between them and ε_{op} and ε_s are the optical and static dielectric constants of the solvent. Values of 6 and 4 Å were used for r_P and r_Q and 12 Å was used for d_c. The free energy change can be calculated using the Weller equation 4.7 [41]

$$\Delta G^0 = E_{ox} - E_{red} - E_{0,0} - \frac{e^2}{2}\left(\frac{1}{r_P} + \frac{1}{r_Q} \right)\left(\frac{1}{\varepsilon_{ACN}} - \frac{1}{\varepsilon_s} \right) - \frac{e^2}{\varepsilon_s\, d_C} \qquad (4.7)$$

where E_{ox} and E_{red} are the electrochemical oxidation and reduction potentials of the donor and acceptor measured in acetonitrile, $E_{0,0}$ is the excitation energy of **PA** (3.6 eV), d_c is the centre-to-centre charge separation distance, ε_{ACN} is the dielectric constant of acetonitrile and ε_s is the dielectric constant of the solvent used for the electron transfer studies (dichloromethane).

To calculate λ_o and ΔG° values the optical and static dielectric constants of the solvents are required. Dielectric properties of solvents are known to be temperature dependent and hence from equation 4.6 and 4.7 it follows that λ_o and ΔG° values are temperature dependent. To fit the observed data to the Marcus equation we need to know λ_o and ΔG° values at the various temperatures.

ε_s and ε_{op} values for dichloromethane at several temperatures in the 230 - 280 K range are reported by Liu *et. al.*[12] For the present studies we required ε_s and ε_{op} values at 220 and 298 K also. In order to obtain these values we have plotted the reported values of ε_s and ε_{op} against temperature. Linear plots (r > 0.99)

were obtained in both the cases, which indicated that changes in ε_s and ε_{op} with temperature are linear. Values of ε_s and ε_{op} for dichloromethane at 220 and 298 K were obtained by extrapolation of these plots.

Dielectric constant of acetonitrile at any temperature T can be obtained from the following empirical relation.[13]

$$\varepsilon_{ACN} = 37.45 - 0.155 \, (T - 293) \tag{4.8}$$

In Table 4.10, we have presented calculated values of λ_o and $\Delta G°$ for the systems at various temperatures. From Table 4.10 it can be seen that as the temperature is decreased λ_o shows an increase while $\Delta G°$ shows a decrease.

Table 4.10. Static (ε_s) and optical (ε_{op}) dielectric constants for dichloromethane and calculated λ_o and $\Delta G°$ values for the donor-acceptor systems at various temperatures.

Temp. K	ε_s	ε_{op}	λ_o, eV	$\Delta G°$, eV		
				PA/5	PA/6	PA/7
298	8.65	2.028	0.6795	-0.5041	-1.164	-1.404
280	9.70[a]	2.045[a]	0.6946	-0.521	-1.180	-1.421
270	10.29[a]	2.054[a]	0.7015	-0.528	-1.189	-1.429
260	10.88[a]	2.063[a]	0.7074	-0.535	-1.195	-1.435
250	11.47[a]	2.072[a]	0.7117	-0.541	-1.201	-1.441
240	12.06[a]	2.081[a]	0.7162	-0.547	-1.207	-1.447
230	12.65[a]	2.091[a]	0.7189	-0.551	-1.211	-1.451
220	13.23	2.100	0.7211	-0.556	-1.216	-1.456

[a] Taken from reference 12

The values of λ_o, ΔG° and observed values of k_{et} at 298 K were then substituted in equation 4.5 to obtain H_{el}. The value obtained was 3.94 cm^{-1}. Assuming that H_{el} values are temperature independent, we have calculated k_{et} values at various temperatures using equation 4.5. Calculations were actually performed for all the four possible situations, which include: (a) constant ΔG° and λ_o (k^a_{cal}); (b) Constant ΔG° and temperature dependent λ_o (k^b_{cal}); (c) constant λ_o and temperature dependent ΔG° (k^c_{cal}) and (d) temperature dependent ΔG° and λ_o (k^d_{cal}). Calculated values for **PA/5** system are presented in Table 4.11 along with observed values.

Table 4.11. Observed (k_{et}) and calculated (k^a_{cal} - k^d_{cal}) electron transfer rate constants for PA/5 system at various temperatures. For calculations equation 4.5 was used.

Temp. K	k_{et}	k^a_{cal}	k^b_{cal}	k^c_{cal}	k^d_{cal}
	10^7 s^{-1}	10^7 s^{-1}	10^7 s^{-1}	10^7 s^{-1}	10^7 s^{-1}
298	90.15 ± 7.6	90.15	90.15	90.15	90.15
280	84.80 ± 8.5	84.14	75.05	97.36	87.14
270	82.71 ± 8.2	80.58	67.79	99.61	84.42
260	80.07 ± 7.8	76.86	61.39	101.89	82.40
250	73.50 ± 5.9	72.97	55.53	103.27	80.01
240	71.37 ± 5.5	68.93	49.85	104.60	77.55
230	66.04 ± 2.6	64.73	43.53	103.88	74.54
220	60.05 ± 1.9	60.38	40.50	103.96	72.39

An inspection of Table 4.11 reveals that rate constants calculated assuming

situation (a) (*ie.* temperature independent λ_o and $\Delta G°$) are the closest to observed

values. This is plotted in Figure 4.12, where the triangles represent the observed

values and the solid line is a plot of k^a_{cal} *vs.* temperature. The second best fit is

provided by k^d_{cal} (obtained using temperature dependent λ_o and $\Delta G°$ values) and

this is shown as the dotted lines in Figure 4.12. k^b_{cal} values show a steep decrease

with decrease in temperature, whereas, k^c_{cal} values show an increase as

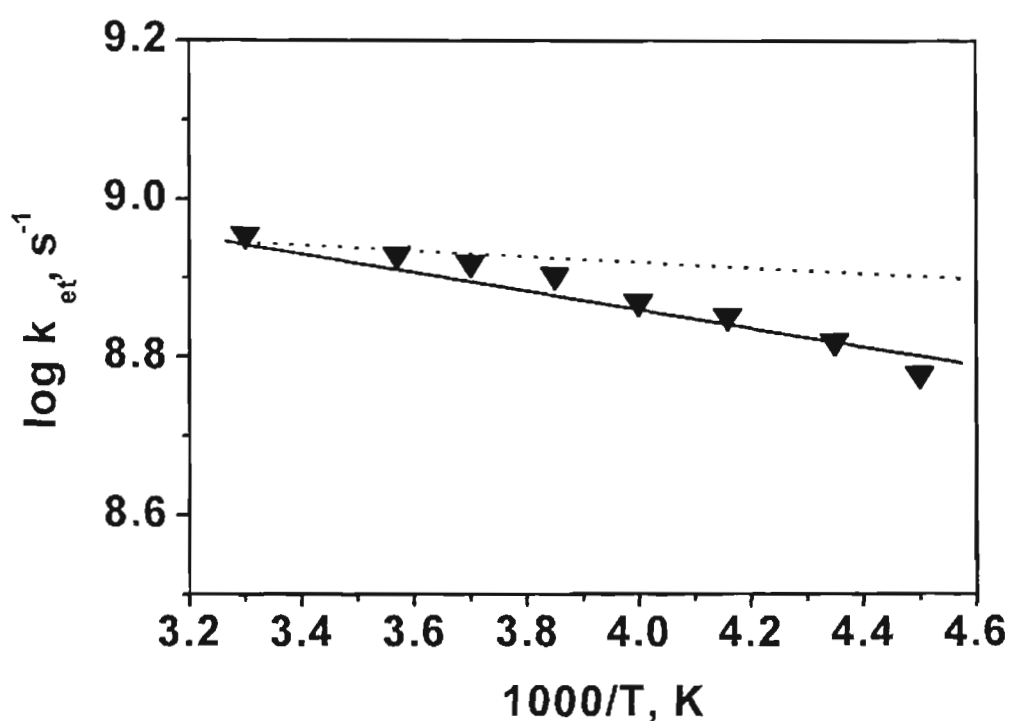temperature falls. It is clear that these two situations are not applicable here.

Figure 4.12. Temperature dependence of rate constants (k_{et}) for the PA/5 system in dichloromethane. ▼ are observed values, solid line is a fit to equation 4.5 using temperature independent $\Delta G°$ and λ_o and dotted line is the fit obtained using temperature dependent $\Delta G°$ and λ_o.

It is not clear as to why the k^a_{cal} values provided a better fit compared to the k^d_{cal} values. One possible reason is the choice of the r_p, r_Q and d_c values used in the calculation of λ_o. Slight changes in these values influence the λ_o values drastically and lead to changes in the calculated k_{el} values. Another reason could be the use of temperature independent H_{el} values in these calculations. H_{el} values are related to the coupling between the donor and acceptor and it is generally assumed that these values are temperature independent. In the case of hydrogen-bonded systems donor-acceptor coupling involves the hydrogen bond interface. We have noticed that the association constant for hydrogen bond formation is higher at lower temperatures. Hence we expect that the hydrogen bond interface will be stronger and more rigid at lower temperatures which may lead to changes in the values of H_{el}. Thus the assumption that H_{el} values are temperature independent may not be valid in the present case.

Attempts were made to correlate the observed rate constant for **PA/6** and **PA/7** systems to the Marcus equation. For this purpose we have calculated H_{el} values by substituting the observed k_{el} values at 298 K in equation 4.5. The values obtained were 2.04 and 1.84 cm^{-1} respectively, for **PA/6** and **PA/7** systems. Theoretical rate constants were then calculated for all the four cases for these two systems and the values are presented in Table 4.12 and 4.13.

Table 4.12. Observed (k_{et}) and calculated (k^a_{cal} - k^d_{cal}) electron transfer rate constants for PA/6 system at various temperatures. Equation 4.5 was used for the calculations.

Temp. K	k_{et} $10^7 s^{-1}$	k^a_{cal} $10^7 s^{-1}$	k^b_{cal} $10^7 s^{-1}$	k^c_{cal} $10^7 s^{-1}$	k^d_{cal} $10^7 s^{-1}$
298	46.88 ± 2.3	46.86	46.86	46.86	46.86
280	44.78 ± 2.0	45.64	50.67	40.88	45.71
270	49.38 ± 1.9	44.87	52.39	37.43	44.48
260	48.64 ± 1.8	44.02	53.71	34.77	43.64
250	50.71 ± 1.8	43.08	54.75	32.03	42.40
240	52.06 ± 1.4	42.06	55.75	29.30	41.08
230	49.95 ± 1.0	40.94	56.04	26.93	39.51
220	51.53 ± 1.0	39.71	56.09	24.60	37.76

Table 4.13. Observed (k_{et}) and calculated (k^a_{cal} - k^d_{cal}) electron transfer rate constants for PA/7 system at various temperatures. Equation 4.5 was used for the calculations.

Temp. K	k_{et} $10^7 s^{-1}$	k^a_{cal} $10^7 s^{-1}$	k^b_{cal} $10^7 s^{-1}$	k^c_{cal} $10^7 s^{-1}$	k^d_{cal} $10^7 s^{-1}$
298	4.45 ± .60	4.45	4.45	4.45	4.45
280	4.16 ± .45	3.78	4.74	3.05	3.87
270	4.28 ± .47	3.41	4.79	2.46	3.52
260	3.99 ± .37	3.06	4.73	2.00	3.20
250	4.31 ± .48	2.71	4.59	1.60	2.84
240	4.84 ± .50	2.38	4.43	1.25	2.49
230	4.73 ± .51	2.06	4.12	0.99	2.14
220	4.41 ± .44	1.76	3.78	0.75	1.77

An inspection of Table 4.12 shows that these calculations have not yielded temperature independent rate constants for the **PA/6** system. k^a_{cal}, k^c_{cal} and k^d_{cal} values increase with temperature while k^b_{cal} shows the opposite trend. Values of k^a_{cal} and k^d_{cal} are very similar at all the temperatures. In Figure 4.13 experimental k_{et} values ($\blacktriangledown$) for this system are plotted along with k^a_{cal} (solid line) and k^b_{cal} (dotted line) values. Calculated fits are close to the observed values at higher temperature but deviates significantly as the temperature is lowered. Inspection of Table 4.13, where the observed and calculated electron transfer rate constants for the **PA/7** systems are presented, also yielded similar conclusions. For this case also experimental k_{et} values ($\bullet$) are plotted in Figure 4.13 along with k^a_{cal} (solid line) and k^b_{cal} (dotted line) values. It can be seen from the figure that, for the **PA/7** system, k^a_{cal} fit deviates significantly at lower temperatures, whereas the k^b_{cal} fit matches reasonably well with the observed values.

Our analysis has shown that the classical Marcus equation can not adequately explain the temperature independent electron transfer rate constants observed for the **PA/6** and **PA/7** systems. Examination of equation 4.5 shows that temperature independent behaviour can be expected when $\Delta G^o = -\lambda$. Under such conditions the free energy of activation, $\Delta G^\# = 0$ and the rate constant of electron transfer will be almost temperature independent. Examination of Table 4.10 shows that for both **PA/6** and **PA/7** systems, at all the temperatures, $\Delta G^o \neq -\lambda$.
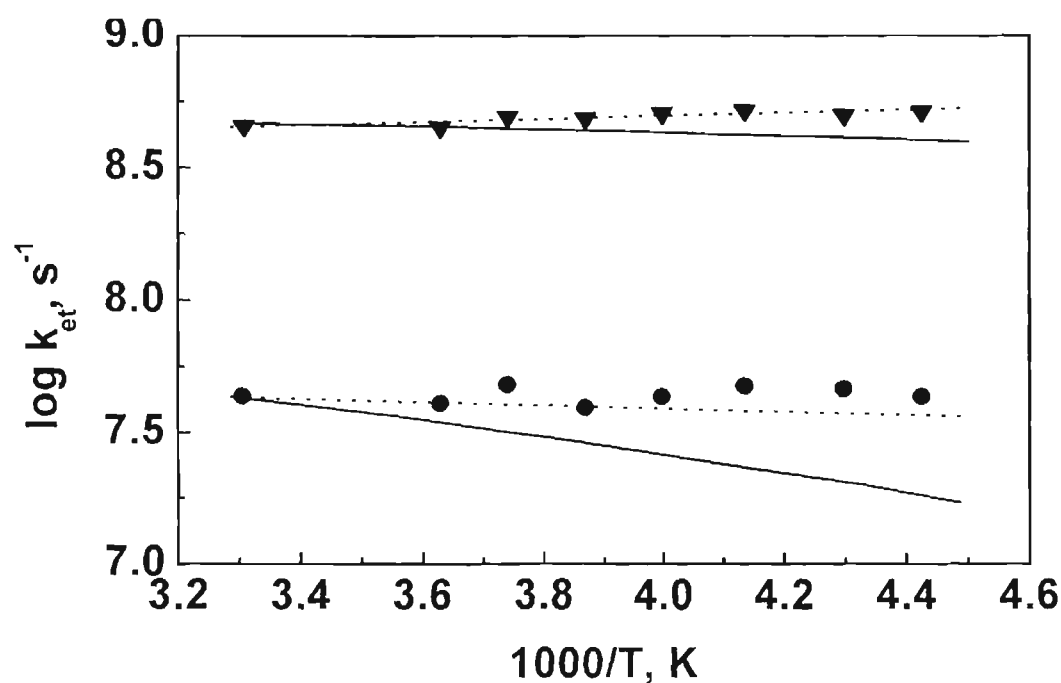
Figure 4.13. Temperature dependence of electron transfer rate constants for the PA/6 (▲) and PA/7 (●) systems. Solid lines are fits to equation 4.5 using constant ΔG° and λ_o values. Dotted lines are fits obtained using constant ΔG° and temperature dependent λ_o values.

Thus the possible reason of $\Delta G^\circ = -\lambda$, for observing the temperature independent behaviour for **PA/6** and **PA/7**, can be ruled out. As mentioned previously, temperature independent electron transfer rate constants were observed in the inverted region by others also and the reason suggested for this is the following.

According to Marcus theory electron transfer can occur only at the intersection of two potential surfaces. In the inverted region, where the vibrational wave functions of the reactant and product are embedded, the dominant reaction pathway may involve nuclear tunneling *via* one or more high frequency vibrational

modes. It was found that under these conditions the electron transfer process is better described by equation 4.9. [42-46]

$$k_{el} = 2\pi/\hbar \ H_{el}{}^2 (4\pi\lambda_o k_B T)^{-1/2} \sum_{m=0}^{\alpha} (e^{-s} s^m /m!) \exp\{-[(\lambda_o + \Delta G^o + mh\nu)^2/4\lambda_o k_B T]\} \quad (4.9)$$

where, m is an integer and $s = \lambda_i/h\nu$. Equation 4.9 is based on the golden rule in which the Frank-Condon term is calculated by a quantum mechanical treatment and the solvent modes are calculated by a classical treatment. In this equation the high frequency quantum modes are represented by a single (average) vibrational mode. The high frequency intramolecular vibrational excitations of the donor and acceptor centres provide several parallel channels involving the vibrational excitations of these modes, which are induced by electron transfer. In the inverted region, this leads to a reduction in the effective free energy gap and a lowering of the activation energy and this leads to substantial modification of electron transfer rates. It can be shown that in the limiting case of $h\nu \ll k_B T$, equation 4.9 will be identical to equation 4.5.

We have made an attempt to fit the observed data for **PA/6** and **PA/7** to equation 4.9. For electron transfers involving aromatic molecules a skeletal vibration of $h\nu = 1500$ cm^{-1} was used by several authors and we adopted this value for our calculations.[11,16] Values of $h\nu$, λ_o, ΔG^o and k_{el} (at 298 K) were substituted in equation 4.9 to obtain H_{el} values. $H_{el} = 2.06$ and 1.14 cm^{-1} were obtained for **PA/6** and **PA/7** systems, respectively. These values were subsequently used to

calculate the rate constants at various temperatures for the four different situations: (a) $\Delta G°$ and λ_o constant (k^a_{cal}); (b) $\Delta G°$ constant and λ_o temperature dependent (k^b_{cal}); (c) $\Delta G°$ temperature dependent and λ_o constant (k^c_{cal}) and (d) $\Delta G°$ and λ_o temperature dependent (k^d_{cal}). The calculated values along with the experimental values of k_{et} for **PA/6** are given in Table 4.14 and for **PA/7** are given in Table 4.15.

Table 4.14. Observed (k_{et}) and calculated (k^a_{cal} - k^d_{cal}) electron transfer rate constants for PA/6 system a various temperatures. Equation 4.9 was used for the calculations.

Temp. K	k_{et} 10^7 s^{-1}	k^a_{cal} 10^7 s^{-1}	k^b_{cal} 10^7 s^{-1}	k^c_{cal} 10^7 s^{-1}	k^d_{cal} 10^7 s^{-1}
298	46.88 ± 2.3	46.86	46.86	46.86	46.86
280	44.78 ± 2.0	46.55	49.49	43.61	46.49
270	49.38 ± 1.9	46.36	50.70	41.78	45.97
260	48.64 ± 1.8	46.16	51.65	40.47	45.72
250	50.71 ± 1.8	45.96	52.45	39.14	45.28
240	52.06 ± 1.4	45.74	53.23	37.84	44.83
230	49.95 ± 1.0	45.51	53.64	36.80	44.29
220	51.53 ± 1.0	45.27	53.94	35.80	43.70

Table 4.15. Observed (k_{et}) and calculated (k^a_{cal} - k^d_{cal}) electron transfer rate constants for PA/7 system a various temperatures. Equation 4.9 was used for the calculations.

Temp. K	k_{et}	k^a_{cal}	k^b_{cal}	k^c_{cal}	k^d_{cal}
	$10^7 \, s^{-1}$	$10^7 \, s^{-1}$	$10^7 \, s^{-1}$	$10^7 \, s^{-1}$	$10^7 \, s^{-1}$
298	$4.45 \pm .60$	4.45	4.45	4.45	4.45
280	$4.16 \pm .45$	4.32	4.77	3.90	4.32
270	$4.28 \pm .47$	4.25	4.91	3.65	4.24
260	$3.99 \pm .37$	4.18	5.01	3.45	4.17
250	$4.31 \pm .48$	4.10	5.07	3.26	4.07
240	$4.84 \pm .50$	4.03	5.13	3.07	3.97
230	$4.73 \pm .51$	3.96	5.14	2.93	3.87
220	$4.41 \pm .44$	3.89	5.12	2.78	3.73

Inspection of Tables 4.14 and 4.15 reveals that the calculated k^a_{cal} - k^d_{cal} values do not match exactly with the observed values. k^a_{cal}, k^c_{cal} and k^d_{cal} values show slight increase with temperature while k^b_{cal} show the opposite trend. Notice, however, that k^a_{cal} and k^d_{cal} values are very similar and their deviation from the observed values are only marginal at all temperatures. In Figure 4.14 we have reproduced the observed k_{et} values along with the k^a_{cal} fit to equation 4.9 (solid lines). Since k^a_{cal} and k^d_{cal} values are very similar, k^d_{cal} fit will also be equally good.
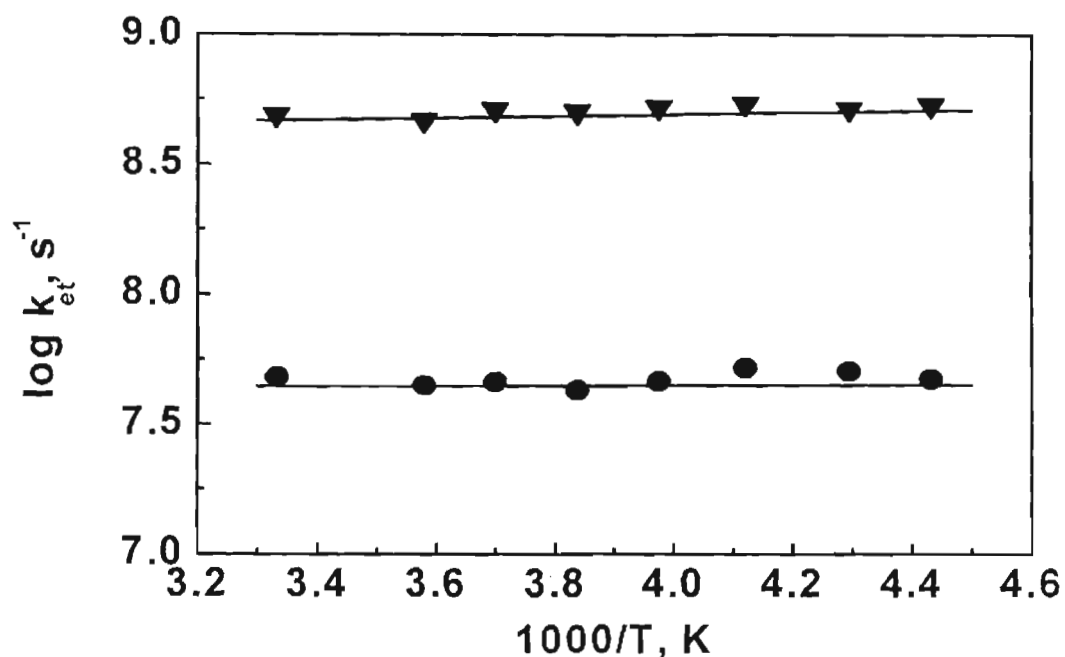
Figure 4.14. Temperature dependence of rate constants (k_{et}) for the PA/6 ($\blacktriangledown$) and for the PA/7 ($\bullet$) systems in dichloromethane. Solid lines are fits to equation 4.9 using temperature independent λ_o and $\Delta G°$ values.

A comparison of Figures 4.13 and 4.14 shows that the golden rule expression is more appropriate to describe the temperature dependence of electron transfer reactions for **PA/6** and **PA/7** systems which fall in the inverted region, compared to the classical Marcus equation 4.5. It is to be noted here that the coupling constant H_{el} is assumed to be temperature independent in these calculations. As mentioned previously, H_{el} values can be temperature dependent in the case of hydrogen-bonded systems. Better fits to the data may be obtained if this factor is also taken into consideration.

4.5. Conclusions

This chapter reports the first study on the temperature dependence of electron transfer in hydrogen-bonded donor-acceptor systems. We have studied the temperature dependence in three hydrogen-bonded systems, one of which belong to the normal region and the remaining two fall in the inverted region. Our results show that the Marcus treatment provides a good estimate of the temperature dependence of electron transfer rates in the normal region. Electron transfer rates for the systems in the inverted region were nearly independent of temperature and could be adequately explained by the golden rule expression. Our results thus are similar to those obtained by Liang *et al.*[10] and Kroon *et al.*[13] for covalently linked donor-acceptor systems. It is concluded that the temperature dependence of electron transfer rates in hydrogen-bonded systems are similar to those in covalently linked systems. The temperature independent electron transfer processes reported here for the systems in the inverted region also resemble the temperature independent electron transfer processes in photosynthetic reaction centres and may throw some light on the understanding of this important problem.

4.6. Experimental Section

4.6.1. Methods

The absorption spectra were recorded on a Shimadzu-3101PC UV-Vis-NIR scanning spectrophotometer. Fluorescence spectra were recorded on a SPEX Fluorolog F112X spectrofluorimeter. Fluorescence decays were measured with a

time correlated single photon counting fluorimeter (Edinburgh Instruments FL900CD) equipped with a pulsed hydrogen discharge lamp operating at 0.4 bar. For lifetime measurements, the probe concentrations were 1×10^{-5} M and quencher concentrations were in the range of $(1 - 2) \times 10^{-3}$ M. The excitation was at 345 nm and the emission was collected at 375 nm. Temperature control over the range + 25 °C to – 50 °C (± 0.1 °C) was provided by a Lauda model RC 6 CP low temperature thermostat.

4.6.2. Materials

All the probes and quencher molecules used for this study were available from studies reported in earlier chapters. The dichloromethane used for fluorescence lifetime measurements were rigorously dried and deaerated before use.

4.7. References

1. Baggot, J. E. in *Photoinduced Electron Transfer, Part B*; Fox, M. A., Channon, M., Eds.; Elsevier: Amsterdam, 1988; p 385.

2. Baggot, J. E.; Pilling, M. J. *J. Chem. Soc., Faraday Trans.* **1983**, *1*, 79.

3. Baggot, J. E.; Pilling, M. J. *J. Phys. Chem.* **1980**, *84*, 3012.

4. Anderson, S.; Constable, E. C.; Seddon, K. R.; Turp, J. E.; Baggot, J. E.; Pilling, M. J. *J. Chem. Soc., Dalton Trans.* **1985**, 2247.

5. Heitele, H.; Michel-Beyerle, M. E.; Finckh, P. *Chem. Phys. Lett.* **1987**, *138*, 237.

6.   Smit, K. J.; Warman, J. M.; de Haas, M. P.; Paddon-Row, M. N.; Oliver, A. M. *Chem. Phys. Lett.* **1988**, *152*, 177.

7.   Liang, N.; Miller, J. R.; Closs, G. L. *J. Am. Chem. Soc.* **1989**, *111*, 8740.

8.   Heitele, H; Finckh, P.; Weeren, S.; Poellinger, F.; Michel-Beyerle, M. E. *J. Phys. Chem.* **1989**, *93*, 5173.

9.   Delaney, J. K.; Mauzerall, D. C.; Lindsey, J. S. *J. Am. Chem. Soc.* **1990**, *112*, 957.

10. Liang, N.; Miller, J. R.; Closs, G. L. *J. Am. Chem. Soc.* **1990**, *112*, 5353.

11. Bixon, M.; Jortner, J. *J. Phys. Chem.* **1991**, *95*, 1941.

12. Liu, J.-Y.; Bolton, J. R. *J. Phys. Chem.* **1992**, *96*, 1718.

13. Kroon, J.; Oevering, H.; Verhoeven, J. W.; Warman, J. M.; Oliver, A. M.; Paddon-Row, M. N. *J. Phys. Chem.* **1993**, *97*, 5065.

14. Chen, P.; Mecklenburg, S. L.; Meyer, T. J. *J. Phys. Chem.* **1993**, *97*, 13126.

15. Fraser, D. D.; Bolton, J. R. *J. Phys. Chem.* **1994**, *98*, 1626.

16. Heitele, H.; Pöllinger, F.; Häberle, T.; Michel-Beyerle, M. E.; Staab, H. A. *J. Phys. Chem.* **1994**, *98*, 7402.

17. Khundkar, L. R.; Perry, J. W.; Hanson, J. E.; Dervan, P. B. *J. Am. Chem. Soc.* **1994**, *116*, 9700.

18. Moser, J. E.; Grätzel, M. *Chem. Phys.* **1993**, *176*, 493.

19. DeVault, D.; Chance, B. *Biophys. J.* **1966**, *6*, 825.

20. Schenck, C. C.; Parson, W. W.; Holten, D.; Windsor, M. W.; Sarai, A. *Biophys. J.* **1981**, *36*, 479.

21. Gunner, M. R.; Robertson, D. E.; Dutton, P. L. *J. Phys. Chem.* **1986**, *90*, 3783.

22. Gunner, M. R.; Dutton, P. L. *J. Am. Chem. Soc.* **1989**, *111*, 3400.

23. Schmid, R.; Labahn, A.; *J. Phys. Chem. B:* **2000**, *104*, 2928.

24. Croney, C. C.; Helms, M. K.; Jameson, D. M.; Larsen, R. W. *J. Phys. Chem. B:* **2000**, *104*, 973.

25. Parson, W. W. *Biochem. Biophys. Acta* **1967**, *131*, 154.

26. Peters, K.; Avouris, P.; Rentzepis, P. M. *Biophys. J.* **1978**, *23*, 207.

27. Fleming, G. R.; Martin, J. L.; Breton, J. *Nature* **1988**, *333*, 190.

28. Kirmaier, C.; Holten, D.; Parson, W. W. *Biochim. Biophys. Acta* **1985**, *810*, 33.

29. Bixon, M.; Jortner, J. *J. Phys. Chem.* **1986**, *90*, 3795.

30. Bixon, M.; Jortner, J. *Chem. Phys. Lett.* **1989**, *159*, 17.

31. Marcus, R. A.; Sutin, N. *Biochim. Biophys. Acta.* **1985**, *811*, 265.

32. Marcus, R. A. *Int. J. Chem. Kinet.* **1981**, *13*, 865.

33. Marcus, R. A.; Siders, P. *J. Phys. Chem.* **1982**, *86*, 622.

34. Siders, P.; Marcus, R. A. *J. Am. Chem. Soc.* **1981**, *103*, 741.

35. Marcus, R. A. *Faraday Discuss. Chem. Soc.* **1982**, *74*, 7.

36. Sutin, N. *Acc. Chem. Res.* **1982**, *15*, 275.

37. Thanasekaran, P.; Rajendran, T.; Rajagopal, S.; Srinivasan, C.; Ramaraj, R.; Ramamurthy, P.; Venkatachalapathy, B. *J. Phys. Chem.* **1997**, *101*, 8195.

38. Turro, C.; Zaleski, J. M.; Karabatsos, V. M.; Nocera, D. G. *J. Am. Chem. Soc.* **1996**, *118*, 6060.

39. Marcus, R. A. *J. Chem. Phys.* **1956,** *24*, 966.

40. Marcus, R. A. *Annu. Rev. Phys. Chem.* **1964,** *15*, 155.

41. Kavarnos, G. J. *Fundamentals of Photoinduced Electron Transfer;* VCH: New York, 1993.

42. Bolton, J. R.; Mataga, N.; McLendon, G. Eds. *Electron Transfer in Organic, Inorganic and Biological Systems*; American Chemical society: Washington. DC, 1991.

43. Jortner, J. *J. Chem. Phys.* **1976,** *64*, 4860.

44. Meyer, T. J. *Prog. Inorg. Chem.* **1983,** *30*, 389.

45. Miller, J. R.; Beitz J. V.; Huddleston, R. K. *J. Am. Chem. Soc.* **1984**, *106*, 5057.

46. Brunschwig, B. S.; Sutin, N. *Comments. Inorg. Chem.* **1987**, *6*, 209.